MODELING, SIMULATION AND APPLICATIONS OF IONIC POLYMER METAL COMPOSITES

Shahin Ranjbarzadeh

Tese de Doutorado apresentada ao Programa de Pós-graduação em Engenharia Mecânica, COPPE, da Universidade Federal do Rio de Janeiro, como parte dos requisitos necessários à obtenção do título de Doutor em Engenharia Mecânica.

Orientador: Fernando Pereira Duda

Rio de Janeiro
Junho de 2017

MODELING, SIMULATION AND APPLICATIONS OF IONIC POLYMER METAL COMPOSITES

Shahin Ranjbarzadeh

TESE SUBMETIDA AO CORPO DOCENTE DO INSTITUTO ALBERTO LUIZ COIMBRA DE PÓS-GRADUAÇÃO E PESQUISA DE ENGENHARIA (COPPE) DA UNIVERSIDADE FEDERAL DO RIO DE JANEIRO COMO PARTE DOS REQUISITOS NECESSÁRIOS PARA A OBTENÇÃO DO GRAU DE DOUTOR EM CIÊNCIAS EM ENGENHARIA MECÂNICA.

Examinada por:

_____
Prof. Fernando Pereira Duda, D.Sc.

_____
Prof. Antonio Guilherme Barbosa da Cruz, D.Sc.

_____
Prof. Carolina Palma Naveira Cotta, D.Sc.

_____
Prof. Marcelo Amorim Savi, D.Sc.

_____
Prof. Angela Cristina Cardoso de Souza, D.Sc.

_____
Prof. Jair Koiller, Ph.D.

_____
Prof. Adriano Maurício de Almeida Côrtes, D.Sc.

RIO DE JANEIRO, RJ - BRASIL
JUNHO DE 2017

Ranjbarzadeh, Shahin

Modeling, Simulation and Applications of Ionic Polymer Metal Composites/ Shahin Ranjbarzadeh. − Rio de Janeiro: UFRJ/COPPE, 2017.

XV,121 p.: il.; 29,7 cm

Orientador: Fernando Pereira Duda

Tese (doutorado) − UFRJ/ COPPE/ Programa de Engenharia Mecânica, 2017.

Referências Bibliográficas: p. 103-121.

1. IPMC. 2. Micropump. 3. Glaucoma. 4. Diabetes. I. Duda, Fernando Pereira. II. Universidade Federal do Rio de Janeiro, COPPE, Programa de Engenharia Mecânica. III. Título

To my parents,

Maryam Massoumian

And Mohammadbagher Ranjbarzadeh

Resumo da Tese apresentada a COPPE/UFRJ como parte dos requisitos necessários para a obtenção do grau de Doutor em Ciências (D.Sc.)

MODELAGEM, SIMULAÇÃO E APLICAÇÕES DE COMPÓSITOS DE POLÍMEROS IÓNICOS E METAL

Shahin Ranjbarzadeh

Junho/2017

Orientador: Fernando Pereira Duda

Programa: Engenharia Mecânica

No presente estudo, um modelo multifísico é organizado para prever o comportamento do composito de polímeros ionicos e metal (IPMC) com resposta elétrica. A abordagem apresentada aqui, envolvendo quimio-eletro-mecânica, as equações de difusão para concentrações iônicas incorporam os termos de migração e difusão; A equação de Poisson é empregada para calcular diretamente a distribuição do potencial elétrico, e a deformação do IPMC é implementada facilmente pelas equações de pequena deformação. A análise é realizada usando o software comercial COMSOL. A resposta do IPMC accionado por eletrodo, incluindo o deslocamento e os perfis de potenciais elétricos são calculados numericamente. Uma das aplicações dos compostos metálicos de polímero iônico é um implante de microbomba oftálmica para remover o excesso de fluido que pode estar causando glaucoma. Portanto, neste estudo, uma microbomba IPMC de baixa energia é projetada e simulada, na qual o fluido é conduzido pela deformação de dois diafragmas IPMC. Os resultados mostram que a microbomba tem a capacidade de transferir o líquido mencionado fora da câmara do olho para reduzir a pressão e o risco de doença. Outra aplicação médica interessante da microbomba IPMC está em dispositivo dispensador de insulina. A simulação da microbomba com o diafragma IPMC confirma que a microbomba IPMC pode gerar um taxa de fluxo suficiente de insulina necessária para o tratamento do Diabetes. Finalmente, propomos um estudo numérico bidimensional sobre o fluxo induzido por um cílio IPMC deformando debaixo de água. Com o objetivo esses resultados, criamos uma microbomba integrada IPMC cilia que contém vários cílios IPMC empregados nos lados superior e inferior do canal fluido. A deformação de cílios de IPMCs empurra e promove escoamento do fluido no canal. Os resultados da simulação numérica mostram que a microbomba gera vazão de fluido com baixo potencial elétrico.

Abstract of Thesis presented to COPPE/UFRJ as a partial fulfillment of the requirements for the degree of Doctor of Science (D.Sc.)

MODELING, SIMULATION, AND APPLICATIONS OF IONIC POLYMER METAL COMPOSITES

Shahin Ranjbarzadeh

June/2017

Advisor: Fernando Pereira Duda

Department: Mechanical Engineering

In the present study, a multiphysics model is presented to predict the behavior of Ionic Polymer Metal Composite (IPMC). The analysis is carried out using commercial software COMSOL. The response of electro actuated IPMC, including the displacement and electric potentials profiles, of the IPMC is numerically calculated. Furthermore, IPMC-fluid interaction is studied with coupling electro-chemo-mechanical model of IPMC with Navier-Stokes equation. The mathematical model used in the numerical analysis consists of three different types of micropumps. Then we focus on the application of IPMC micropump in Biomedical for drug delivery and extracting excess fluid. One of the applications of ionic polymer metal composites is an ophthalmic micropump implant in order to remove excess aqueous humor that may be causing Glaucoma. Therefore, in this study, a low energy IPMC micropump is simulated, in which the fluid is driven by deformation of two IPMC diaphragms. Results show that micropump has the ability to transfer mentioned liquid outside of eye chamber to reduce the pressure and risk of the disease. Another interesting medical application of IPMC micropump is in insulin dispenser device. Simulation of micropump with IPMC diaphragm confirms that IPMC micropump can generate sufficient flow rate of insulin required for treatment of Diabetes. Here, we propose a two-dimensional numerical study on the flow induced by an IPMC cilia vibrating underwater. Concequently, we designed an IPMC cilia integrated micropump that contains various IPMC cilia employed in the upper and bottom side of the fluid channel. Deformation of IPMCs cilia pushes fluid in the channel. Numerical simulation results show that micropump generate fluid flow rate at low electro-potential.

TABLE OF CONTENTS

List of Figures

List of Tables

List of Symbols

p	Pressure	Pa
c	Concentration of the ion species	mol m^{-3}
c_f	Concentration of fixed charge	mol m^{-3}
D	Diffusion coefficient	m^2 s^{-1}
E	Strain tensor	m
E	Young's modulus	Pa
$\mathbf{E_e}$	Elastic strain tensor	m
$\mathbf{E}_0$	Distortion strain tensor	m
F	Faraday constant	C mol^{-1}
I	Identity tensor	
t	Time	s
T	Temperature	K
u	Displacement	m
v	Velocity	m s^{-1}
z	Ion valance	
T	Stress Tensor	Pa
R	Gas constant	J K^{-1} mol^{-1}
d	Electric displacement	C m^{-2}
q	Electric charge density	C m^{-1}
J	Flux of mobile ions	mol m^{-3} s^{-1}
n	Vector normal to given surface	
$P_{osmotic}$	Osmotic Pressure	Pa
c_{ig}	Ion concentration in Gel	mol m^{-3}
c_{is}	Ion concentration in Solution	mol m^{-3}
T	Elastic stress tensor	Pa
D	Symmetric Stretching Tensor	Pa
c_0	Initial Ion Concentration	mol m^{-3}

α	Hydrophilicity coefficient	mol m^{-3}
λ, G	Lame constant	Pa
ψ	Electric potential	V
ε	Permittivity	C^2 N^{-1} m^{-2}
P	Density	Kg m^{-3}
v	Viscosity	m Pa s
μ	Chemical Potential	Joule

List of Abbreviations

IPMC	Ionic Polymer Metal Composite
EAC	Electro Active Ceramic
SMA	Shape Memory Alloy
EAP	Electro Active Polymer
CNT	Carbon Nano Tube
PAMPS	Poly Acrylicamido Methyl Propane Sulfonate
DC	Direct Current
PAA	Poly Acrylic Acid
PVA	Poly Vinyl Alcohol
BDF	Backward Differential Formulation
FSI	Fluid-Structure Interaction
PARDISO	Parallel Direct Sparse Solver
MUMPS	MUltifrontal Massively Parallel Sparse direct Solver
ALE	Arbitrary Lagrangian Eulerian
PDE	Partial Differential Equation
IU	Insulin Unit
IOP	Intraocular Pressure
TBA	Tetra Butyl Ammonium
HDL	High-Density Lipid
IDDM	Insulin-Dependent Diabetes Mellitus
NIDDM	Non-Insulin-Dependent Diabetes Mellitus
GLP	Glucagon-Like Peptide
DPP-4	Dipeptidyl Peptidase-4
ALT	Argon Laser Trabeculoplasty
GUI	Graphic User Interface

CHAPTER I

1. INTRODUCTION

1.1. Introduction

Smart materials have been promoted widely as a key technology that will underpin all manner of novel products with unique capabilities. Many smart materials and products are available commercially and the technologies continue to be the subject of widespread academic research. Nevertheless, there is a widely held view that existing smart materials could find far more widespread uses and the limited commercialization reflects in part the many misconceptions surrounding exactly what smart materials are and what they can do. Although widely discussed in the technical literature and also by the popular press, there is no universally accepted definition of exactly what "smart" or "intelligent" materials are. Many indicate that they are materials which sense some stimulus from the external environment and create a useful response but this would include conventional sensing materials such as Ionic Polymer Metal Composites (IPMCs) which several authors do, indeed, categorize as "smart". However, a more useful view is to consider the response rather than the material itself. Some authorities argue that there are no such things as smart materials but only materials that exhibit certain intrinsic characteristics which can be exploited in products, systems or structures that in turn exhibit "smart" behavior. Examples of this behavior include responses to external stimuli such as self-sensing, self-healing, self-actuating, self-diagnostic and shape changing [1,2].

IPMCs as multi-functional smart materials with actuation, energy harvesting, and sensing capabilities were first introduced in 1997–1998 by Shahinpoor, Bar-Cohen and co-workers as a member of the electroactive polymer (EAP) family based on research work supported by NASA–Jet Propulsion Laboratory (JPL) and under the leadership of Yoseph Bar-Cohen at JPL and Mohsen Shahinpoor [3], director of the University of New Mexico's Artificial Muscles Research Institute. However, the original idea of ionic polymer and polymer gel actuators goes back to the 1991–1993 time period of Osada *et al* [4]. The IPMC actuators, sensors and artificial muscles are composed of a

perfluorinated ion-exchange membrane, which is chemically composited with a noble metal such as gold, palladium, platinum, and silver.

Note that IPMCs are excellent sensors that generate huge outputs in terms of millivolts, which can be employed for the sensing, transduction, and harvesting of energy from wind or ocean waves. These unique materials work perfectly well in a wet environment and thus they are excellent candidates for medical applications. These might range from endovascular steerers and stirrers to enable navigation within the human vasculature; use as deep brain stimulators or employed in flat diaphragm micropumps for precision drug delivery, glaucoma and hydrocephalus; artificial muscles for the surgical correction of ptosis (drooping eyelid syndrome); ophthalmological and vision improvement applications; artificial muscles to assist a failing heart; correction of facial paralysis and other applications in muscular dystrophy; to mediate the control of drainage or flow within the human body; and myriad additional purposes. On the industrial side, due to the fact that the IPMCs are excellent sensors and low-voltage actuators, they can be used for both sensing and simultaneous actuation in many engineering applications Two emerging visions of the future are to see IPMCs heavily utilized in atomic force microscopes as novel and dynamic probes in scanning probe microscopy, as well as robotic surgery to facilitate the conveyance of specific haptic, force, tactile and impedance feedback to surgeons. IPMCs as active substrate and micropillars may be used to monitor nano-bio and cellular dynamics in real time [3,5].

1.2. Motivation

In the recent years, there has been an explosion of advances in the fields of structured and intelligent materials. One of the promising candidates of these materials is IPMC. The IPMCs can undergo large reversible deformation changes in response to a small perturbation in its environment. Due to its unique properties, IPMCs attracted much attention from both academia and industry. Numerous IPMCs have been fabricated and various applications have been identified. Besides experimental design and synthesis of IPMC with different properties and structures, mathematical modeling and computational analysis have come to play an important role in understanding the basic mechanisms such as deformation behavior and response time. There are series of physical and chemical processes that are taking place during deformation of IPMC and it is difficult to quantify

practically. Mathematical modeling can save the money and time as the numerical study can be carried out at a significantly lower cost as compared to practical experiment [6,7].

Ionic electroactive polymers such as polyelectrolytes in a nanocomposite form with a conductive phase such as a metal, a synthetic metal or a conductive polymer of carbon, graphite or graphene are active actuators, sensors and energy harvesters that show large deformation in the presence of a low applied voltage and yet generate a transient voltage signal if subjected to mechanical deformations, as sensors and energy harvesters. In particular, ionic polymer metal composites (IPMCs) have been shown to be excellent candidates for low-voltage biomimetic robotic soft actuation and self-powered biomimetic robotic sensing and energy harvesting [5]. Furthermore, they are good candidates as actuators to use in micropump industry. Because of their lightweight and power to weight ratio, IPMCs are applicable in artificial muscle fabrication and "bending fingers/arms" [8,9].

The applications of the IPMCs rely much on the comprehensive understanding and formulation of their unique properties responsible for the functions. Currently, the understanding of IPMC is still preliminary, which limits the applications of these amazing materials. A good constitutive relation should be able to describe the full stress-strain response while using a minimal number of materials parameters. The understanding of IPMC paves way for manipulating their structures to facilitate shape formations. The development of accurate mathematical models for the mechanical response is still important challenges in the endeavor to create new and better performing IPMCs.

1.3. Objective

Computer simulation is becoming an alternative branch of research complementary to experiments and analytical theory. It offers a lot of advantages, for instance, the freedom to control the parameters of the system and properties of the material, direct access to the microscopic structures and dynamics, and in particular, providing the bridging between the analytical theory and experiment. All this while, most of the research explorations of these fascinating new materials are based on experimental trial-and-error, which is very time-consuming. These have hindered the development of new materials and delayed the transfer of new applications from the laboratory to the marketplace. The need to bring innovative and high-quality products to market in the

shortest time is driving the use of models that can speed up the design and realization process. On top of that, the experimentalists might find it difficult or impossible to carry out their jobs as intended under extreme environment parameters. In contrast, a computer simulation of the material, for example, in extremely low pressure or high temperature or even an impulse forces or sinusoidal pulse would be completely viable. Furthermore, in order to precisely control the deformation feature of the IPMCs by means of a computer, for example in the biomimetic walking machine, a model algorithm is necessary to be implemented in the computer system. With the knowledge of modeling and computational tools in handy, design and simulation of the IPMCs for various engineering application is just one-click apart.

The main purpose of this thesis is to model and simulate the behaviors of IPMCs in response to the externally applied electrical field and then study IPMC-fluid interaction with coupling Navier-Stokes equation and explain the experimental phenomena within a theoretical framework. In the present work, an approach to a fully coupled three-field description using the finite element method is used. The mathematical model of electric stimuli IPMCs and IPMC-fluid interaction is solved numerically to study

- The concentration distributions of different ion species within the IPMC.
- The electric potential distribution across the domain of IPMC.
- The behavior of IPMC in response to the stimulation of externally applied electric field.
- The distinct effects of the various physical and chemical factors by means of systematically and independently varying their property parameters.
- Modeling and simulation of IPMC application as a micropump in the treatment of Glaucoma and Diabetes.
- Investigation of IPMC-fluid interaction and suggest a new structure for IPMC cilia integrated micropump.

1.4. Outline of the thesis

This dissertation is organized into six chapters, and a brief summary for each chapter is given as follows.

Chapter one, Introduction, briefly gives the overview of the nature of the IPMCs and their distinctive characteristics. Then, the motivations and objectives of the present work are presented, followed by the outline of the thesis. In chapter two, the IPMC is defined first with a description of the formation and structure. Then applications of IPMC are discussed, and in the area of biomedical, Diabetes and Glaucoma are targeted. Later, a literature survey is performed on the research history and the existing mathematical modeling, in which more attentions are drawn at the IPMCs. Chapter three deals with the fundamental theory and the mathematical formulation for deformation of IPMC is developed for simulations of bending of the IPMC with applying electro-potential. Chapter four covers numerical method including the finite element method and especially the implementation of governing equations in COMSOL Multiphysics.

Numerical investigation and results of this work are then outlined in chapter five. Three-dimensional simulation of IPMC is demonstrated. Model of IPMC deformation coupled with Navier-Stokes and interaction of IPMC-fluid is investigated in three different scenarios. The first case, IPMC micropump is employed as a part of insulin dispenser device for treatment of Diabetes. Treatment of Glaucoma presented with double diaphragm IPMC micropump in the second scenario and last section is focused on IPMCs cilia and their application as an integrated micropump with a new structure in the last case. In addition, several parameters are considered to analyze and discuss their effects on IPMC based micropump. Chapter six concerns the conclusions and suggestions.

CHAPTER II

2. LITERATURE REVIEW

2.1. Introduction

Materials exhibiting coupled phenomena such as pH, temperature, and electro-potential affecting mechanical deformation and vice versa (Shape Memory Alloys, thermoelastic materials), could be put to intelligent use in many engineering applications. Such materials are classified as `Smart'. Ionic Polymer Metal Composite (IPMC) strips are an example of one such material [10].

IPMC strips respond to an electric potential applied across two electrodes and undergo mechanical deformation. Conversely, when the strip is bent, an electric potential is developed across the surface of the strip. Given its large bending deflection with low actuation voltage input property and the converse effect, IPMC strips show promise in engineering applications such as in actuators, sensors, and energy and force transducers. Further IPMC strips have been used in space and planetary applications like soft robotic actuators (dust wipers), biomedical applications (gastrointestinal endoscopic devices), and artificial muscles. A wider list of applications ranging from mechanisms, robotic toys and actuators, human machine interfaces, and planetary and medical devices can be found in the literature [11-16]. In this chapter literature review survey structure, fabrication, applications, and modeling of IPMC to gain a deep understanding of this class of material.

2.2. Structure of IPMC

An IPMC is a porous charged polymer, saturated with an electrolytic solvent and plated by two metallic electrodes. A difference in voltages between the electrodes generates mechanical deformations (actuation mechanism) which in turn yield a difference in voltages between the electrodes (sensing mechanism). The electrolytic solution comprises mobile ions and an uncharged solvent. The actuation mechanism is based on ion mobility. Because of the difference in voltages between the electrodes, mobile ions (due to their hydrophilicity) displace the uncharged solvent; the concentration

gradient of the uncharged solvent causes a volumetric dilatation of the hydrophobic polymer which is not uniform along the thickness, hence a dilatation gradient. Thus, the polymer is deformed without any mechanical forces acting on it during the actuation mechanism [17].

IPMC strips are made up of an ionic polymer, like Nafion (perfluorosulfonate made by DuPont) or Flemion, which has fixed anions in the polymer network. This ionomeric polymer network is neutralized with an ionic solution with solvents like water and cations like (Li^+) or tetrabutylammonium ions (TBA^+). The surface is composited with a conductive medium like platinum or gold electrodes. A schematic of an IPMC strip is shown in Figure 2.1. When an electric potential is applied between the two surface electrodes, the IPMC strip bends. Redistribution of the mobile ions and water molecules due to various physical processes like diffusion, electrophoretic solvent transport, and diffusion-deformation coupling gives rise to the electromechanical behavior [18,19].

IPMCs are generally fabricated through an electroless chemical reduction process, consisting of the diffusion, adsorption, and reduction of a metal salt onto an ionomeric membrane. Nafion and Flemion are typically used as the ionomers, and noble metals, such as platinum, gold, or silver serve as the electrode material. The electroless chemical reduction is often followed by an ion-exchange process, in which the sample is immersed in a solution to replace hydrogen ions with the select counterion species. Water is typically used as solvent and several counterions, such as lithium, sodium, and potassium have been considered in the literature [20]

The type of polymer base (Nafion or Flemion), the mobile cations, and the type of solvent along with their composition affects the response of the IPMC strip. Under the application of a step voltage, Nafion-based IPMC strips bend towards the anode. Flemion based IPMC strips show an initial fast bending movement towards the anode side and then a slow relaxation towards the cathode side. The tip displacement response, when a step voltage is applied differs, depending on the type of free mobile cations even for a Flemion based sample. Response time depends on the dimension of IPMC strip (length, thickness, and width), type of polymer, mobile ions, electrodes and applied electro-potential [21,22].

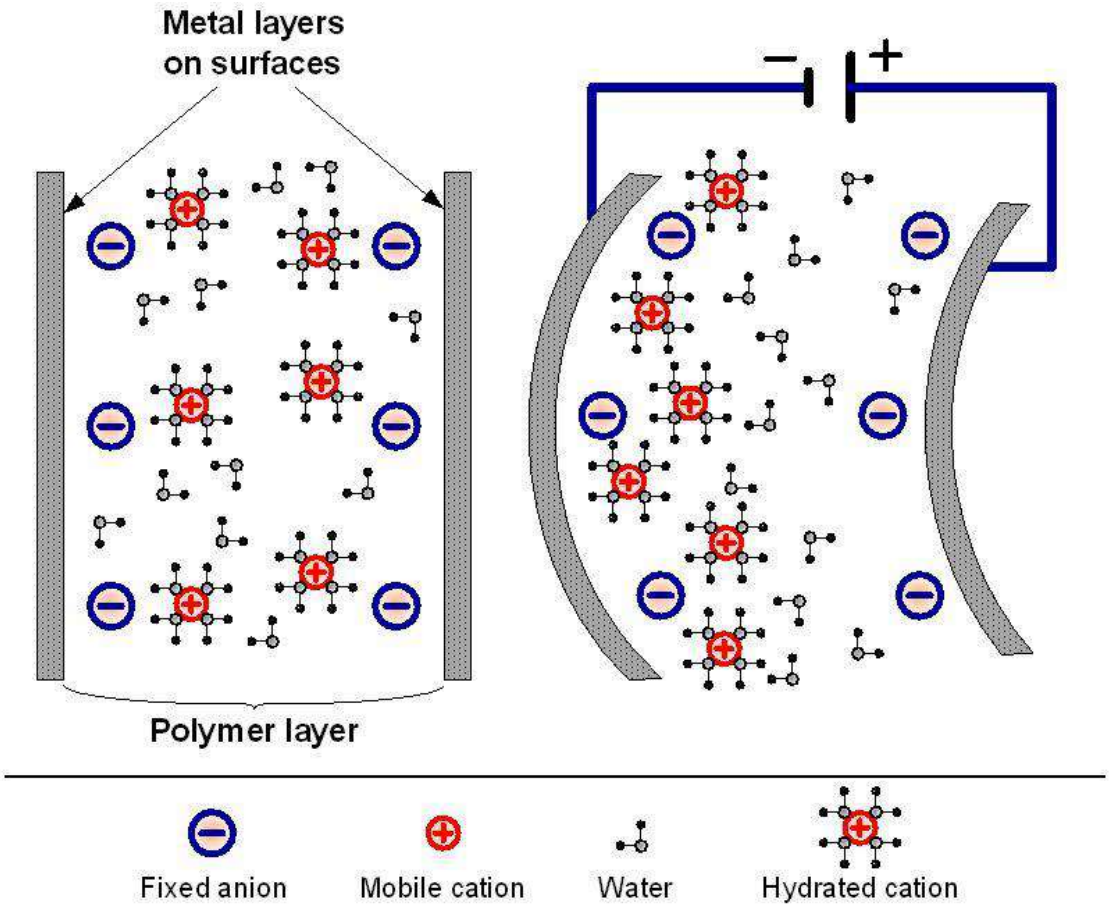

Figure 2.1: A schematic of a typical IPMC strip and its actuation principle. The IPMC strip bends toward the anode when an electric potential is applied across the surface of the strip [21].

The current state-of-the-art IPMC manufacturing technique incorporates small amount (< 10 wt.%) of nanoparticles (layered silicate [montmorillonite], fumed silica, carbon nanotubes [CNTs], etc.) into the Nafion has been proven to affect the ionic and mechanical properties of Nafion. In general, the nanocomposites of an organic or nonorganic material increase the modulus of elasticity and lead to better thermal and mechanical stability. This is more important when Nafion is fully hydrated and as a result the elastic constant decreases by several times. The ionic properties of the Nafion nanocomposite may be improved or deteriorated depending on the type and amount of nanoparticles. On the other hand, a major disadvantage of commercially available Nafion resin beads is their very low surface area (0.02 m^2/g), which limits the access to most of the active sites, which as a result hampers the ionic activity. The addition of nanoparticles has been known to increase the surface area and thus ionic acidity. For fabrication of Nafion nanocomposites, typically a known amount of nanoparticles is dispersed in the

Nafion solution and the (nanoparticle)–Nafion solution is stirred or sonicated to achieve a homogenous solution. Using the solution-casting method, membranes with desired thickness can be fabricated. Several types of nanoparticles have been investigated for the fabrication of IPMC soft actuators and sensors, including nonorganic particles (such as silica) and organic nanoparticles (such as CNT and graphene). Due to different preparation processes, morphologies of precipitated metals are significantly different [23, 24].

2.3. Application of IPMC

Consideration of practical applications for electroactive polymers (EAP) commenced only in this decade following the emergence of new materials that induce large displacements. These materials are highly attractive for their low-density and large strain capability, which can be as high as two orders of magnitude greater than the striction-limited, rigid and fragile electroactive ceramics (EAC). Also, these materials are superior to shape memory alloys (SMA) in their temporal response, lower density, and resilience. However, EAP materials reach their elastic limit at low-stress levels, with actuation stress that falls far shorter than EAC and SMA actuators. The most attractive feature of EAP materials is their ability to emulate biological muscles with high fracture tolerance, large actuation strain, and inherent vibration damping. EAP actuation similarity to biological muscles gained them the name "Artificial Muscles" and potentially can be used to develop biologically inspired robots. The limited force actuation of current EAP is constraining the practical applications that can be considered [25,26].

The emphasis of this section is on IPMC, which is bending EAP materials, first reported in 1992. The various issues that can affect the application of IPMC were examined including operation in vacuum, low temperatures, and the effect of the electromechanical and ionic characteristics of IPMC on its actuation capability. The finding that IPMC can be activated at low temperatures and vacuum, paved the way for the serious consideration of this class of materials for space applications. IPMCs bending characteristics offered the potential to address the critical issue of planetary dust that affects solar cells and imaging instruments on such planets as Mars [27].

Our vision of the future of IPMC artificial muscles may be summarized below in terms of both medical and industrial applications. Note that IPMCs are excellent sensors that generate huge outputs in terms of millivolts, which can be employed for the

sensing, transduction, and harvesting of energy from wind or ocean waves. These unique materials work perfectly well in a wet environment and thus they are excellent candidates for medical applications. These might range from endovascular steerers and stirrers to enable navigation within the human vasculature; use as deep brain stimulators or employed in flat diaphragm micropumps for precision drug delivery, glaucoma and hydrocephalus; artificial muscles for the surgical correction of ptosis (drooping eyelid syndrome); ophthalmological and vision improvement applications; artificial muscles to assist a failing heart; correction of facial paralysis, facioscapulohumeral and other applications in muscular dystrophy; to mediate the control of drainage or flow within the human body; and myriad additional purposes. On the industrial side, due to the fact that the IPMCs are excellent sensors and low-voltage actuators, they can be used for both sensing and simultaneous actuation in many engineering applications. In the sensing mode, they have a very good bandwidth to sense low as well as high frequencies, in contrast to piezoelectric materials such as PZT (Lead Zirconate Titanate) or lithium niobate, which are only suitable for high-frequency sensing. Two emerging visions of the future are to see IPMCs heavily utilized in atomic force microscopes as novel and dynamic probes in scanning probe microscopy, as well as robotic surgery to facilitate the conveyance of specific haptic, force, tactile and impedance feedback to surgeons. IPMCs as active substrate and micropillars may be used to monitor nano-bio and cellular dynamics in real time [28-34].

There is great potential for Nafion-based IPMCs in nano-to-micro-to-macro size ranges, as materials that could provide new applications in miniature scales have emerged. With the development of microfabrication technology, intense research efforts have been made towards microfluidic systems and micro liquid handling devices. Micropumps are one of the crucial components for moving liquids in the miniaturized systems and the most important part of micropump is actuators. Their compact size and ability to handle very small and precise volumes of liquid make them attractive for applications in microfluidic systems, biotechnology, microchemical analysis systems, drug delivery systems, and chip-integrated cooling systems. Due to IPMC actuators characteristics, IPMC based micropump is a promising candidate in biomedical applications to deliver drugs or extract fluid [35].

2.4. Micropump

In the past few years, there has been a growing interest in the development of microfluidic systems for various applications including biological and chemical analysis, lab on chip diagnostics and drug delivery. Micropump is a pivotal component in such microfluidic systems as it is essential for micro liquid handling and thus micropump has become an important research area. A micropump is a device which can be used to generate controlled flow rate in the range of μl/min to ml/min. During recent years several different micropumps have been reported based on different principles and actuation mechanisms including electro-osmotic, electromagnetic, piezoelectric, electrostatic, shape memory alloy [36].

Among various actuation possibilities, IPMC actuation offers advantages in terms of high deflection, low weight, fast mechanical response and ease of integration. IPMC actuated valveless micropumps have advantages of simple structure and improved reliability due to the elimination of valves [10].

In the past decade, a large number of micropumps have been developed to deliver and transport a wide range of liquids. These micropumps produce a flow rate ranging from a few μl/min to ml/min, and a pressure varying from a few Pa to several hundred kPa or more. Micropumps can be classified into two groups: mechanical micropumps (with moving parts) and non-mechanical micropumps (without moving parts). Some examples of mechanical micropumps include but are not limited to thermos pneumatically driven peristaltic pumps, electrostatically driven reciprocating pumps, piezoelectric micropumps, and shape memory alloy micropumps. Non-mechanical micropumps use a variety of electric-fluid interactions to generate forces in the liquid, such as electrokinetic micropumps, magnetohydrodynamic micropumps, and electrohydrodynamic micropumps [37].

As with many technologies, each method has its advantages and disadvantages that depend upon the particular application. A comprehensive overview of micropumps is given elsewhere [38]. Since the focus of this work is on the application of IPMC in micropump and apply the model of IPMC-fluid interaction to simulate IPMC based micropump, only micropumps working based on this principle will be discussed in the following.

Mechanical micropump in general consists of a fluid chamber, diaphragm, inlet, and outlet. Figure 2.2 presents schematic of a basic micropump. Micropump operations divide into two steps suction mode and pump mode. In the first step (suction) as shown in figure 2.3 inlet is open and the outlet is closed, the diaphragm is deformed outward and sucks the fluid into the chamber. In the second step (pump) as presented in figure 2.4 inlet is closed and the outlet is open so with bending of diaphragm fluid pushed out of the chamber. So there are three main parameters include velocity and pressure field of fluid and deformation of IPMC diaphragm to investigate and analyze the operation of micropump. The flow rate of micropump calculated by the fluid velocity at the outlet and volume of fluid pumped in each cycle obtained from the displacement of IPMC diaphragm. It is possible to make some graphs that relate flow rate or fluid velocity with applied electro-potential to the IPMC diaphragm for specific micropump structure and dimension. This information would be useful for fabrication of IPMC micropump in a wide range of applications.

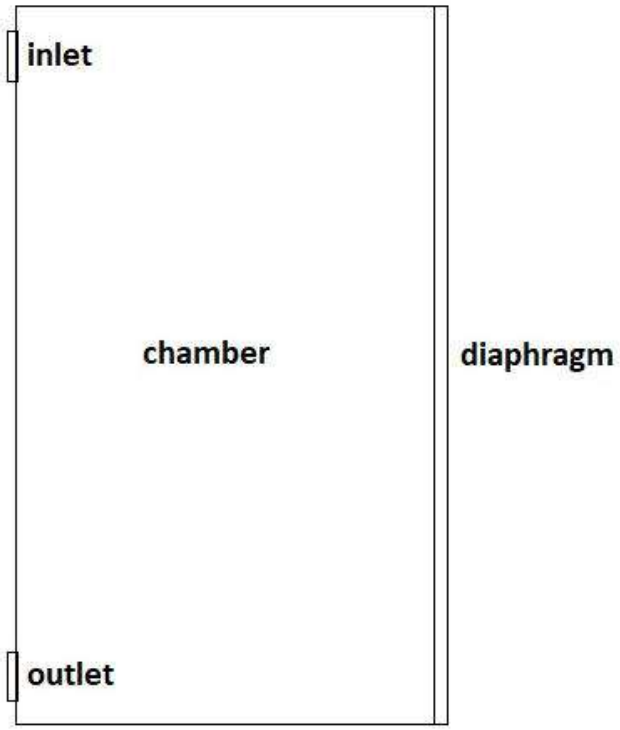

Figure 2.2: Micropump schematic includes the diaphragm, a fluid chamber, inlet, and outlet.

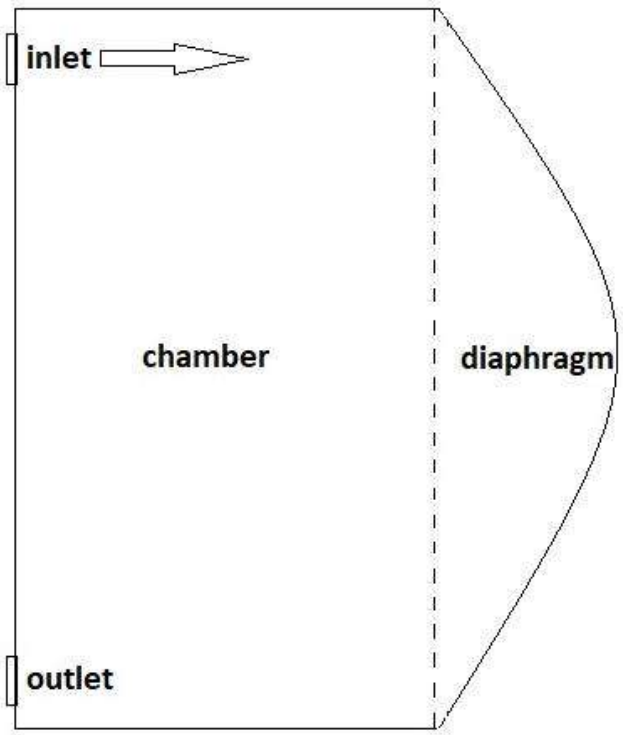

Figure 2.3: Micropump schematic in suction mode.

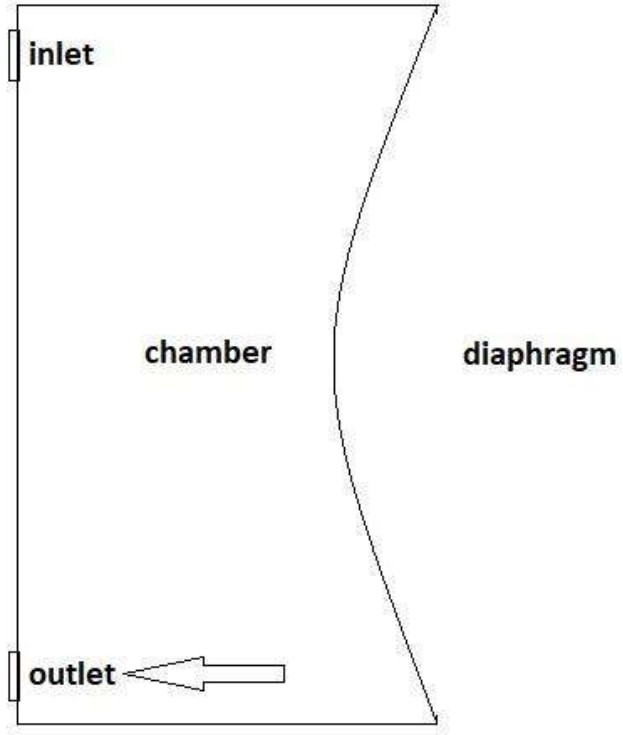

Figure 2.4: Micropump schematic in pump mode.

Nozzle/diffusers micropumps rely on fluidic structures that act either as a diffuser or a nozzle depending on the direction of fluid flow. Typically, they have a lower flow restriction in the direction of the diffuser, resulting in net fluid flow in that direction during pumping. The structure as presented in figure 2.5 comprises a pair of nozzle-diffuser elements and a fluid chamber. In the supply mode, the diaphragm deflects upward which results in a negative pressure inside the fluid chamber due to which fluid is drawn into the chamber via the inlet (diffuser) and outlet (nozzle). As the pressure drop across a nozzle is higher compared to that across a diffuser, more fluid is drawn via the inlet compared to that via the outlet. In the pump mode, the diaphragm moves downward thus creating a positive pressure and more fluid leaves via the outlet (diffuser) compared to that via the inlet (nozzle). Thus, a net flow from the inlet to the outlet is achieved [36].

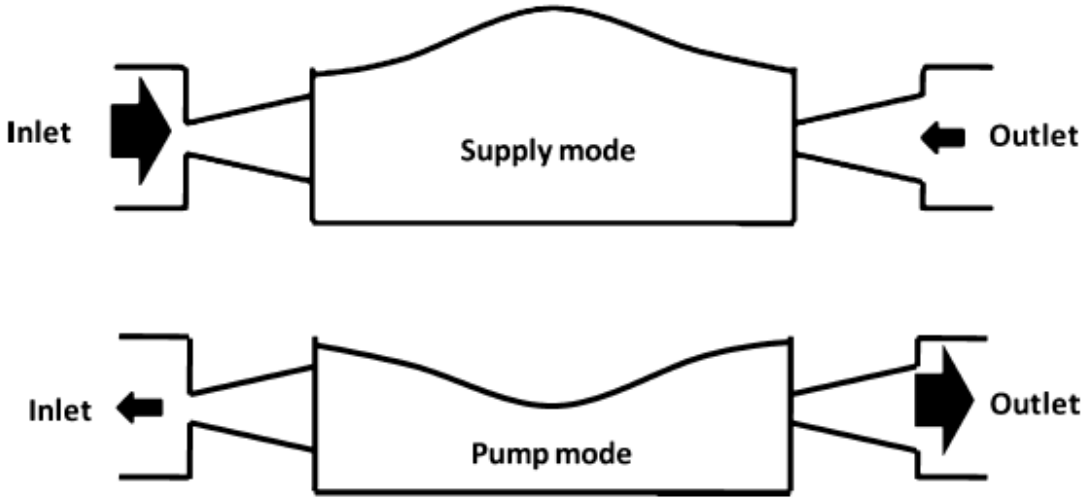

Figure 2.5: Working principles of nozzle/diffuser micropump [36].

Among other actuation mechanisms, the piezoelectric actuators are the most popular for micropump applications because they normally have a short response time and a high output force, but compared to IPMCs their high operational voltages are considered disadvantage in biomedical applications and especially in implanted micropump. Numerous research groups have been active in developing and modeling IPMCs micropumps. A review of some researches related to IPMC based micropumps will be presented in following. Guo *et al.* [39] proposed a double chamber IPMC micropump that each chamber consists two IPMC diaphragms. He experimentally

obtained a flow rate of 4.5 µl/min to 37.8 µl/min. Later Pak *et al.* [40] described the fabrication and characteristics of a nozzle/diffuser IPMC micropump with measured flow rate of about 9.97 µl/min when the input voltage was 8V. Lee *et al.* [41] presented the design and flow rate predictions of an IPMC actuator-driven valveless micropump. He utilized finite element analysis to optimize diaphragm then used the flow resistance coefficient equations at very low Reynolds numbers to reach output flow rate of 8.2 µl/s. Naguyen *et al* [42] fabricated a flap valve IPMC micropump and introduced the concept of flexible support. He recorded a maximum flow rate of 760 µl/min at an applied voltage of 3V. Santos *et al.* [43] fabricated and investigated two different diaphragms of IPMC then based on previous work, he fabricated an IPMC micropump with 8.02 µl/s outflow rate. Nam *et al.* [44] reported a novel design of IPMC diaphragm that helped to produce larger deformation. Unlike conventional method of using a single piece of IPMC clamped at all edge, he used several IPMC clamped at the single edge. Recently, Kawun *et al.* [45] suggested a thin PDMS nozzle/diffuser IPMC based micropump with a peak flow of 135 µl/min for the treatment of Glaucoma.

2.5. Diabetes treatment

Diabetes Mellitus is a group of physiological dysfunctions characterized by hyperglycemia, defined by The American Diabetes Association as "a condition characterized by hyperglycemia resulting from the body's inability to use blood glucose for energy…" It occurs due to body`s hormonal dysfunctions that lead to insulin resistance, inability to produce insulin or excessive glucagon secretion. It can also be defined as a disease of dysregulation of metabolic functions, with the main dysregulation being of the glucose metabolism [46].

Insulin is the hormone that triggers body cells to take up glucose, in order to use it as energy. It is produced by beta cells located in the pancreas in the region known as islets of Langerhans. The main factor that stimulates insulin secretion is the elevation of the concentration of glucose in the blood, such as after a meal (known as a postprandial state). Insulin acts by binding to specific receptors on the membrane of adipose, muscle and liver cells. In each of these cells, it achieves different objectives: storage of fat for further use from the body in adipose cells, the transformation of glucose into glycogen, that are used as energy for muscle extension, in muscle cells and stimulates glucose

storage in the liver. The disease cannot be cured but can be successfully treated. Diabetes can be considered a chronic degenerative disease. It is associated with, but not limited to, five complications: retinopathy, neuropathy, nephropathy, cardiovascular complications and delayed wound healing. Periodontal disease and depression are also related to Diabetes [47,48].

There are two types of diabetes: Type-1 or Insulin-dependent diabetes mellitus (IDDM) is an autoimmune disease that leads to the destruction of pancreatic beta-cells. Type-2 or Non-insulin-dependent diabetes mellitus (NIDDM) is a progressive impairment of glucose regulation due to insulin resistance and dysfunctional pancreatic beta cells.

Insulin-dependent diabetes

Type-1 diabetes is a chronic autoimmune disorder, defined by the body's own immune systems attacking beta cells in the Islets of Langerhans, damaging them which eventually reduces or eliminates insulin production. It is usually determined by people younger than 30 years old as it is associated with the acute crisis of symptoms as soon as the disease develops. Its incidence has risen across 5the past decade and this pattern is expected to be maintained until 2020. Type-1 diabetes manifests in genetically susceptible individuals, but it is only precipitated due to some environmental factors, such as viral or bacterial infections [49].

Non-insulin-dependent diabetes

Type-2 Diabetes is characterized by insulin resistance, where the muscles or adipose cells do not respond well to increased blood insulin levels, whereas beta-cells are intact. Type-2 diabetes sets on later at patients' lives and results in the impairment of glucose regulation. Type 2 is more common, being responsible for 95% of all the cases in the USA as of 2015. Due to its various symptoms, diabetes is associated with early mortality and as a result, increasing level of morbidity [46,48].

Risk factors associated with NIDDM are a sedentary lifestyle, unhealthy eating habits, low levels of HDL (high-density lipids in the blood), and obesity, with the latter being the most important one. Obesity can lead to insulin resistance. Age, heredity, ethnicity, and hypertension are also criteria for testing for diabetes in asymptomatic adults [49,50].

Along with insulin deficiency, come alterations in other hormones that are also relevant to glucose homeostasis. Glucagon, which synthesizes glucose, glucagon-like peptide 1 (GLP-1) that increases insulin and suppresses glucagon secretion from the pancreas and amylin that modulates glucagon, and is released in response to food intake, are all affected by diabetes, by virtue of being produced and released by the alfa and beta cells in the pancreas. Some symptoms associated with diabetes are excess volumes of urine (polyuria), weakness, fatigue, weight loss and increased appetite. These are due to water loss that happens because of an osmotic effect caused by the excess glucose in the blood. Another indication of diabetes is yeast infections in the urinary tract [51-53].

In Brazil, self-referred Diabetes prevalence has been estimated at 6,2% and it increases as age increases, following the global trend and the morbidity has increased when polled by national health organs. Overall, it was estimated in 2015 that more than 9 million people are affected, higher than 2006 estimative and in line with the projection for 2010-2030. This fact corroborates with increasing numbers of obesity and aging population [54].

Diagnose for diabetes usually includes measurement of glucose in the blood, in short-term and long-term variations. Another important measurement to be made is that of HbA1c, which is a glycosylated hemoglobin. As glucose flows through the blood, it may attach to a hemoglobin. The ratio of measured HbA1c to free hemoglobin is representative of glucose in the blood. The goal in treating diabetes is to keep HbA1c levels <7%. All measurements are utilized to inform the patient and the physician on what kind of treatment should be followed [50,52].

Diabetes is related to multiple complications, affecting multiple parts of the body, that can be separated into two categories, related to which blood vessel are damaged by Diabetes: microvascular and macrovascular. Macrovascular complications, such as strokes and heart attacks happen due to higher blood pressure. The main mechanism is atherosclerosis [48,54].

Typical Diabetes treatment starts with monitoring of glucose levels in the blood and insulin supplement injections to complement the body's own production. The patient is able to monitor glucose levels at different points during the day, at least three times per day, for patients carrying out insulin treatment. However, the first line of treatment suggested is the administration of metformin, along with lifestyle changes, then

proceeding to insulin if results are not achieved or another medication is glucose levels are not below the threshold [51,55].

Lifestyle changes, such as the adoption of regular exercise have been shown to improve blood glucose control, reduce cardiovascular risk factors and contribute to weight loss, while also preventing type-2 diabetes onset in high-risk individuals. Recommended exercise levels are of 150 minutes a week. Medical Nutrition Therapy is also of major relevance to diabetes treatment. The focus of the diet should be to promote tight control of glucose levels and limit complications. Smoking cessation is highly recommended for diabetes patients, as studies and trials showed that smoking has heightened the risk of morbidity and premature development of microvascular complications [48,50,52].

There are other treatments besides insulin, such as medication to decrease glucose production by the liver, increase fat tissue and muscle tissue sensitivity to insulin and stimulating beta cells to release more insulin. These may be utilized in conjunction with insulin therapy and with each other. Non-insulin treatment may focus on re-establishing the balance of the other hormones affected by diabetes. However, it is impractical to inject directly either GLP-1, due to its rapid degradation by another enzyme DPP-4 or Amylin because it forms an insoluble precipitate. The treatment then consists of administering agonists, medicine that is analog to the body produced hormones [48,56].

Exenatide is one of the agonists, a GLP-1 mimetic, enhancing insulin secretion and suppress higher than normal glucagon levels after meals. Some side effects include mild nausea and vomiting, however, they only happened when patients were still being introduced to the treatment. Also related to GLP-1 is sitagliptin, a DDP-4 inhibitor. That means the GLP-1 stays longer in the serum and is able to act for longer. With that, it's able to reduce glucose levels in the blood, while having fewer side effects than other GLP-1 agonists. The main concern when using sitagliptin is pancreatitis. Liraglutide is a GLP-1 analog, which altered composition makes it 97% homologous to GLP-1 while making it more resistant to DDP-4 degradation, enabling once-daily administration. It enhances insulin secretion [47,57].

Pramlintide is an amylin analog, that contains a chemically altered amylin molecule. This alteration makes it possible to keep it in subcutaneous space for enough

time to the body to assimilate it. It has the same mechanism of actuation as amylin, slowing gastric emptying and enhancing satiety by reducing postprandial glucagon secretion. The side effects follow suit of other medicine, evoking nausea, vomiting, and anorexia, but only during an adaptation period [51].

Insulin therapy takes place in different forms, adapted to the patient. There are short-acting, intermediate-acting and long-acting formulas, that may be utilized a different number of times a day. When diabetes is still on the onset, outside critical situations, insulin shots are rarely the first treatment suggested. Usually, medication such as sulfonylureas and metformin are used first to try and control the disease by stimulating insulin production and glucose reduction, if glucose blood goals are not achieved, insulin treatment is started, at first in conjunction with other agents [49,57].

Initially, single insulin injections are utilized at night, in order to balance fasting blood glucose. This is known as basal insulin. This helps other agents keep glucose levels balanced throughout the day. Although useful, this approach is not able to keep glucose levels in check if there are no dietary adjustments, or if postprandial and daytime hyperglycemia still happens. At this stage, although there are no studies indicating consensus best course of action, a physiological regimen of insulin therapy should take place [59].

Therapy should be adjusted to the patient's needs and life schedule. It can be comprised of administering insulin injections after meals (bolus insulin), either with or without the injection required to keep low glucose levels at night. Another option is insulin injections containing intermediate and fast-acting doses, which are to be used with a strict dietary and activity schedule. Whatever treatment is chosen, the goal is still to keep fasting glucose and postprandial glucose levels balanced. Treatment then should carry on with regular blood glucose levels monitoring, during the day and at longer periods, in order to adjust medication and dosage. Metformin use is recommended as a complementary medication at this stage since it is an insulin sensitizer. Figure 2.6 shows examples of insulin treatment administration [57,59].

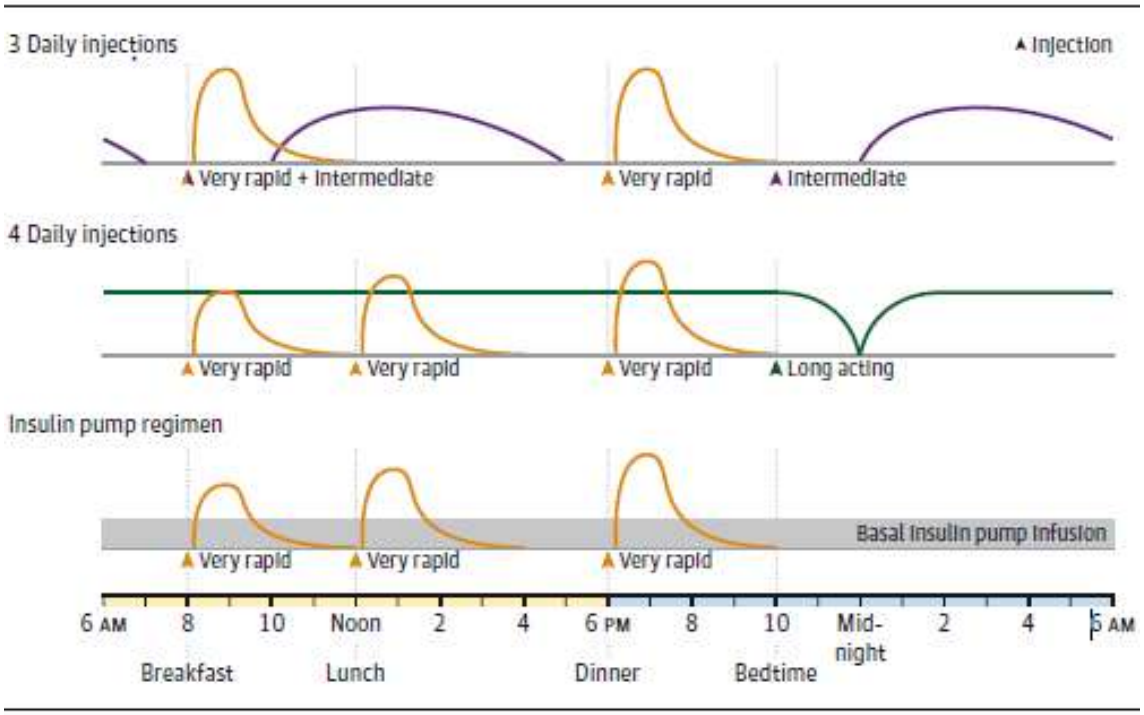

Figure 2.6: Examples of insulin treatment administration [57].

Since insulin treatment is constant and to be done for long periods of time, it needs to be carried out unsupervised for most of the time if the quality of life of the patient is to be retained. Along with nutrition changes, the patient must be willing to comply with the treatment. The standard mean of injecting insulin is a vial and syringe. However, fear of needles and preconceptions about pain levels, self-injection concerns and social bias towards injections are all deterrent factors in insulin treatment. These factors end up influencing doctors, that will delay insulin treatment unless completely necessary, risking letting some complications set on the patient [57,60].

With that in mind, insulin pens were developed as an alternative to vials and syringes. There are two types of pens: reusable ones, with cartridges that are replaced as they are used and disposable pens, prefilled with insulin. These reduce a lot of the risks and perceptions about standard insulin treatment: They avoid the risk of dosing error via electronic functions embedded in some and some use smaller needles, that reduce pain. Studies show that patients are significantly more willing to carry on insulin treatment while using pen systems, reporting smaller missed programmed shots, no reports of pain, feeling socially accepted and increased usability. Both methods are shown to equally reduce glucose levels in the blood, however, pens, being mechanically more complex, are more prone to breaking. They are also, for those of reusable nature, more likely to be

infected by exterior agents. Pen systems are also more expensive and insulin cartridges are not always interchangeable between manufacturers [49,59].

Another option is inhaled insulin formulations, via aerosol. Since there is a large surface area in the lungs and absorption is quicker than subcutaneous injection, inhaled insulin has upsides compared to the other methods. They are used for postprandial doses, not usable for basal dosage. It is shown that although less efficient than insulin injections, inhaled insulin is preferred by patients, so it should be considered as a vital alternative. It is not shown to be completely safe, however, especially for people with impeded pulmonary function or pulmonary disease [58,60].

Finally, insulin pumps that act on continuous subcutaneous infusion are also an alternative. They are used to keep postprandial levels of glucose balanced. They work by keeping in insulin reservoir next to the body and having a needle that acts as catheter connected to subcutaneous tissue. The needle needs to be changed from time to time to avoid infection. This kind of treatment is based on the continuous release of insulin throughout the day. It keeps glucose levels balanced throughout the day, and it is able to account for variations in glycemic levels in case of patient misestimating sugar intake or exercise effects. There is some commercial insulin dispenser device including Tandem (t: Slim and t: Flex), Roche (Accu-chek combo), Insulet (OmniPod), Animas (vibe) and V-Go [60,61].

Compared to insulin injection treatment, the insulin pump showed less glycemic fluctuations as shown in figure 2.7. The reduction in glycemic fluctuations allows patients to reduce glycated hemoglobin levels without increasing the risk of hypoglycemia. Insulin-pump therapy may also lessen the problems of glycemic control associated with injections because it allows for more flexible, reprogrammable basal insulin rates and extended-wave insulin profiles that can reduce the risk of hyperglycemia after fatty meals [58].

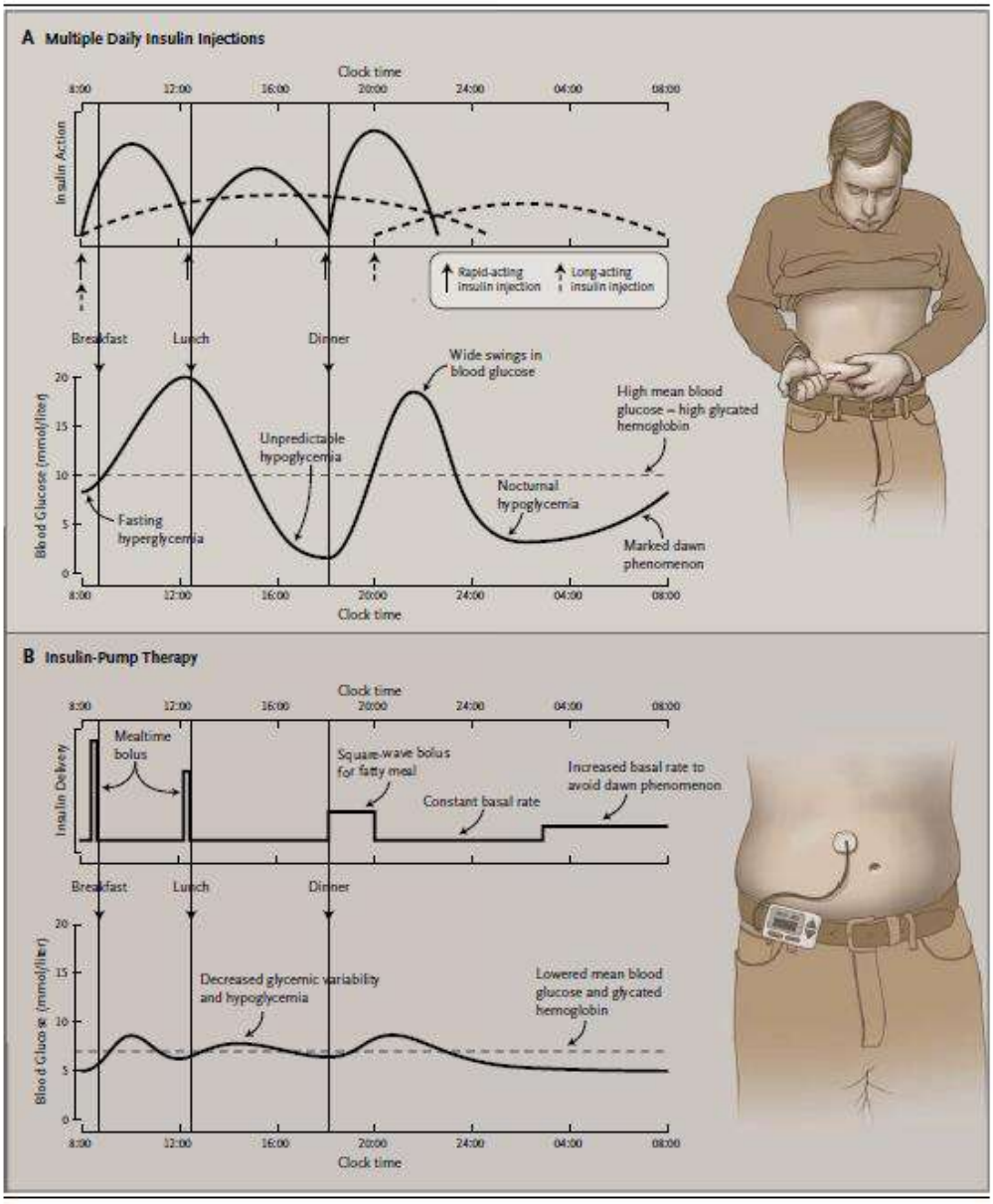

Figure 2.7: Insulin Pump treatment compared to multiple injections a day [58].

Due to its continuous nature and ability to compensate for total lack of insulin secretion, insulin pumps are fit for type-1 diabetes. By taking into consideration the ability to monitor blood glucose levels and manual or automatically adjustable insulin release make insulin pumps a viable alternative treatment. Since the treatment is more expensive and conventional multiple injections are shown to achieve acceptable control, pumps are indicated to people who are unable to control hyperglycemia or hypoglycemia with conventional methods [53,62].

However, insulin pumps are shown to be able to control glycemic levels better than self-injections, keeping not only glucose levels but also glycated hemoglobins lower.

This is also true for type-2 diabetes patients. The risk of severe complications and overall insulin dosage are reduced when using pumps, while also keeping the patient less time in hyperglycemia since there is no need for high insulin injections. Insulin pump treatment was shown to not increase weight gain and it has also been concluded that insulin pumps improve the quality of life and are preferred over multiple-dose injections [58,61].

The drawbacks come from the fact that rigorous control is needed and the patient needs to be diligent and technically trained to operate the pump. The pump is also not being able to compensate for insulin demand in case of alterations and if pump malfunction occurs, hyperglycemia may happen faster. Overall, as insulin pump technology improves, it may become the preferred alternative to diabetes treatment, as monitoring improves and the pump becomes able to compensate for unexpected variations in glycemic levels [60,63].

IPMCs are very well suited to medical applications, due to its softness, flexibility, biocompatibility. Recent researchers delineate a wide range of applications including insulin dispenser pump. IPMCs are useful to fabricate small-scale pumps, able to serve as diaphragm actuators. The use of micropumps in the field of Medical Care is promising for the delivery of drugs and extracting body fluids. An area where this technology could be applied is in the treatment of Diabetes. So we presented and studied an IPMC micropump with single IPMC diaphragm for insulin delivery. Then we applied mentioned governing equation before to simulate IPMC micropump for insulin delivery.

2.6. Glaucoma treatment

In the recent years, many microfluidic devices have been developed in a wide range of applications, such as biology, chemical analysis systems, micro drug delivery systems, fuel cell, bionic devices, and cooling systems [64–69]. A microfluidic device typically requires components such as micropumps, microvalves, micromixers, and microheaters for separating, mixing and manipulating of fluids [70,71]. With recent advances in smart materials, main advantages of ionic polymer metal composites (IPMCs) have been found over conventional electroactive materials, such as large deformation, low voltage actuation, low weight and biocompatibility [72]. Due to these characteristics, IPMCs are a promising candidate for application in micropumps, microvalves, and microsensors. In the trend of developing new devices for biomedical

applications, micropumps have received great attention. One of these applications is an ophthalmic micropump implant in order to remove excess aqueous humor that may be causing Glaucoma. Glaucoma is the second leading cause of blindness in the world and a term used to describe a group of multi-factorial and complex eye diseases that cause irreversible gradual vision loss. High pressure due to aqueous humor accumulation in anterior chamber was known as the main risk factor of Glaucoma [73].

As of 2013, Glaucoma affects 60.5 million people worldwide and had 3.54% of the prevalence for populations aged 40 – 80. Statistically, glaucoma affects more men than woman, and is more prevalent with people of African ancestry, although it`s not clear why sex or ethnicity have any influence on the disease. These numbers, however, don`t represent the full extent of the disease, since it is mostly undetected until the disease is at an advanced stage. It is also known that glaucoma is an age-related disease, with the mean age of onset being 60 years old. Some of the risk factors associated with the disease are age, African descent, a thicker cornea, family glaucoma history and high intraocular pressure. In Brazil, it is no different. There are no precise numbers of how many people were diagnosed by Glaucoma. In 2007, estimates indicated that around 2 million people had the disease, but only 500.000 were known [74,75].

The eye is a complex human organ composed of different structures and elements as shown in figure 2.8 and understanding some of these structures eases understanding of this chapter. Willoughby defines the eye as having three layers: The outer layer, containing the sclera, an outer coat issue which function is to protect the eye from external impacts and keep its shape, and the cornea, responsible for directing the light to the interior of the eye via refraction while also keeping the eye free from infection. The conjunctiva, a transparent membrane, covers the sclera. The middle layer is the iris, that regulates the amount of light reaching the retina, the ciliary body that controls the lens and regulates aqueous production and the choroid, a vascularized site that provides oxygen to the retina. The anterior chamber, where aqueous fluid flows are located right above the ciliary body. The final inner layer is the retina, which gives visual feedback of the eye, composed of a complex arrangement of neurons, capable of processing light [76].

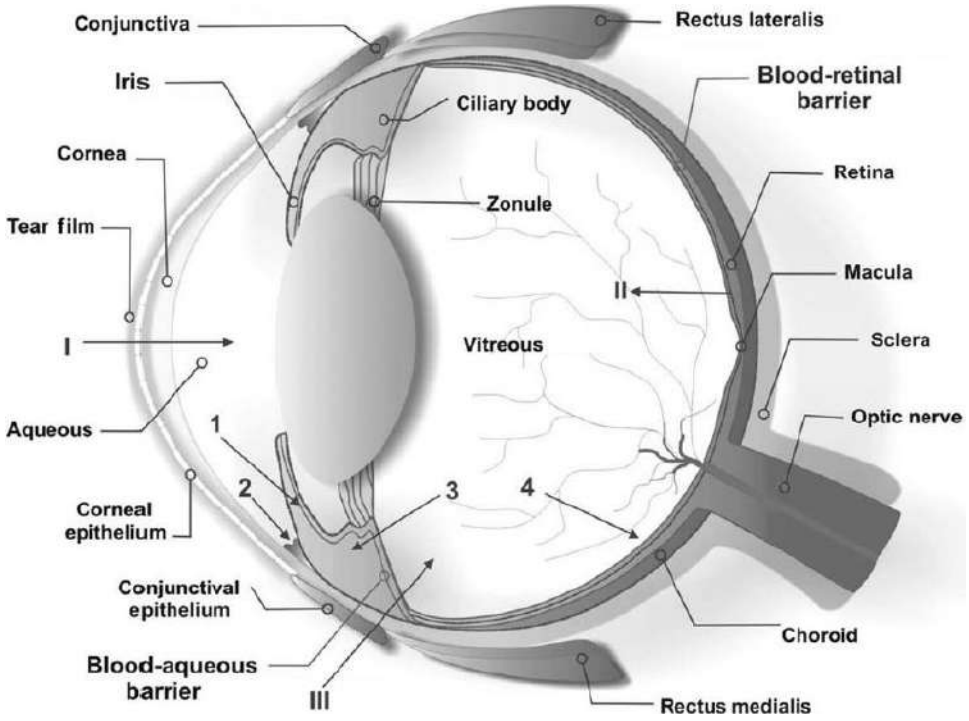

Figure 2.8: Schematic representation of the eye [76].

Glaucoma is a term used to describe a group of eye diseases that causes irreversible gradual vision loss that results in the destruction of optic nerves in the back of the eye. It is considered an optic neuropathy that progressively causes structural (optic disc damage) and functional (loss of visual field) alterations to the eye. The main structural alteration is damage to the retinal ganglion cells located at the optic disc, alongside changes in the form of the retina, the main one being the cupping of the optic disc, disrupting axonal transport from the eye [75].

The optic disc is where nerve fibers (axons) pass out of the eye, transporting visual information and vital cell organelles. Usually, the aspect of nerves and disc is such that there will be a paler central depression of the disc. However, as the disease progresses and more cells die the cup/disc ratio increases. As these cells die, the visual field is reduced and the environment may become more toxic, leading to a snowball effect. Loss of optic nerve tissue results in excavation or “cupping” of the optic nerve head, which is best viewed by direct ophthalmoscopy. Figure 2.9 shows glaucomatous excavation of the optic nerve with the vertical cup-to-disk (C:D) ratio of 0.8. With a vertical C:D ratio 0.6 or greater, glaucoma should be suspected. The main functional alteration associated with glaucoma is a loss of visual field, initially affecting peripheral vision and progressing into total blindness. Glaucoma differs from other optic neuropathies by its slow progression over long periods of time, months to years [75,77].

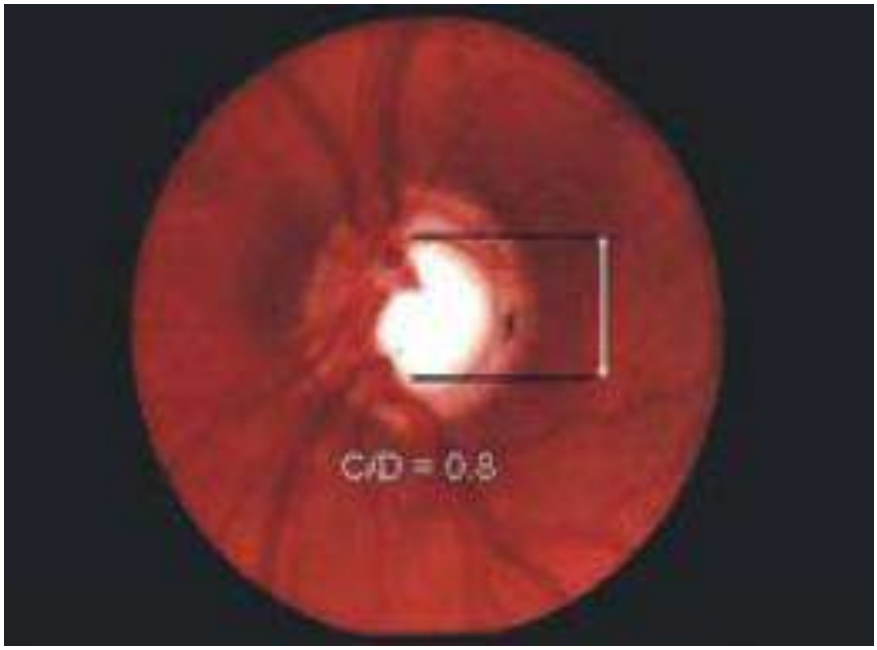

Figure 2.9: Glaucomatous excavation of the optic nerve [77].

Glaucoma is the leading cause of irreversible blindness in the world and due to its lack of early observable symptoms, it is hard to diagnose in its early stages as the only detectable signs are a progressive loss of visual feedback and morphologic changes to the optic disc. Detailed eye examining with exams such as tonometry, ophthalmoscopy, perimetry, gonioscopy, and pachymetry is required to detect glaucoma properly. It is observed that glaucoma is undiagnosed in 90% of people affected by the disease [78].

There are two main types of glaucoma: open-angle and angle-closure as shown in figure 2.10. Angle-closure glaucoma is largely as asymptomatic as open-angle, however, in 25% of the cases, patients suffer from a crisis marked by symptoms, blurry vision, nausea pain. Angle-closure glaucoma is responsible for twice as much the cases of full vision loss as open-angle glaucoma. This type of glaucoma is caused by the closure of the angle between the iris and cornea, that may be the result of increased resistance to flow from the posterior to the anterior eye chamber; obstructing the main flow of aqueous humor to the trabecular meshwork. If left unchecked the iris may adhere to the meshwork, resulting in chronical increased intraocular pressure. Features such as corneal edema, unreactive pupil, shallow anterior chamber and very high intraocular pressure are associated with angle-closure glaucoma [75,79].

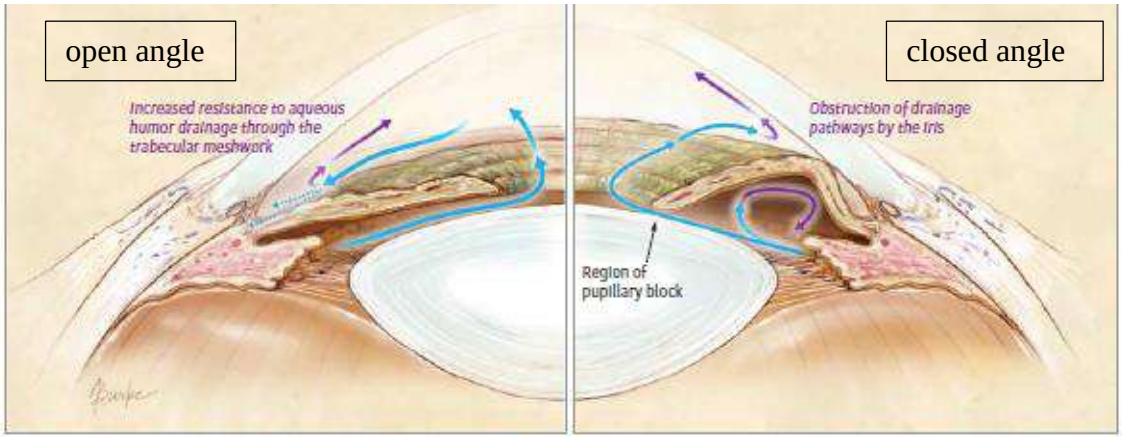

Figure 2.10: Aqueous humor drainage pathway in open angle and closure angle glaucomatous eye [75].

To understand the role of intraocular pressure in causing glaucoma, it is important to understand the flow of aqueous humor inside the eye. Aqueous humor is the fluid, very similar to water, that balances out blood pressure in the eye and takes nutrients to eye components that are not vascularized such as the lens and corneal endothelium. Aqueous humor is produced in the posterior chamber at the level of the ciliary body at a rate of 2–3 µl/min, connected into the posterior chamber, where it flows through, around the lens, passing through the pupil and ends in the anterior chamber. Then it is drained by the trabecular meshwork, reaching the episcleral venous system where it will be reassimilated This is the main path of aqueous humor, however, about 10% of the liquid will flow through what is known as the uveoscleral pathway, interstitial spaces between the iris and ciliary body. Figure 2.11 shows the circulation of aqueous humor [80,81].

In the glaucomatous eye, the liquid flow may become unbalanced due to a myriad of factors, such as increased production without an increase in the outflow, or trabecular meshwork blockage. Although it is not a direct cause of glaucoma, increased ocular pressure is related to glaucoma's associated factors, such as stress in the sclera and damage to the optic nerve. It is uncertain how exactly the pressure relates. It is known that initial raised IOP alters the optic disc the environment of axons, which may make it harmful, further accelerating axon degeneration via apoptosis. The higher the pressure, higher is the likelihood to develop glaucoma and it worsens faster than at typical IOP levels. Table 2.1 shows properties of aqueous humor [82].

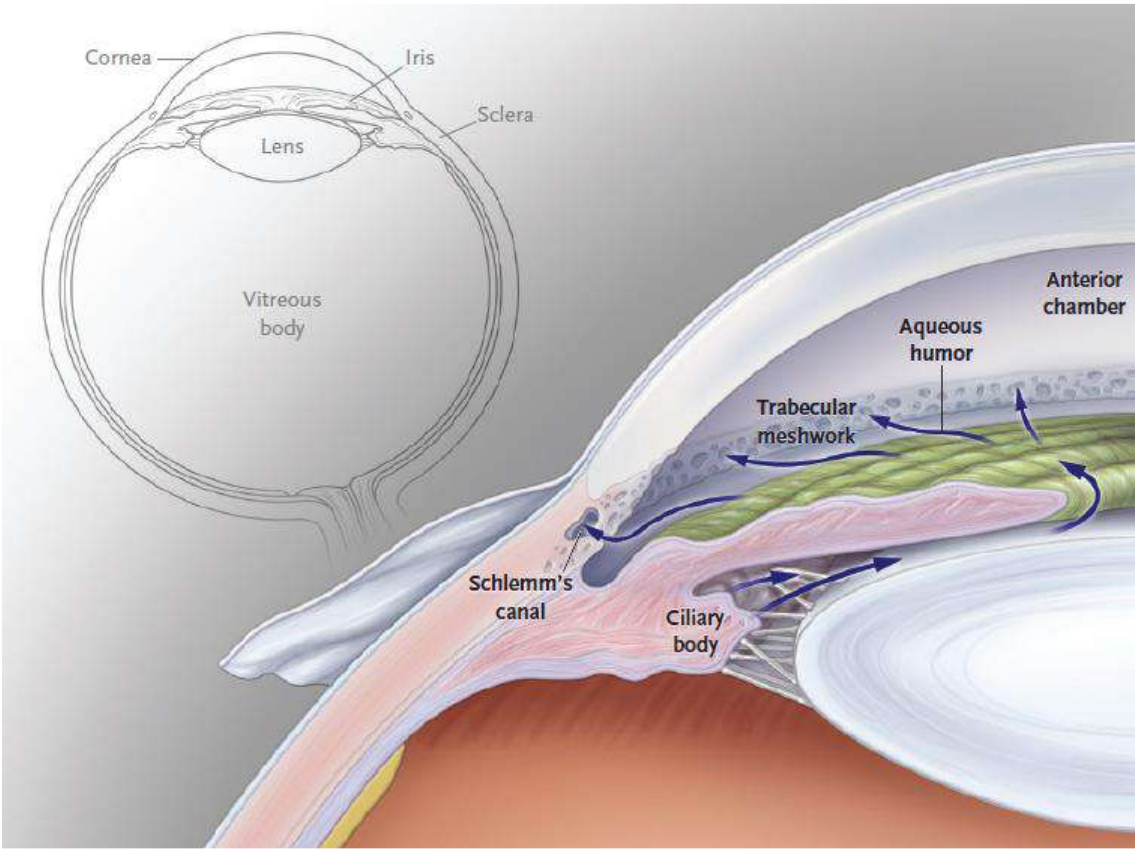

Figure 2.11: Circulation of the aqueous humor [81].

However, most patients with ocular hypertension will not develop glaucoma. Despite that, there are statistical studies that show treatment for ocular hypertension reduces the risk of this condition evolving into glaucoma. Studies suggest that IOP fluctuations over long periods are related to an increase in lost visual field from glaucoma, especially for patients with low mean IOP. That means reducing IOP fluctuation might be as beneficial to glaucoma treatment as reducing absolute IOP levels [83].

Table 2.1: Properties of aqueous humor [82].

Characteristic	Typical Value
Radius of anterior chamber (m)	5.5×10^{-3}
Total width of anterior chamber (m)	11×10^{-3}
Height of anterior chamber (m)	2.75×10^{-3}
Dynamic viscosity of aqueous humour (Pa.s)	1.0×10^{-3}
Density of aqueous humour (km/m^3)	1.0×10^{-3}

There are three main treatment methods for Glaucoma: eye drops, which work by increasing outflow of aqueous humor [75], incisional surgeries [84,85] and implants of shunt devices [86]. Shunt devices do that by inserting a tube into the anterior chamber with the outlet being under the conjunctiva. All methods having mediocre rates of success, especially over long periods due to increased flow resistance due to scarring, biofouling and increasing ocular pressure [86,87].

As it has been discussed, intraocular eye pressure is the main risk factor associated with glaucoma. It has been determined that for patients with established glaucoma, but without abnormal eye pressure, treatment for reducing intraocular pressure is always recommended, as it slows down progression. Mechanisms that may achieve this goal consist of reducing aqueous humor production, increasing outflow via one of the pathways or both or even creating other pathways in the case of incisional surgery. The goal for managing glaucoma is preserving visual function with minimum side effects as possible. This is done by setting a target intraocular pressure level and utilizing the appropriate treatment. This target needs to be constantly reassessed as treatment continues [84].

The first line of treatment for open-angle glaucoma is usually eye drops medication. These are based on factors such as cost, adverse effects, and dosing schedules. These have different acting principles and side effects. Prostaglandin analogs, such as latanoprost, are the main ones utilized, achieving reduced IOP by increasing uveoscleral pathway flow. However, they may induce conjunctival hyperemia, discoloration of the iris and macular edema. In the case of contraindication of intolerance, other medication may be utilized Beta-Adrenergic Blockers and Alfa-Adrenergic agonists, carbonic anhydrase inhibitors are alternatives, albeit more dangerous, as they have contraindications against patients with asthma, renal problems and headaches [75].

Incisional surgery is the alternative to eye drops usage in glaucoma treatment. In the case of angle-closure glaucoma due to the possibility of crisis, it is usually the first line of treatment adopted with iridotomy, where the iris is punctuated with a laser to end pupillary blocks. Surgery is utilized when other medications do not achieve the desired intraocular pressure reduction if there are counter-indications [78,85].

Trabeculectomy is the first surgery tried in primary open glaucoma cases and the usual follow up to iridotomy, in angle closure cases, if standard medication fails. The

goal is to create a path from the anterior chamber to the conjunctiva by removing part of the iris, and creating an incision on the sclera. It is also standard to create a small bleb, a trapdoor structure that assimilates the removed liquid so that it can later be reassimilated by the eye. There is a need for thorough postoperative care, with the need for antibiotics and steroids to reduce infection and control inflammation. Follow-up visits to the doctor also include adjustments to control IOP: if it is too high, it can be lowered by massaging the bleb or changing the sutures and if it is too low, steroids drop quantity may be lowered to allow for more scarring [85,87].

Trabeculectomy short-term complications may occur due to the initial failure to lower IOP. As the conjunctiva scars, less aqueous fluid is filtrated, which contributes to this phenomenon. Another reason for IOP staying elevated or increasing is fluid misdirection, where the fluid drains over the exit instead of forward, which may push the lens, the iris and increase flow resistance by blocking the drainage angle [84].

Another possible complication is IOP levels becoming too low. This occurs because of possible leakage in the bleb or excessive filtering. Reduction of IOP levels may lead to cataract or bleeding in the eye, which may also result in decreased vision. Long-term complications are often the same as short term, but also include infection, which may be very dangerous due to access to the interior of the eye offered to microorganisms from the new aqueous pathway. Due to all these factors, trabeculectomy is not expected to control IOP forever, being considered a success if control is achieved for 7-8 years. If necessary, trabeculectomy can do again as a follow-up, but not a third time [84,85].

Another important technique is laser trabeculoplasty. The procedure of this surgery showed in figure 2.12 The goal is to use localized laser burns in the trabecular meshwork in order to reduce fluid resistance by shrinking collagen that tightens the adjacent tissues and reduce trabecular pores. However, it is postulated that the laser may alter cell physiologic characteristics, reducing flow resistance. The burns are placed 360° around the eye, although 180° may achieve similar results [75,85].

Results of ALT (argon laser trabeculoplasty) trials show that ocular pressure curves are lower along with peak pressure. Other medications are still needed, like in trabeculectomy. However, there are mixed reports on ALT success over extended periods, so that even though ALT may control IOP in about 63% of the cases over four years, this

value decreases as time goes on, with patients requiring additional surgery. IOP levels tend to return to unacceptable for some patients, and doing the surgery again is dangerous, as there are reports of high increase again, with lower success rate and chronic pressure elevation that may lead to accelerated vision loss [88].

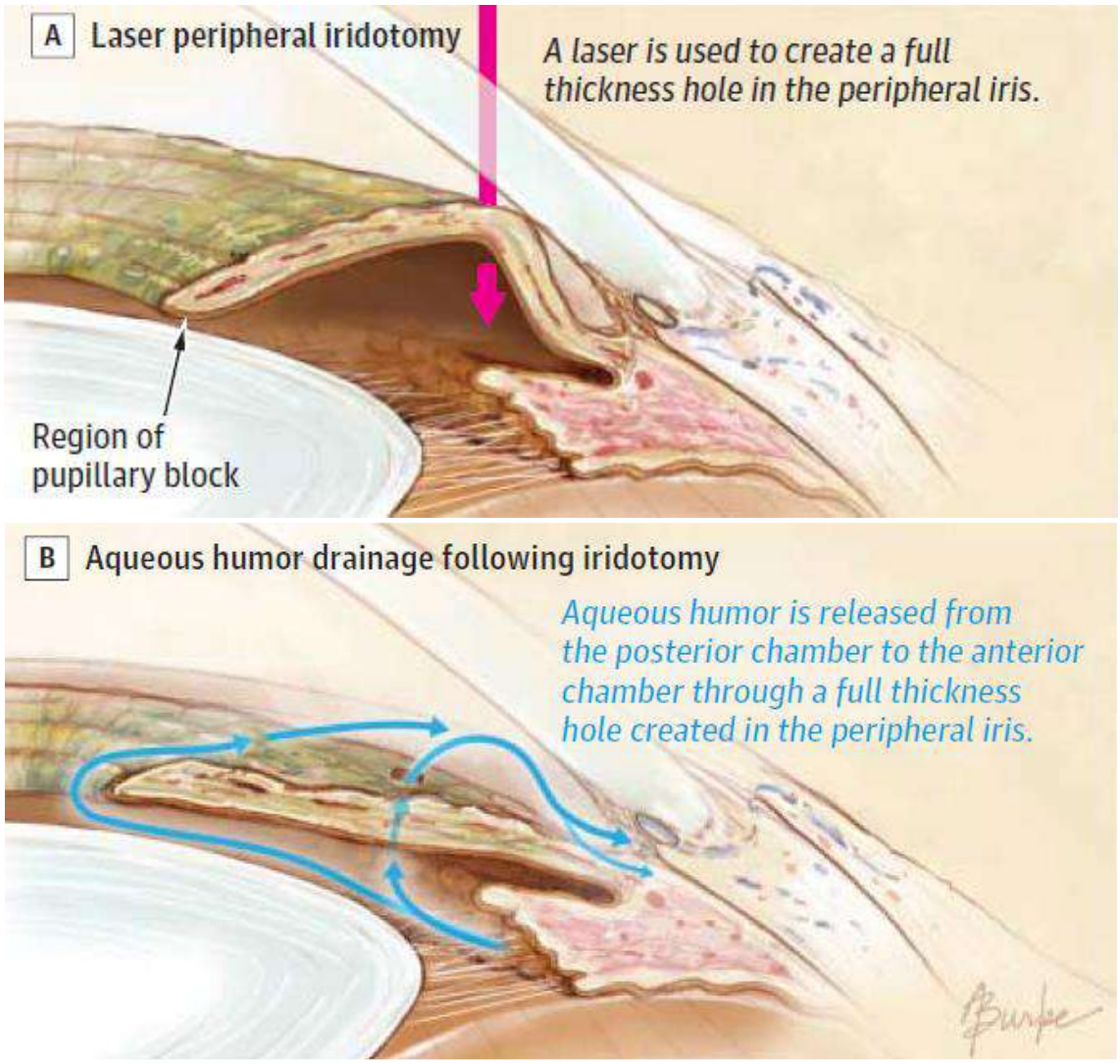

Figure 2.12: Laser trabeculoplasty procedure [75].

Glaucoma drainage implants, or aqueous shunts or eye-tube shunts are another options of treatment. They are based on creating an alternate pathway for aqueous humor, channeling fluid from out of the eye through a tube, ending in a plate, that acts as the base for the formation of a subconjunctival bleb. The inlet of the tube is placed within the anterior or posterior chamber of the eye and tube follows through to the end plate placed under the conjunctiva. There are many different devices available: the single and double Molteno plates, which are based on the first design by Molteno in 1969 [89]; the Baerveldt implant [90], which is similar to the Molteno as both offer no resistance to fluid flow; the

Ahmed and Krupin implants [91], that are valved. These implants are all based on the concept idea of having a tube ending in a plate, differing between each other in the size of the plate, the materials utilized and modifications on sutures and ligatures. They all offer advantages and disadvantages. Figure 2.13 shows Ahmed implant [86,87].

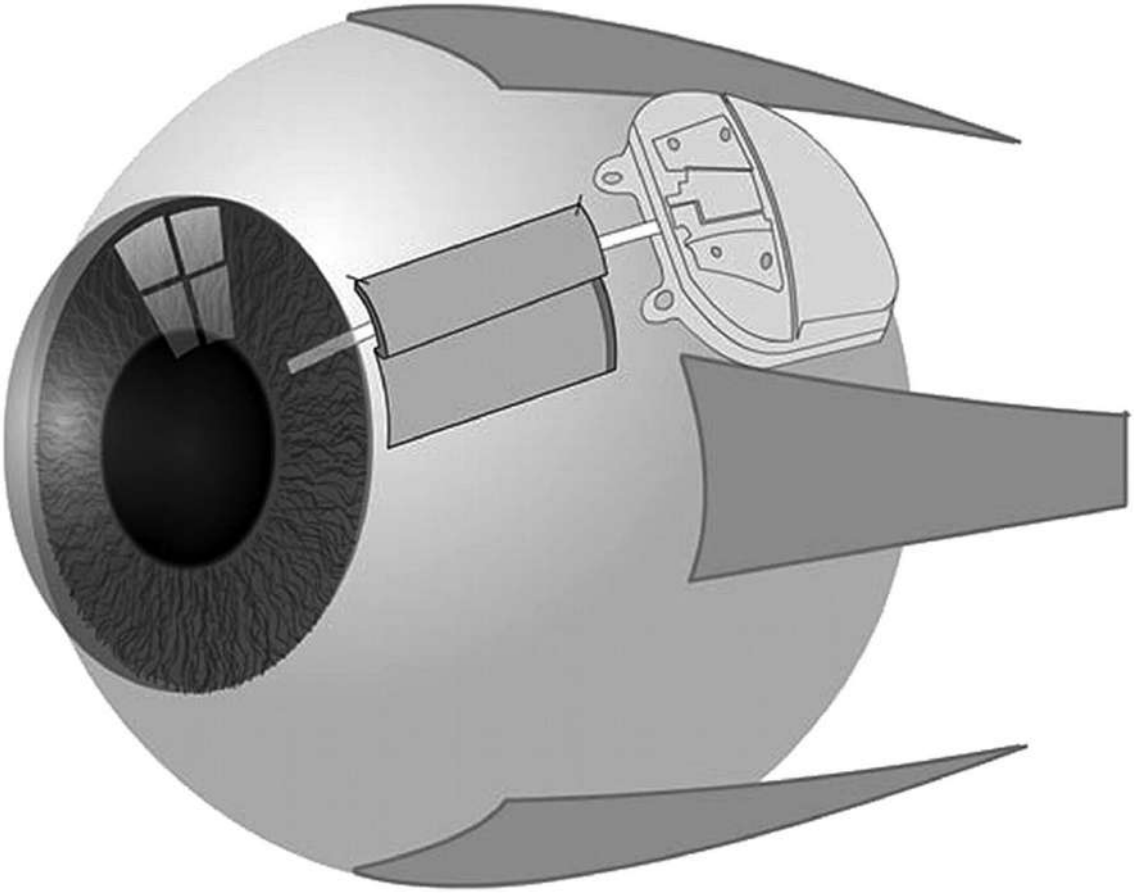

Figure 2.13: Ahmed Glaucoma drainage implant installed in the eye [92].

Complications of aqueous shunt implantation are immediate postoperative hypotony, excessive capsule fibrosis and clinical failure, erosion of the tube or the plate edge, strabismus and rarely infection. Hypotony is the result of not enough resistance to liquid flow from the bleb, especially on the non-valved implants, however, it seems that fluid may leak from the insertion site, which would also be a reason for hypotony. The proper bleb takes 1-4 weeks to develop, needing artificial modifications such as releasable sutures, stents or tube occlusion did for that period [87].

Postoperative elevated intraocular pressure derives from the opposite reason: After 3-6 weeks after the operation, the bleb may become inflamed and there is a high occurrence of scarring. This capsular fibrosis causes a postoperative hypertensive phase,

with increased resistance to flow. It has been suggested that the presence of aqueous humor in contact with sub conjunctival space may accelerate a fibrotic response from the organism. Other possible reasons are the shape, surface area, and materials of the end plate, with the ones that are smaller and more rigid, are subject to micro motion and inflammation. During this phase, if the pressure keeps high levels for too long, it is usually alleviated by ocular massage and medication that helps return the normal fluid flow. Cases that do not respond to these solutions may be solved by needling or in more extreme cases, surgical removal of the bleb [87,93].

As excessive fibrous reaction happens in the beginning stages of postoperative care and this period is when drainage devices tend to fail more, it is postulated that bleb fibrosis is the major cause of drainage device failure. So maintaining proper bleb form is of utmost importance, it needs to be thin and permeable to provide IOP reducing, although there is uncertainty to the factors that cause fibrosis [86].

A study from Gardiner *et al* [94], shows that when scarring occurs, if the scar has capillaries able to absorb fluid, IOP will increase but may still be controlled, since the increased vascularization does not compensate for the lowered hydraulic conductivity. However, a bleb scar that lacks capillaries to absorb fluid, may cause IOP to increase as much as 10 mmHg. This implies that a thick scar cap is more likely to keep IOP elevated, whereas diffuse scarring will keep proper hydraulic conductivity and help in keeping IOP levels low. Tube erosion happens in the case of poor suturing techniques and tube misplacement on the sclera. It has been shown that with a double thickness patch graft, erosion may be eliminated.

A “trabeculectomy vs tube” study show tube shunts are more likely to maintain IOP control and avoid hypotony or reoperation for more time than trabeculectomy, with equal medical management after two years. The shows that postoperative complications are less prevalent in tube shunt surgeries than in trabeculectomy for 1 year. However, for the following five years there are no significant differences in serious complications requiring reoperation between both methods [78].

Considering all, it is clear that achieving reduced eye pressure is one of the best ways to curb glaucoma in its early stages or after it is already established. However, none of the main ways of treatment act on the moment when eye pressure is elevated since there are no ways to monitor eye pressure throughout the day. We propose a novel

technique to reduce eye pressure when it is at its highest by IPMC actuators and possibly helping cure the advance of the disease.

2.7. IPMC Cilia

Ionic polymer metal composites (IPMCs) are an emerging class of electroactive polymers that are finding growing applications. A key application of IPMCs is within biomimetic miniature swimmers, as originally proposed by Shahinpoor [95] and later developed by different research groups like Guo *et al.* [96], Yeom *et al*. [97] and Shen *et al*. [98] In these studies, vibrating IPMCs are utilized as underwater propulsors, based on their ability to operate in wet environments with low actuation voltage.

An IPMC-based tadpole robot was designed and realized by Kim *et al*. [99], and the thrust and swimming speed were measured as functions of the vibration frequency. The thrust generated by IPMCs with patterned electrodes was investigated by Kim *et al*. [100] using a fixed propulsor connected to a load cell. Jellyfish robots incorporating IPMCs have been studied by Yeom *et al*. [101]. A curved IPMC actuator was considered and the thrust and swimming speed of the jellyfish robot was measured in his work. IPMCs were used as the tail of robotic fish of varying dimensions, and theoretical insights were proposed to shed light on the physics of propulsion by Shen *et al*. [98] and like Guo *et al.* [96]. Chen *et al*. [101] designed a robotic ray using two IPMC wings. Hubbard *et al*. [102] investigated the possibility of exploring patterned IPMCs to enable bending and twisting motions for underwater propulsion of robotic fish. Cha *et al*. [103] presented a comparison between IPMC-based biomimetic swimmers and other robots.

As the interest in IPMC-based underwater propulsion grows, the need for understanding and predicting the hydrodynamics generated by an IPMC vibrating underwater in a viscous fluid has become more pressing. Abdelnour *et al*. [104] presented a two-dimensional (2D) numerical study on the flow induced by an IPMC vibrating along its fundamental mode. Numerical results presented there in demonstrate the central role of vorticity generation and shedding from the IPMC tip on thrust generation. The effect of higher modes in IPMC-based underwater propulsion was investigated by Lee *et al*. [105]. The main focus of these noteworthy efforts is to demonstrate the feasibility of

IPMCs as a miniaturized, maneuverable, and wireless biomimetic underwater robotic swimmer.

2.8. Modeling of IPMC

After observation of electrolytically activated contraction of the polymer by Hamlen [106] in 1965, many attempts were made extensively to investigate the swelling mechanism of the electric-sensitive polymers and hydrogels. Tanaka [107] explained reported progressive collapse of a weakly ionized polycationic gel in contact with a metal anode, immersed in acetone-water (50:50) mixture under an electrode potential difference ranging from 1.25 to 2.15 V. Gel deswelling was ascribed to the electrophoretic attraction of the charged gel network to the electrode resulting in the generation of a mechanical stress gradient (orthogonal to the electrode) squeezing the gel.

Osada's team [108-111] developed an electrically activated artificial muscle with the hydrogels. He reported PAMPS and other gels shrinking and water exudation when in contact with carbon electrodes under DC excitation. The phenomena were tentatively ascribed to the concomitant electrophoretic attraction of the gel to the electrode and electrostatically induced gel dehydration. Shiga [112-114] investigated the swelling and bending deformation of PAA subjected to an electric field and analyzed an electrically controlled ionizable hydrogel as the active material in adaptive structures. Shahinpoor [115] and Li [116] fabricated the ionic polymer-metal composite (IPMC) to use for tissue engineering.

De Rossi *et al*. [117,118], working with PAA-PVA gels in solution with a slightly higher potential difference at the electrodes observed gel swelling or shrinking governed by water electrolysis at interfaces, resulting in local pH changes. Gel bending under the action of an electric field was first reported by Shiga and Karauchi [119] under appropriate conditions and geometry.

Electric responsive hydrogels are usually made of polyelectrolytes and an insoluble, but swellable, polymer network which carries cations or anions. This system can transform chemical free energy directly into mechanical work to give an isothermal energy conversion. A typical function of a hydrogel containing ionic groups is to bend reversibly under the influence of a DC electric field, making it useful in some actuators

driven by an electric field. From the theoretical point of view, the response mechanism of the electric-sensitive hydrogels is similar to that of pH-sensitive hydrogels [120].

When an electric field is applied to the bath solution, mobile ions will redistribute in the hydrogels and surrounding solution. The diffusion gives rise to the ionic concentration differences between the interior hydrogel and exterior solution because of the fixed charge groups that are bound to the cross-linked macromolecular chains. As a result, an osmotic pressure is generated by the concentration differences, which drives the swelling or shrinking of the hydrogel. The deformation of the hydrogel redistributes the diffusive ions and fixed charge groups, which causes new ionic concentration differences and the hydrogel deforms again. The recurrent kinetics will stop when the hydrogel reaches an equilibrium state. It can also explain the process how chemical energy converts to mechanical energy in the process. From the theoretical point of view, the response mechanism of the electric-sensitive hydrogels is similar to that of pH-sensitive hydrogels [121-123].

The most fundamental model for the swelling behavior of hydrogel presented by Flory [124] and Huggins [125]. It was derived based on simple lattice model theory and mean field approximation, traditionally used to calculate entropy change of polymer-solvent system contributed by mixing of solvent molecules with a long chain of the polymer network. The drawback of this theory is that it could not predict the swelling behavior of network in a good solvent. Later study revealed that interaction of gels in a good solvent has stronger concentration dependence than that originally proposed in the Flory-Huggins theory.

In the 1950s, Flory and Rehner [126,127] were the first to formulate a macroscopic theory for investigating the swelling of network structures. This model is an extension of Flory-Huggins theory that accounted for the elastic deformation of gels upon the absorption and desorption of water. It was further developed into a well-known Flory´s mean field theory.

Flory´s mean field theory treats the equilibrium swelling of the hydrogel-solvent system as a balance between the mixing, elastic and ionic free energies. Despite its popularity, Flory´s mean field theory has a certain drawback. While it could predict continuous and slightly discontinuous volume change of hydrogel, it could not adequately predict swelling behavior involved large discontinuous volume changes, which was first

postulated by Dusek [128] and Patterson [129] and experimentally confirmed by Tanaka [130] in 1978.

One of the first groups who quasi-statically investigated the dynamic behavior of ionic polymer gels in electric fields was Doi *et al*. [131], Shiga and Kurauchi [112] and Shahinpoor [115]. Brock *et al*. [132] have given a coupled formulation for the ion dynamics and a theory for large displacements.

Grimshaw *et al*. [133] have presented a coupled formulation for chemically and electrically induced swelling in polyelectrolyte gels. De Gennes *et al*. [134], discuss the mechanoelectrical effects in ionic gels are described, while Tamagawa and Taya [135] and Li *et al*. [136] consider the ion distribution and the ion transport by applying a chemo-electric model. De and Aluru [137] proposed a chemo-electro-mechanical model for the simulation of pH-sensitive hydrogel while using a multiphysics modeling approach. Li and Lai [138] simulated ionic-strength-sensitive hydrogels using a meshless simulation technique. Wallmersperger *et al*. [139-141] have published electrochemical and electromechanical formulations for ionic gels under chemical and electrical stimulation. The modeling of temperature-sensitive polyelectrolyte gels has been performed by Keller *et al*. [142]. Gerlach *et al*. [143] developed chemical and pH-sensors based on the swelling of hydrogels. Equilibrium swelling of hydrogels in aqueous solutions based on thermodynamics has been investigated by Orlov *et al*. [144,145] and Ermatchkov *et al*. [146,147].

The mass transport within membranes as well as the swelling behavior of gels has been described by Kind *et al*. [148]. The mass transport measurements in membranes were performed by means of in situ Raman spectroscopy, for the modeling, a multicomponent transport model was used by Scharfer *et al*. [149]. Yoon *et al*. [150] used the fluorescence microscopy to track the kinetics of micron-size hydrogel layers and verified the linear theory of poroelasticity. Prudnikova and Utz [151] have experimentally investigated the electrochemical equilibrium properties of poly (acrylic acid/acrylamide) hydrogels and compared the results to the one predicted by theory with an overall satisfactory outcome. In Mann *et al*. [152], the swelling of charged hydrogels is discussed. A review article on gel swelling theories has been published by Quesada- Perez *et al*. [153].

Sun *et al*. [154] and Van Loon *et al*. [155] presented a triphasic and quadriphase mixture theory for the simulation of hydrated tissues, respectively. The swelling of charged tissues and gels in the framework of the theory of porous media has been investigated by Ehlers *et al*. [156] and Acartürk [157]. On the atomistic scale, the conformation change of hydrogels in water has been studied by Walter *et al*. [158]. An overview over modeling on different scales has been given by Wallmersperger *et al*. [159]. Experiments and modeling of nonlinear effects in hydrogel-based chemical sensors have been performed by Guenther *et al*. [160]. Bouklas and Huang [161] compared the linear poroelasticity theory and a nonlinear theory to study the kinetics of swelling hydrogels. They have demonstrated that within the linear regime, both theories have yielded consistent results. Lucantonio and Nardinocchi [162] also investigated the bending deformation of gel bars through a stress-diffusion mechanism in the absence of the electric field. Their model has been developed based on a thermodynamically consistent theory of poroelasticity. In the special issue on "responsive gels" [163], e.g. phase field model simulations of hydrogel dynamics under chemical stimulation [164] and simulation results of tracer diffusion in hydrogels [165] were published. In addition, the modeling and simulation of pH-sensitive hydrogels [166] and experimental results on the diffusion of polyethylene glycol in N-isopropyl acrylamide (NIPAAm) hydrogels with Raman spectroscopy [167] were released within this special issue. A theory for the behavior of solid undergoing a macroscopic or mechanical process due to solid deformation and a microscopic or chemical process due to chemical species migration through the solid was developed by Duda *et al.* [168]. The theory was applied to study diffusive dynamical processes of one- dimensional problem.

Due to the complexity of the governing physics and the coupling nature of the problem, the available modeling approaches for hydrogels and IPMC still present a wide gap between theory and practice. This work, therefore, intends to bridge between the hydrogels and IPMC and contribute to the modeling and simulation of IPMCs applications in biomedical. Throughout the years, many attempts have been made to constitutively model IPMCs using different methods. With the development and applications of IPMCs, various constitutive models have been proposed to capture certain features of the mechanical behavior of IPMCs. Following section reviews some of the most important contributions from the existing literature that deals with the mechanical models of hydrogels to obtain a better understanding of IPMC modeling fundamentals.

Broadly, they can be categorized into equilibrium volume model, multi phasic model, transport model and thermodynamic model.

It is well known that an elongated strip of an anionic hydrogel bends towards the cathode in an electric field. Doi and coworkers [131] have provided a comprehensive theory to explain this behavior. The theory is based on equilibrium in the interface of Gel and Solution that explained by Flory. According to Flory, the equilibrium volume of gel achieved by the following condition

$$P_{osmotic} + RT \sum \ (c_{ig} - c_{is}) = 0 \quad (1)$$

where $P_{osmotic}$ is the osmotic pressure of a neutral gel in which ionic group of the gel are not dissociated at all, R is the gas constant, T is the absolute temperature, and C_{is} and C_{ig} denote the ionic concentration of species i in the outer solution and in the gel. Subscript i stands for A (Na^+), B (Cl^-), H^+ and OH^-.

When there is no charge in gel, the volume of gel is determined by two opposite effects. First is an interaction between gel and solvent, which tends to swell or shrink. Second is network elasticity that resists the deformation. These two effects are both included in $P_{osmotic}$ and $P_{osmotic}$ determine the equilibrium volume of neutral gel. If the gel has charge, the concentration of free ion inside and outside of gel is not equal, so this unbalance create an additional term ($RT \sum \ (c_{ig} - c_{is})$) to osmotic pressure and swells the gel.

Based on thermodynamic stability conditions, equation 1 indicates that if $P_{osmotic}$ increases by applying electric field, the gel swell while gel shrink if $P_{osmotic}$ decreases.

Hydrogel volume transition involves intricate chemical process, hydrophilic, hydrophobic, electrostatic interactions and mechanical deformation [169]. To accurately capture features of hydrogel volume transition behavior, it is necessary to develop a model, which is able to describe the multi-physics complexity. The multi-phase model considers hydrogel to be a mixture of several phases. The hydrogel is visualized to be a charged porous matrix saturated with fluid dissolved with ions. The fundamental work of the mixture theory was developed by Gibbs [170] who formulated a thermodynamic theory describing the mechanical behavior of liquid-swollen solid, assuming these two

phases are under equilibrium. Later, Truesdell [171] extended the mixture theory by introducing balance equations of mass, momentum, and energy to the system. Then, Morland [172] used volume fraction concept in connection with mixture theory. Mow and co-workers [173-175] included the osmotic effect to the mixture theory and formulated the well-known tri-phasic models. Below, we briefly describe the key features of the triphasic model.

Assumptions in the multiphasic model:

- The mixture is incompressible, that is, both fluid and solid are incompressible.
- No chemical reactions exist between the three phases.
- The inertia effects and body forces are neglected.
- The process is assumed to be isothermal.
- The volume fraction of the ions is neglected compared to those of the solid and fluid.
- The solid matrix is entirely elastic and initially isotropic. No shear stress in the fluid phase associated with mixture deformation.

In the multi-phasic theory, the hydrogel is divided into solid phase, water phase, and ion phase containing both anion (denoted as -) and cation (denoted by +), each phase has a density and velocity. Balance equations like balance of mass, momentum and energy must be established for each phase in consideration of all interactions and external agencies.

The multi-phase theory considers hydrogel as a mixture of four components including water, polymer matrix, anion, and cation. It is formulated by considering the interaction between each phase. This model could predict the transient and equilibrium behavior of hydrogels with/without charge under any solvent condition and electric stimulus. This model has already been used to investigate the swelling, shrinking, and bending behavior of electric-stimulus-responsive hydrogel subjected to external electric field [176]. Since the composition of the hydrogel is similar to the hydrated tissue, this model is also used to study the response of soft tissue under compression and indentation [177, 178]. Lai and co-workers applied the model to study the electric potentials inside a charged soft hydrated biological tissue [179]. Both streaming potential originates from the movement of ions convected by fluids, and diffusion potential, caused by ions

diffusion from high concentration to low concentration, contribute to the electric potential of a hydrated tissue. However, the porous polymer matrix follows a linear elastic constitutive relation. This assumption constrains the model to be only applicable to hydrogels with small volume change. Besides, the model does not consider the change of material properties during the volume transition process, leading to inaccuracy in large deformation region. In the next section, transport model will be discussed and related formulation will be presented.

In transport model, hydrogel volume transition is diffusion-driven. The solvent and ion diffusion controls the osmotic pressure, the stress states and the swelling behavior of the hydrogels. Wallmerperger and coworkers formulated a model that couples chemical, electrical and mechanical field for ionic hydrogels [139,140]. This model includes Nernst-Planck equation, Poisson equation, and mechanical equilibrium equations to describe the multi-physical behavior of hydrogel under the electric stimulus.

This model simplifies the interactions in hydrogel systems and is capable of predicting both transient and equilibrium phase transition behavior of ionic hydrogels. This model has been used to predict the electric potential, ions concentration and osmotic pressure with ionic hydrogel under multi-stimuli. The transport model also explains the bending behavior of the ionic hydrogels under electric stimulus [140].

The exact electric potential and swelling ratio within the hydrogel and at the hydrogel/solvent interface can be calculated by numerically solving previous equations. However, this transport model neglects the interaction between polymer and water, which may contribute to swelling. Thus, this model can only be applied for certain hydrogels where swelling mainly depends on ionic diffusion. Whereas for neutral hydrogels or ionic hydrogels where swelling results from the hydrophilicity of the polymer, this model may not be able to give an accurate prediction.

Following the field theory by Biot [180] and Gibbs [170], Suo and coworkers [181-183] formulated a hydrogel theory that couple large deformation and diffusion. When the hydrogel is immersed in water, small molecules immerse into the polymer network causing the expansion of the polymer chains. This theory assumes that there are two modes of deformation within the hydrogel system. The first mode, that is, the short-term mode, results from local rearrangements of water molecules. This mode is accompanied by rearrangement of polymer chains. The time scale of this mode is material

size independent. Whereas the second mode, namely the long-term mode, is caused by the migration of water molecules into the polymer matrix. This mode is governed by diffusion and is sample size dependent. Both modes lead to the shape and volume change of the hydrogel. Since the first mode, which corresponds to polymer chain rearrangement, is much faster than the second diffusion-dominating mode, it is assumed that the first mode is instantaneous whereas the second mode is time dependent. The detailed theory can be derived from the laws of thermodynamics and kinetics laws.

The physical background of the different actuation behavior of Nafion- and Flemion-based ionic polymer metal composites (IPMCs) was not completely understood. Therefore, it was very complicated to derive a physical model for numerical predictions of the bending behavior. In 1992, the active behavior of IPMCs (plated with conductive metal on their surfaces) was demonstrated by Oguro *et al*. [184]. The sensing response under the application of a mechanical deformation was also found in the 90s by Sadeghipour *et al*. [185] and Shahinpoor *et al*. [186]. These properties allow for the IPMCs to be used as electromechanical sensors and actuators.

Although a lot of progress has been made in the development of ionomeric transducers in recent years, there is still a wide gap in understanding the fundamental mechanisms occurring inside IPMCs; so there exist a lot of different models trying to explain these mechanisms. Some reviews of available physics-based models of IPMC actuation are published by Shahinpoor and Nemat-Nasser [187,188]. Kanno *et al*. [189] have introduced a simple linear approximate dynamic model for an ionic conducting polymer gel film actuator (ICPF). Tadokoro *et al*. [190] have presented a model for Nafion-Pt composite actuators and a physicochemical actuator model of ICPF for robotic applications. Mallavarapu and Leo [191,192] have discussed the feedback control of the bending response of ionic polymer actuators, and Newbury and Leo [193] have introduced an electrical model for ionic polymer transducers (IPTs). Farinholt and Leo [194] have investigated the charge sensing phenomena in IPTs. Nemat-Nasser *et al*. [195] have presented an electromechanical model and a micromechanical actuation model [196] for ionic polymer-metal composites. In these studies, electrostatic forces and the ion transport are regarded as the main mechanisms for the mechanical actuation and different kinds of parameters such as mobile ions, electrode morphologies, hydration, temperature, and ion concentration are investigated [197,198].

A continuum model and its electric equivalent circuit representation for the electromechanics of IPMCs have been derived by Branco *et al*. [199], while a beam theory for the modeling of an IPMC actuator has been published by Lee *et al*. [200]. Xiao and Bhattacharya [201] have given a model describing the electro-mechanical properties of ionic polymers, Weiland and Leo [202,203] have performed a computational micromechanics model for ionic polymer cluster energetics and Farinholt and Leo [204] have modeled the electrical impedance response of ionic polymer transducers by considering the electro-mechanical coupling. Wallmersperger and Leo [205-207] have developed a chemo-electro-mechanical model describing the ionic transport and electromechanical transduction in ionomeric polymer transducers. This model has been extended for high-surface area electrodes by Wallmersperger *et al*. [208-210]. In He *et al*. [211], a comparison of the modeling of ion transport in high strain, ionomers is performed by the Monte Carlo method and the continuum model.

Other electro-mechanical models for IPMC have been published, e.g., by Pugal *et al*. [212,213]. Nardinocchi *et al*. [214] have given a thermodynamically based multiphysics model for IPMCs, Enikov and Seo [215] have performed an electromechanical numerical analysis of muscle-like ionic polymer actuators, Chen *et al*. [216] presented a dynamic model for ionic polymer-metal composite sensors, and Bonomo *et al*. [217] have published a nonlinear electrical model for ionic polymer-metal composites as actuators. Charge dynamics in ionic polymer-metal composites, as well as an electromechanical model for sensing and actuation of ionic polymer metal composites, has been published by Porfiri [218,1219]. In Cha and Porfiri [220], the chemoelectrical behavior of IPMCs is described through the modified Poisson-Nernst-Planck framework by including steric effects. Aureli and Porfiri [221] studied the nonlinear sensing behavior of IPMCs in response to mechanical deformations; this work is based on the Poisson-Nernst-Planck framework. A mixture theory framework for the mechanical modeling of IPMCs and of species interactions occurring therein is given by Bufalo [130]. The nonlinear capacitance and electromechanical response of ionic liquid polymers have been studied by Davidson and Goulbourne [222].

One of the most important areas of research is the development of theoretical models and concepts for the mechanisms that give rise to the coupled electromechanical response. These models and theories are used to study how individual constituents of an IPMC strip affect the overall electromechanical response and various physicochemical

and mechanical properties of IPMC strips. This facilitates the design of IPMC strips, which show an efficient, robust, and reliable response.

Another approach in modeling is to macroscopically and phenomenologically capture the force-voltage-beam configuration response so that they can be used in the design and analysis of systems involving IPMC strips as components. Given that the state of many of these applications is still conceptual and under development, these models would be of significance.

The typical beam or plate-like configuration of the IPMC is governed by the need for an electric field across the polymer. When the IPMC strips are used in actuators, information about the beam configuration as a function of time under the application of external mechanical loads and electric potential would be useful. This calls for an actuator model, which relates electrical input to the mechanical output. When it is used in sensors, knowledge relating the electrical potential and charge developed across the surface of the strip as a function of time when the strip is deformed would be useful. This calls for a sensor model, which relates mechanical input to the electrical output. State-space models offering ordinary differential equations to simulate these complex electromechanical responses are of immense value for material characterization and design of applications.

It would be beneficial in the design process to use a model based on physical principles, which are thermodynamically consistent and addresses all the above requirements. Such a model, if versatile, would also be able to simulate different electromechanical responses. Amongst others, thermodynamically consistent, physics based, mixture theoretic and micromechanical models have been reported. Being interested more in the micromechanical behavior rather than an input-output response; these models would be better suited for accurate analysis at final stages of design. It provides one such model based on the micromechanical approaches. Such models, based on beam theories, are of particular interest due to usability and lesser computational costs.

CHAPTER III

3. FUNDAMENTAL THEORY

3.1. Introduction

In order to study the IPMC micropump, we need a mathematical model to predict the behavior of IPMC deformation in contact with the fluid and its effects. In this chapter, theory and mathematical formulation of the IPMC-fluid interaction presented and described. The mathematical (electro-chemo-mechanical) model that describes the behavior of IPM under applied electro-potential adapted from Nemat-Naaser *et al* [195], Wallmersperger *et al* [214], and Nardinocchi *et al* [206]. We assumed IPMC body B immersed in fluid region R with IPMC-fluid interface S. The section (3.2) deals with basic theory and mathematical formulation of IPMC (Solid) deformation and section 3.2 concerns about the fluid region and coupling the governing equations. Exact boundary conditions depend on geometry and detail of problems (IPMC deformation and micropump).

3.2. IPMC actuation

The mechanisms of IPMC actuator or sensing are driven by the change in the solvent concentration induced by electrically and mechanically driven migration of the mobile cations which drag solvent molecule along them. Their physics-based model may be described by considering the electric field in the polymer and boundaries, chemical field and mechanical field in the polymer. Let us consider a material IPMC-like body B composed of an elastic solid and a one-component interstitial solute. This body, from now on identified with the region occupied by its solid component in a fixed reference configuration, is the stage of three interdependent phenomena, namely electrical, solid deformation and solute diffusion in the polymer. The state of B at time t is defined in terms of solid displacement $\mathbf{u}(x,t)$, solute concentration $c(x,t)$ and the electrical potential $\psi(x,t)$, which respectively assign to each material point x in B the corresponding displacement, solute content and electrical field per unit reference volume at time t.

Let **u** be the vector field describing the displacement suffered by the IPMC-like body. The deformation field corresponding to **u** is **E**, which is a small deformation setting and is given by symmetric part of displacement gradient. Let us call **E** the visible deformation and decompose it into two contributions, one due solute (mobile cation concentration) change with no change in stress, distortion $\mathbf{E}_c$, and one due to stress with no solute change, elastic deformation $\mathbf{E}_e$:

$$\mathbf{E} = \text{sym}\, \nabla \mathbf{u}, \tag{2}$$

Additive decomposition

$$\mathbf{E} = \mathbf{E_c} + \mathbf{E_e}, \tag{3}$$

We assume that the distortion field $\mathbf{E_c}$ is induced by solvent migration occurring in the IPMC when hydrated and stimulated electrically and mechanically. The form of such a field ensures the model includes the solute transport within the flux of the cations carriers through the introduction of a hydrophilicity coefficient α. Only one mobile ion species is employed in the model. Thus, the distortion $\mathbf{E_0}$ is represented as:

$$\mathbf{E_c} = \alpha\,(c - c_0)\mathbf{I}, \tag{4}$$

where c measures the concentration of mobile cations and c_0 is the solute concentration in the reference configuration. The structure of equation (4) says that the solvent migration induces volumetric deformations.

The distortion $\mathbf{E_c}$ would be visible if the boundary layers consisting of clusters embedded in the elastic polymer matrix were free from the constraint of the remaining part of the IPMC.

Balance Equation

In absence of external forces per unit volume and neglecting the inertial forces, the local balance equations of mechanics yields:

$$\text{div}\, \mathbf{T} = 0, \tag{5}$$

Where **T** denoting the stress field.

We have from equations (3) and (4)

$$\dot{\mathbf{E}} = \dot{\mathbf{E}}_\mathbf{e} + \alpha \dot{c}\mathbf{I}, \tag{6}$$

Due to the much larger propagation speed in the electric field compared to the diffusion speed in the chemical field, the equations of the electrostatics are used to describe the electrical physics of the body. Hence, the variation of the electric potential field in the IPMC-like body is governed by the basic electrostatics equation prescribing that:

$$q = \text{div}\,\mathbf{d}, \tag{7}$$

$$q = F(c - c_0), \tag{8}$$

Here, the vector field **d** describes the electric displacement and the scalar field q is the total electric charge density (per unit volume) contributed from electrons, ions, and fixed charges.

The balance equation for the flux **J** of the mobile cations per unit time is formulated through the appropriate conservation law. We assume that changes in the concentration of the cations in any part of the hydrated body are most generally brought about by diffusion across the boundary if any internal sources are absent. Thus, the flux **J** satisfies the following:

$$\dot{c} = -\text{div}\,\mathbf{J}, \tag{9}$$

Thermodynamical Equation

Here, we derive from basic thermodynamical issues the equations providing the stress **T**, the electric field **e**, and the chemical flux **J** in the IPMC-like body. The same approach may be employed when considering large deformations of the IPMC-like body which induce more complex couplings among the mechanical and electrochemical fields. Our starting point is the assumption of the existence of a free internal energy φ measuring the energy available to any part of the body. The dissipation principle requires that the rate of energy dissipation (defined as the difference between the working extended along a process and the time derivative of the free energy) should be non-negative, at all times. With regard to the free energy, we assume that, at each point, the value of the free energy per unit reference volume depends only on the value of the elastic deformation $\mathbf{E}_e$, the electric displacement **d**, and the cation concentration *c* at that point:

$$\varphi = \hat{\varphi}(\mathbf{E}_e, \mathbf{d}, c), \tag{10}$$

$$\mathbf{T} = \frac{\partial \hat{\varphi}(\mathbf{E_e},\mathbf{d},c)}{\partial \mathbf{E_e}}, \tag{11}$$

$$\nabla\psi = -\frac{\partial \hat{\varphi}(\mathbf{E_e},\mathbf{d},c)}{\partial \mathbf{d}}, \tag{12}$$

$$\mu = \frac{\partial \hat{\varphi}(\mathbf{E_e},\mathbf{d},c)}{\partial c} + F\psi - \alpha \mathrm{tr}\mathbf{T}, \tag{13}$$

where μ is the electrochemical potential. Defining the electric field **e** as

$$\mathbf{e} = -\nabla\psi, \tag{14}$$

Note that the equations of the electrostatics are used to describe the electric physics of the body, because of the smaller propagation time scale in the electric field compared to the diffusion time scale in the chemical field.

The free-energy response $\hat{\varphi}$ describes three contributions, elastic $\widehat{\varphi_m}$, chemical $\widehat{\varphi_c}$, and Electric $\widehat{\varphi_e}$, that is,

$$\hat{\varphi}(\mathbf{E}_e, \mathbf{d}, c) = \widehat{\varphi_m}(\mathbf{E}_e) + \widehat{\varphi_e}(\mathbf{d}) + \widehat{\varphi_c}(c), \tag{15}$$

$$\hat{\varphi}(\mathbf{E}_e, \mathbf{d}, c) = \frac{1}{2}\mathbb{C}\mathbf{E}_e \cdot \mathbf{E}_e + \frac{1}{2\varepsilon}\mathbf{d} \cdot \mathbf{d} + f(c), \tag{16}$$

With

$$\widehat{\varphi_c}(c) = \mu_0 c + k_B T c(lnc - 1), \tag{17}$$

$$\mathbb{C}\mathbf{E}_e = 2G\mathbf{E}_e + \lambda(\mathbf{E}_e \cdot \mathbf{I})\mathbf{I}, \tag{18}$$

$$\widehat{\varphi_m}(\mathbf{E}_e) = \frac{1}{2}(\lambda|tr\mathbf{E}_e|^2 + 2G|\mathbf{E}_e|^2), \tag{19}$$

where λ and G are the Lame modules, ε is the electric permittivity, μ_0 is the reference chemical potential of the cations, k_B is the Boltzmann constant, and T is the temperature. f (c)

Constitutive Equations

The aforementioned choices imply that

$$\mathbf{J} = -D\left(\nabla c + \frac{F}{RT}c\nabla\psi - \frac{\alpha}{RT}c\nabla \mathrm{tr}\mathbf{T}\right), \tag{20}$$

The first term on the right-hand side of Eq. (20) represents the diffusive flux due to the gradient of concentration in the domain. This term is identical to the Fick's first law of diffusion equation. The second and third term represents the migration flux arising from the gradient of the electrical potential.

where D is the diffusion coefficient of the solute in the solid and R is the gas constant. Note that Eq. (20) describes the flux of ions resulting from the diffusion of cations solute and a migrative component due to the electric and mechanical fields. It is interesting to note that Eq. (20) is akin to the so-called Nernst-Plank equation for chemical species motion in fluid media.

The full electro-mechano-chemical problem is defined through the following coupled sets of field equations.

Electric physics:

$$\operatorname{div}\mathbf{d} = \mathrm{F}(\mathrm{c} - \mathrm{c}_0), \mathbf{d} = -\varepsilon\nabla\psi, \tag{21}$$

Chemical physics:

$$\dot{c} = \operatorname{div}\mathbf{J},\ \mathbf{J} = -D\left(\nabla c + \frac{F}{RT}c\nabla\Phi - \frac{\alpha}{RT}c\nabla\mathrm{tr}\mathbf{T}\right), \tag{22}$$

Mechanical physics:

$$\operatorname{div}\mathbf{T} = 0, \mathbf{T} = \lambda\mathrm{tr}(\mathbf{E_e})\mathbf{I} + 2\mathrm{G}\mathbf{E_e} - (3\lambda + 2\mathrm{G})\alpha\,(c - c_0)\mathbf{I}, \tag{23}$$

where $\mathbf{C}$ is the elasticity tensor, which provides the mechanical characteristics of the body.

The partial differential equations (PDEs) need a set of initial and boundary conditions. We assume that $c(x,0) = c_0(x)$ for any x. Then, boundary conditions for the electric, chemical, and mechanical equations depending on the specific problem under investigation have to be specified to solve the governing equations. For the chemical field, a zero-flux boundary condition over all the boundary is specified to model ion blocking surfaces:

$$\mathbf{J}.\mathbf{n} = 0, \tag{24}$$

When the behavior of the IPMC-like body as the actuator is analyzed, we prescribe:

$$\psi = 0, \psi = \psi^*, \tag{25}$$

on the both surfaces, at top and bottom respectively, and null electric displacement on the rest of the boundary.

3.3. IPMC-fluid interaction

The mechanisms of IPMC actuator or sensing are driven by the change in the solvent concentration induced by electrically and mechanically driven migration of the mobile cations which drag solvent molecule along them. We described governing equations of IPMC deformation under electric potential in section 3.2. To describe IPMC-fluid interaction throughout this section, we shall concentrate on the coupling between the electro-chemo-mechanical theory of IPMC deformation and Navier-Stokes equations.

Here, mentioned electro-chemo-mechanical theory is used to generate fluid motion actuated by IPMC diaphragm or cilia in micropump. In the framework of the continuum fluid mechanics, fluid velocity v and pressure p are governed by the following bulk equations (or Stokes equations):

$$\rho \dot{\mathrm{v}} = \mathrm{div}(-p\mathbf{I} + 2\rho\nu\mathbf{D}), \tag{26}$$

$$\mathrm{tr}\mathbf{D} = \mathrm{div}\ \mathrm{v} = 0, \tag{27}$$

where $\mathbf{D} = 1/2\ (\mathrm{grad\ v} + (\mathrm{grad\ v})^{\mathrm{T}})$ is the symmetric stretching tensor, ρ is the density and ν is the kinematic viscosity. Note that the inertial and external body force are neglected, which is reasonable in applications involving a Reynolds number sufficiently small and dominant pressure forces. Further, v is subject to the in compressibility constraint (27).

The aforementioned governing equations must be supplemented by boundary conditions that involve the interactions between the IPMC and the fluid environment. For instance, if we suppose that IPMC is in contact with an environment wherein the chemical potential of the solute is constant and equal to μ_f and the chemical equilibrium is achieved. The attaining boundary conditions are

$$\mu = \mu_f,\ \mathbf{J} \cdot \mathrm{n} = 0, \tag{28}$$

where n is the exterior unit normal to the surface of IPMC. The boundary conditions for the electrostatic environment are

$$\psi = 0, \psi = \psi^*, \mathbf{d} \cdot \mathrm{n} = 0, \tag{29}$$

The theoretical multiphysics model presented in the previous section has been implemented and subsequently solved numerically in the finite element software COMSOL Multiphysics. Briefly, the model consists of the full coupled electro-mechano-chemical model (21), (22), and (23), which is solved in the IPMC domain B, and a fluid part, solved with the incompressible Navier-Stokes equations (26) in the flow domain R. Described model and related governing equations in this chapter, predicted the response of IPMC under applied electro-potential and its effect on fluid environment.

CHAPTER IV

4. NUMERICAL METHOD

4.1. Introduction

The numerical analysis is performed by solving governing equations through finite element methods. COMSOL Multiphysics has been chosen as a finite element commercial software to implement the equations. We used different modules of COMSOL include Transport Diluted Species (Nernst-Plank equation), Electrostatic AC/DC (Poisson equation), Weak Form PDE mode, Structure Solid Mechanic (mechanic equations), Laminar Fluid (Navier-Stokes), and Fluid-Structure Interaction (FSI).

COMSOL Multiphysics is a powerful interactive environment for modeling and solving all kinds of scientific and engineering problems. The software provides a powerful integrated desktop environment with a *Model Builder* where we get a full overview of the model and access to all functionality (that we used). With COMSOL Multiphysics we can easily extend conventional models for one type of physics into multiphysics models that solve coupled physics phenomena and do so simultaneously. Accessing this power does not require an in-depth knowledge of mathematics or numerical analysis. Using the built-in *physics interfaces* and the advanced support for material properties, it is possible to build models by defining the relevant physical quantities such as material properties, loads, constraints, sources, and fluxes rather than by defining the underlying equations. We can always apply these variables, expressions, or numbers directly to solid and fluid domains, boundaries, edges, and points independently of the computational mesh. COMSOL Multiphysics then internally compiles a set of equations representing the entire model. We access the power of COMSOL Multiphysics as a standalone product through a flexible graphical user interface (GUI) or by script programming in Java or the MATLAB® language (requires the COMSOL LiveLink for MATLAB). Using these physics interfaces, we can perform various types of studies including:

- Stationary and time-dependent (transient) studies

- Linear and nonlinear studies
- Eigenfrequency, modal, and frequency response studies

When solving the models, COMSOL Multiphysics uses the proven *finite element method (FEM)*. The software runs the finite element analysis together with adaptive meshing (if selected) and error control using a variety of numerical solvers. The studies can make use of multiprocessor systems and cluster computing, and we can run batch jobs and parametric sweeps. A more detailed description of this mathematical and numerical foundation is in the *COMSOL Multiphysics Reference Guide*. COMSOL Multiphysics creates *sequences* to record all steps that create the geometry, mesh, studies and solver settings, and visualization and results in presentation. It is therefore easy to parameterize any part of the model: Simply change a node in the model tree and re-run the sequences. The program remembers and reapplies all other information and data in the model. Partial differential equations (PDEs) form the basis for the laws of science and provide the foundation for modeling a wide range of scientific and engineering phenomena [223].

The optional modules are optimized for specific application areas and offer discipline-standard terminology and physics interfaces. For some modules, additional material libraries, specialized solvers, element types, and visualization tools are also available. This section briefly describes the modules and details we performed the simulations.

4.2. Electrostatic AC/DC

The AC/DC Module is used by engineers and scientists to understand, predict, and design electric and magnetic fields in static, low-frequency and transient applications. Simulations of this kind result in more powerful and efficient products and engineering methods. It allows its users to quickly and accurately predict electromagnetic field distributions, electromagnetic forces, and power dissipation in a proposed design. Compared to traditional prototyping, COMSOL helps to lower costs and can evaluate and predict entities that are not directly measurable in experiments. It also allows the exploration of operating conditions that would destroy a real prototype or be hazardous.

The AC/DC Module includes stationary and dynamic electric and magnetic fields in two-dimensional and three-dimensional spaces along with traditional circuit-

based modeling of passive and active devices. All modeling formulations are based on Maxwell's equations or subsets and special cases of these together with material laws like Ohm's law for charge transport. The modeling capabilities are accessed via a number of predefined physics interfaces, referred to as AC/DC physics interfaces, which allow us to set up and solve electromagnetic models [223].

The AC/DC interfaces cover electrostatics, DC current flow, magnetostatics, AC and transient current flow, AC and transient magnetodynamics, and AC electromagnetic (full Maxwell) formulations. Under the hood, the AC/DC interfaces formulate and solve the differential form of Maxwell's equations together with initial and boundary conditions. The equations are solved using the finite element method with numerically stable edge element discretization in combination with state-of-the-art algorithms for preconditioning and solution of the resulting sparse equation systems. The results are presented in the graphics window through predefined plots of electric and magnetic fields, currents and voltages or as expressions of the physical quantities that we can define freely, and derived tabulated quantities (for example resistance, capacitance, inductance, electromagnetic force, and torque) obtained from a simulation [223].

The work flow in the module is straightforward and is described by the following steps: define the geometry, select materials, select a suitable AC/DC interface, define the boundary and initial conditions, define the finite element mesh, select a solver, and visualize the results. All these steps are accessed from the COMSOL Desktop. The solver selection step is usually carried out automatically using the default settings, which are already tuned for each specific AC/DC interface.

The AC/DC Module provides a unique environment for simulation of AC/DC electromagnetics in 2D and 3D. This module is a powerful tool for detailed analysis of coils, capacitors, and electrical machinery. With this module, we can run static, quasi-static, transient, and time-harmonic simulations in an easy-to-use graphical user interface. The AC/DC interfaces are fully multiphysics enabled couple them to any other physics interface in COMSOL Multiphysics or the other modules. By combining the definition of the potential with Gauss' law, we can derive the classical Poisson's equation. This equation is used in the Electrostatics interface. It is worth noting that Gauss' law does not require the charge distribution to be static. Thus, provided dynamics are slow enough that induced electric fields can be neglected and hence a scalar electric potential is justified,

the formulation can be used also in the Time Dependent study type. That typically involves either prescribing the charge dynamics or coupling a separate formulation for this. For the DC field, Poisson's equation is solved for the electric potential. In this case, the electrodes must only be represented as boundary conditions (fixed or floating potential). Figure 4.1 illustrates the detail of sub branch electrostatics AC/DC.

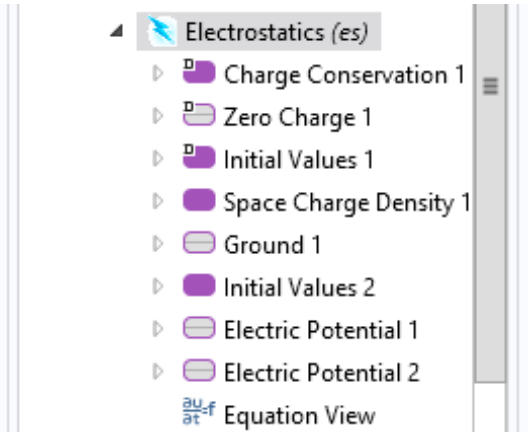

Figure 4.1: Electrostatics AC/DC branch details.

4.3. Transport of Diluted Species

Mass transfer is an important part of chemical engineering because this field considers the conversion of one type of substance into another. This occurs through chemical reactions, although separation and other unit operations are an important part. Transport of Diluted Species interface can be used to model the transport of a diluted species in chemical systems by convection and diffusion. In the Transport of Diluted Species interface, Fick's law describes the diffusive transport in the flux vector. Fick's law is adequate when the diffusing species is dilute with respect to a solvent. Assuming a binary mixture of solute A in solvent B, concentrations of up to 10 mol% of A can be considered dilute. The Transport of Diluted Species interface, found under the Chemical Species Transport branch, is used to calculate the concentration field of a dilute solute in a solvent. Transport and reactions of the species dissolved in a gas, liquid, or solid can be handled with this interface. The driving forces for transport can be diffusion by Fick's law, convection when coupled to a flow field, and migration when coupled to an electric field. The interface supports simulation of transport by convection and diffusion in 1D, 2D, and 3D as well as for axisymmetric components in 1D and 2D. The dependent variable is the molar concentration, *c*. Modeling multiple species transport is possible,

whereby the physics interface solves for the molar concentration, c_i, of each species *i*. The Transport of Diluted Species Interface provides a predefined modeling environment for studying the evolution of chemical species transported by diffusion and convection [223].

4.4. Fluid-Structure Interaction

Using the Fluid-Structure Interaction (FSI) interface, found under the Fluid Flow branch when adding a physics interface, we can model phenomena where a fluid and a deformable solid affect each other. The physics interface models both the fluid domain and the solid domain (structure) and includes a predefined condition for the interaction at the fluid-solid boundaries. An ALE formulation is used for incorporating the geometrical changes of the fluid domain. The fluid can be either compressible or incompressible. The flow regime can be laminar or turbulent. The solid domain has the same options as in a Solid Mechanics interface, including contact conditions and also nonlinear materials if the Nonlinear Structural Materials Module or Geomechanics Module is available. Using a stationary or a time-dependent study, the Fluid-Structure Interaction interface models two-way coupling between solids and fluids. There are, however, special study steps available in order to model one-way coupled fluid-structure interaction. The Fluid-Structure Interaction interface is available for 3D, planar 2D, and 2D axisymmetric geometries. In planar 2D, the physics interface uses the assumption that the structures deform in the plane strain regime. This means that the interpretation of the results is values "per meter thickness," and there is no specific thickness to specify. When the Fluid-Structure Interaction interface is added, the following default nodes are added to the Model Builder: Fluid Properties, Linear Elastic Material, and Free Deformation (for the mesh movement and default boundary conditions) in the domains; Wall (for the fluid), Prescribed Mesh Displacement (for the mesh movement), and Free (for the solid mechanics, which initially is not applicable to any boundary because the default settings assume a fluid domain) as default boundary conditions; and Initial Values. In addition, for the fluid-solid boundary, a Fluid-Solid Interface Boundary node adds the fluid-structure interaction. This node is only applicable to interior fluid-solid boundaries [223].

The Solid Mechanics (solid) interface, found under the Structural Mechanics Fluid Mechanics branches when adding a physics interface, is intended for general structural analysis of 3D, 2D, or axisymmetric bodies. In 2D, plane stress or plane strain

assumptions can be used. The Solid Mechanics interface is based on solving the equations of motion together with a constitutive model for a solid material. Results such as displacements, stresses, and strains are computed. The functionality provided by the Solid Mechanics interface depends on the products we are using. The Acoustics Module, MEMS Module, and Structural Mechanics Module add several features, for example, geometric nonlinearity and advanced boundary conditions such as contact, follower loads, and nonreflecting boundaries. The default material is a Linear Elastic Material. Figure 4.2 presents the detail of fluid-structure module in COMSOL.

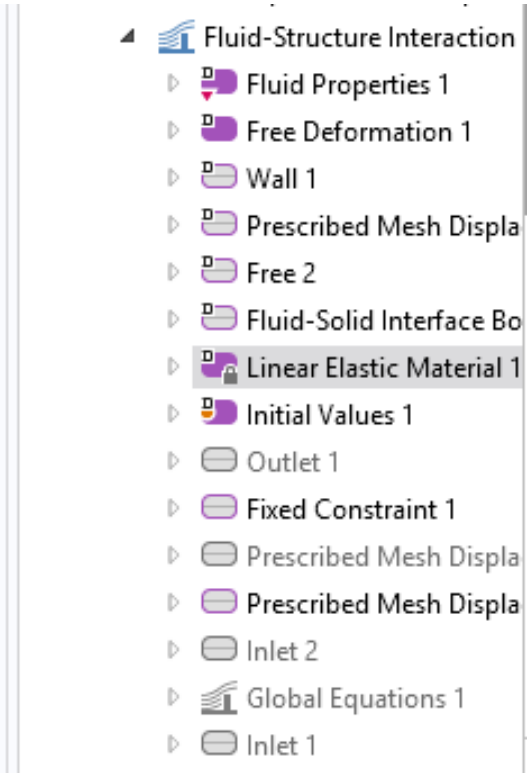

Figure 4.2: Fluid-structure interaction branch and details.

4.5. Weak Form

The term *weak form* is borrowed from mathematics, but in this context, it has a slightly different meaning; this implementation incorporates capabilities in addition to those defined in the mathematical weak form. Moreover, knowledge of the mathematical weak form is not a prerequisite to using the COMSOL Multiphysics implementation. The distinguishing characteristics of the weak form in COMSOL Multiphysics are that it makes it possible to:

• Enter certain equations that can be derived from an energy principle in a very compact and convenient form. Such equations, for example, arise in structural mechanics.

• Add and modify non-standard constraints, such as various contact and friction models.

• Use the *test operator* to conveniently work with problems in variational calculus and parametric optimization. COMSOL Multiphysics provides the possibility to add weak form contributions to any physics interface in the model. In addition, add *weak constraints*, which, for example, provide accurate fluxes and reaction forces [223].

In the Model Wizard, add weak form interfaces on all domain levels: Weak Form PDE on domains, boundaries, edges (in 3D models), and for points. All the interfaces are found under the Mathematics>PDE Interfaces branch in the Model Wizard. In all of them, weak expressions can be added, which COMSOL Multiphysics adds to the overall equation. Adding one of these interfaces creates a PDE node for PDE modeling using a weak formulation. Also, add a Weak Form PDE on the domain level to any other PDE interface. When this interface is added, these default nodes are also added to the Model Builder: Weak Form PDE, Zero Flux (for a Weak Form PDE on the domain level only), and Initial Values. Right-click the main PDE node to add other nodes that implements other boundary conditions, for example. On the domain level, edge level, and boundary levels the same boundary conditions can be used as for the Coefficient Form PDE and General Form PDE. To implement the equations using the Weak Form PDE mode, we require the governing equation introduced before to be recast in their weak form, namely

$$\int_B \varepsilon(\tilde{\mathbf{u}}) \cdot \mathbf{T}\, dv - \int_{\partial B} \tilde{\mathbf{u}} \cdot \mathrm{t}\, da = 0, \tag{30}$$

$$\int_B \tilde{c}\dot{c}\, dv - \int_B \nabla\tilde{c} \cdot \mathbf{J}\, dv + \int_{\partial B} \tilde{c}\mathbf{n} \cdot \mathbf{J}\, da = 0, \tag{31}$$

$$\int_B \nabla\tilde{\psi} \cdot \mathbf{d}\, dv - \int_{\partial B} \tilde{\psi}\mathbf{n} \cdot \mathbf{d}\, da + \int_B \tilde{\psi} q\, dv = 0, \tag{32}$$

for all independent-time function chosen in an appropriate functional space.

An alternative way of implementing equation (30) is to use the Solid Mechanics interfaces of the Structural Mechanics physics module and introduce the solute contribution, as a Weak Contribution mode in the IPMC domain.

$$-\int \varepsilon(\tilde{\mathbf{u}}) \cdot (3\lambda + 2G)\alpha(c - c_0)\mathbf{I}\, dv = 0, \tag{33}$$

See the COMSOL Multiphysics Modeling Guide for implementation details. In addition, we have used the COMSOL physics module Transport of Diluted Species interface to implement the ion transport equation and the AC/DC Module to implement the electrostatic equation (Poisson). The weak form (30-33) accounts for the mechanical, chemical and electric boundary conditions which depend on the specific problem under investigation.

4.6. Particle Tracing

Particle tracing provides a Lagrangian description of a problem, in which the particles are treated as distinct entities instead of a continuous distribution. The particle trajectories are computed by solving ordinary differential equations using Newton's law of motion. Newton's law of motion requires specification of the particle mass and all forces acting on the particle. The forces acting on particles can be divided into two categories, those due to external fields and those due to interactions between particles. Forces due to external fields are typically computed from a finite element model, using the physics interfaces available in COMSOL Multiphysics.

For each particle, a second-order ordinary differential equation is usually solved for each component of the position vector. This means that three ordinary differential equations are solved for each particle in 3D and two in 2D. At each time step, the forces acting on each particle are queried from the external fields at the current particle position. If particle-particle interaction forces are included in the model, then they are added to the total force. The particle position is then updated, and the process is repeated until the specified end time for the simulation is reached. Since the Particle Tracing Module uses a very general formulation for computing particle trajectories, the physics interfaces can be used to model charged particle motion in electromagnetic fields, large scale planetary and galactic movement, and particle motion in laminar, turbulent, and multiphase fluid systems.

The Particle Tracing Module is available to assist with these types of modeling problems. In this study, we used this module to predict the position of the particle released in the fluid when IPMCs cilia deform under electro potential. It is possible to model particle tracing with COMSOL Multiphysics provided that the impact of the particles on the flow field is negligible. First, we compute the flow field, and then, as an analysis step, calculate the motion of the particles. The motion of a particle is defined by Newton's second law. Examples of forces acting on a particle in a fluid are the drag force, the buoyancy force, and the gravity force. The drag force represents the force that a fluid exerts on a particle due to a difference in velocity between the fluid and the particle. It includes the viscous drag, the added mass, and the Basset history term. Several empirical expressions have been suggested for the drag force. One of those is the one proposed by Khan and Richardson [224]. That expression is valid for spherical particles for a wide range of particle Reynolds numbers. 3000 particles with 5 μm diameter released in the channel [223].

4.7. Meshing

The Mesh nodes enable the discretization of the geometry into small units of simple shapes, referred to as "mesh elements". A mesh is a result of building a meshing sequence. A meshing sequence corresponding to geometry consists of Meshing Operations and Attributes. The attribute nodes store properties that are used by the operation nodes when creating the mesh. Building an operation node creates or modifies the mesh on the part of the geometry defined by the operation node's selection. Some of the operation nodes use properties defined by attribute nodes; for example, the Free Tetrahedral node reads properties from the Distribution and Size attribute nodes. For some operation nodes, we can right-click to add local attribute nodes as subnodes. Properties defined in local attribute nodes of an operation node override the corresponding properties defined in global attribute nodes (on the same selection).

2D Geometries

The mesh generator discretizes the domains into *triangular* or *quadrilateral* mesh elements. If the boundary is curved, these elements represent an approximation of the original geometry. The sides of the triangles and quadrilaterals are called *mesh edges*,

and their corners are *mesh vertices*. A mesh edge must not contain mesh vertices in its interior. The boundaries defined in the geometry are discretized (approximately) into mesh edges, referred to as boundary elements (or *edge elements*), which must conform with the mesh elements of the adjacent domains. The geometry vertices are represented by vertex elements.

3D Geometries

The mesh generator discretizes the domains into *tetrahedral*, *hexahedral*, *prism*, or *pyramid* mesh elements whose faces, edges, and corners are called *mesh faces*, *mesh edges*, and *mesh vertices*, respectively. The Distribution node was used to specify the distribution of mesh elements along an edge, for example. Predefined distribution type was selected to specify properties of a predefined distribution method. It could be a geometric sequence (exponentially increasing or decreasing element size) or an arithmetic sequence (equal distance between elements); see COMSOL Manual for details.

To create a mapped quadrilateral mesh (that we used for IPMC) for each domain, the mapped mesher maps a regular grid defined on a logical unit square onto each domain. The mapping method is based on transfinite interpolation. The settings in the Size and Distribution nodes used by a Mapped node determine the density of the logical meshes. For the mapping technique to work, the opposite sides of each logical unit square must be discretized by the same number of edge elements. By default, the relationship between the four sides of the logical unit square and the boundaries around a domain is based on a criterion related to the sharpest angle between boundaries. Next distribution option applied at the two edge of IPMC to distribute higher density of elements near the electrodes.

Because of fluid-IPMC interaction in this region we need more detailed elements to solve equations and reach accurate results. There are various options predefined in size selection section from extremely coarse to extremely fine for the size of elements (see figure 4.3). In the most of the cases of two-dimensional analysis, we used finer option to mesh IPMC and fluid with the elements size in the range of 1.6 μm to 112 μm. Normally the smallest element size applied to IPMC-fluid interface and biggest to the triangular structure of fluid. For the rest of system (fluid), the triangular element formation was chosen.

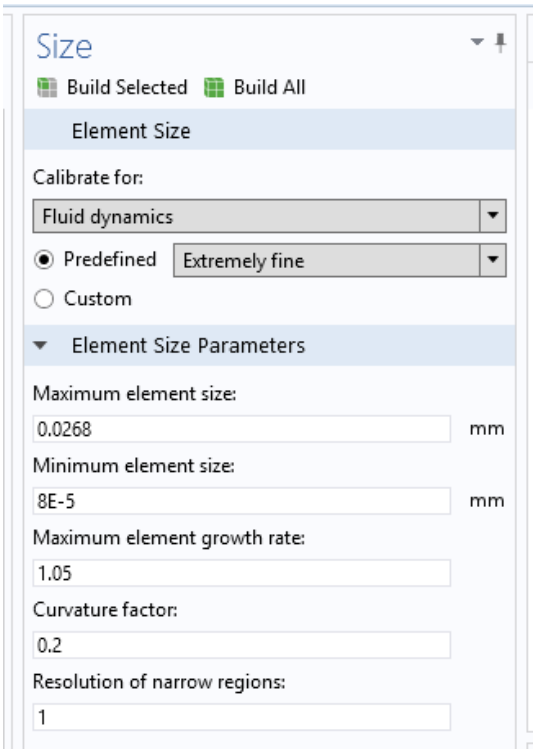

Figure 4.3: Mesh generation and element size selection in COMSOL.

4.8. Moving Mesh

The Moving Mesh interface (ALE), found under the Mathematics>Deformed Mesh branch when adding a physics interface, can be used to create models where the geometry, here represented by the mesh, changes shape due to some physical phenomena without the material being removed or added. Arbitrary Lagrangian Eulerian (ALE) is a formulation where a Eulerian equation is transformed into an equation written with respect to a mesh, which can be moving in relation to both the Eulerian frame and the Lagrangian frame. The COMSOL Multiphysics solvers have built-in support for the necessary transformation of derivatives.

The difference between the Deformed Geometry and Moving Mesh interfaces is that the former defines a deformation of the material frame relative to the geometry frame, while the latter defines a displacement of the spatial frame relative to the material frame. The Moving Mesh interface can be used to study both stationary states and time-dependent deformations where the geometry changes its shape due to the dynamics of the problem. For example, it can be used for fluid and solid (IPMC) domains deformations in fluid-structure interaction (FSI) or electrostatic domain deformations in MEMS.

Simulations using moving meshes, with a boundary moving in the normal direction, can sometimes need a stabilizing term to suppress the formation of local boundary segments of high curvature. This can be of particular importance in an automatic re-meshing sequence, where the re-meshing step might amplify local curvature artifacts.

In this study in the fluid-IPMC interaction of micropump simulation, we applied moving mesh to predict the IPMC configuration under electro potential. Furthermore, this deformed configuration employed to obtain fluid velocity and pressure field. Also, it is possible to use deformed IPMC mesh for post processing of results.

4.9. Solver

The process of solving a problem in COMSOL Multiphysics is hierarchical. The Study node is the coarsest level (the top level). It contains of the least amount of detail and defines a Study branch (see figure 4.4). When creating a new model, we can add any of the predefined Study and Study Step Types. At any time, we can also add studies. However, we choose to add a study, a study node is added to The Model Builder including a corresponding *study step* (for example, Stationary), and in some cases, additional study steps. The study step represents the next level of detail. Most study steps are used to control the form of the equations, what physics interfaces are included in the computation, and what mesh is used. A study step Settings window has a Physics and Variables Selection section where inclusion and exclusion of physics interfaces and variables can be adjusted and set. There are also Common Study Step Settings for many of the study features added to a sequence. Study steps correspond to part of a *solver configuration* (solver sequence), which is the next level of detail. There are also study steps for cluster computing, for example, which corresponds to part of the Job Configurations. Solver Configurations contain nodes that define variables to solve for, the solvers and settings, and additional sequence nodes for storing the solution, for example. The solvers also have nodes that can control the solver settings in detail. Knowing The Relationship Between Study Steps and Solver Configurations is useful to help define and edit the settings before computing a solution. Bear in mind, however, the default solver settings defined by the study usually provide a good starting point.

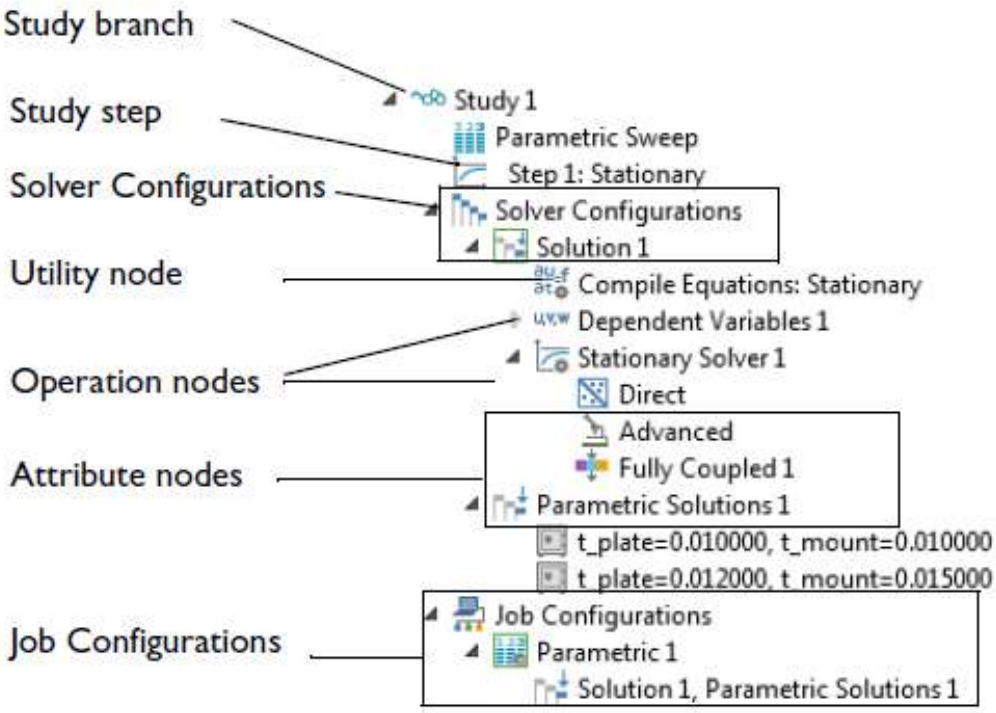

Figure 4.4: An example of the hierarchy under the Study node.

All linear system solvers work on general sparse linear systems of the form $Ax = b$ and use LU factorization on the matrix A to compute the solution x. In doing so, they use a preordering algorithm that permutes the columns of A to minimize the number of nonzeros in the L and U factors. Popular preordering algorithms include Minimum degree, Nested dissection, and Multisection. The MUMPS and SPOOLES solvers run distributed when running COMSOL Multiphysics in distributed mode (on clusters, for example). All linear system solvers benefit from shared memory parallelism (multicore processors, for example); however, MUMPS do so to a slightly lesser extent than PARDISO and SPOOLES.

The MUMPS solver works on general systems of the form $Ax = b$ and uses several preordering algorithms to permute the columns and thereby minimize the fill-in. MUMPS is multithreaded on platforms that support multithreading and also supports solving on distributed memory architectures through the use of MPI. The code is written in Fortran 90. For further details about MUMPS, see COMSOL Manual. The PARDISO Solver works on general systems of the form $Ax = b$. In order to improve sequential and parallel sparse numerical factorization performance, the solver algorithms are based on a Level-3 BLAS update, and they exploit pipelining parallelism with a combination of left-looking and right-looking super node techniques. PARDISO is multithreaded on

platforms that support multithreading. On distributed memory architectures, the solver settings are changed to corresponding MUMPS settings if needed. The code is written in C and Fortran. COMSOL uses the PARDISO version developed by Olaf Schenk and collaborators, which is included with Intel® MKL (Intel Math Kernel Libraries).

Backward differentiation formula (BDF) is a multi-step formula based on numerical differentiation for solutions to *ordinary differential equations*. A BDF method of order *n* computes the solution using a *n*th-grade polynomial in terms of backward differences. The default time-dependent solver for Navier-Stokes is the BDF method with the maximum order set to two. Higher BDF orders are not stable for transport problems in general nor for Navier-Stokes in particular. BDF methods have been used for a long time and are known for their stability. However, they can have severe damping effects, especially the lower-order methods. Hence, if robustness is not an issue, a model can benefit from using the generalized-α method instead. Generalized-α is a solver which has properties similar to those of the second-order BDF solver but it is much less diffusive. Both BDF and generalized-α are per default set to automatically adjust the time step. While this works well for many models, extra efficiency and accuracy can often be gained by specifying a maximum time step. It is also often beneficial to specify an initial time step to make the solver progress smoothly in the beginning of the time series [223].

4.10. Boundary Conditions

In general, the situation consists of an IPMC immersed in the fluid and we study the IPMC-fluid interaction (see Fig. 4.5 for schematics details). The bulk equations must be supplemented by boundary conditions that involve the interaction between IPMC and the fluid. Thus, the essential boundary condition for the displacement field $\mathbf{u} = 0$ are given at the clamped boundary surface $\partial_u B$ and null traction $t = 0$ over the remain boundary $\partial_t B$. For the chemical field, a zero flux boundary condition $\mathbf{n} \cdot \mathbf{J} = 0$ is specified over all the boundary to simulate ion blocking surfaces. For the IPMC actuation, an electric load $\psi = 0$ and $\psi = \psi^+$ are prescribed on the boundary surface ∂B (the left side and the right side of IPMC). At the fluid wall, no slip boundary conditions applied ($v = 0$) and at the interface of IPMC and fluid, fluid velocity is equal to velocity of IPMC deformation ($v = v_w$). Also open boundary conditions prescribed for fluid.

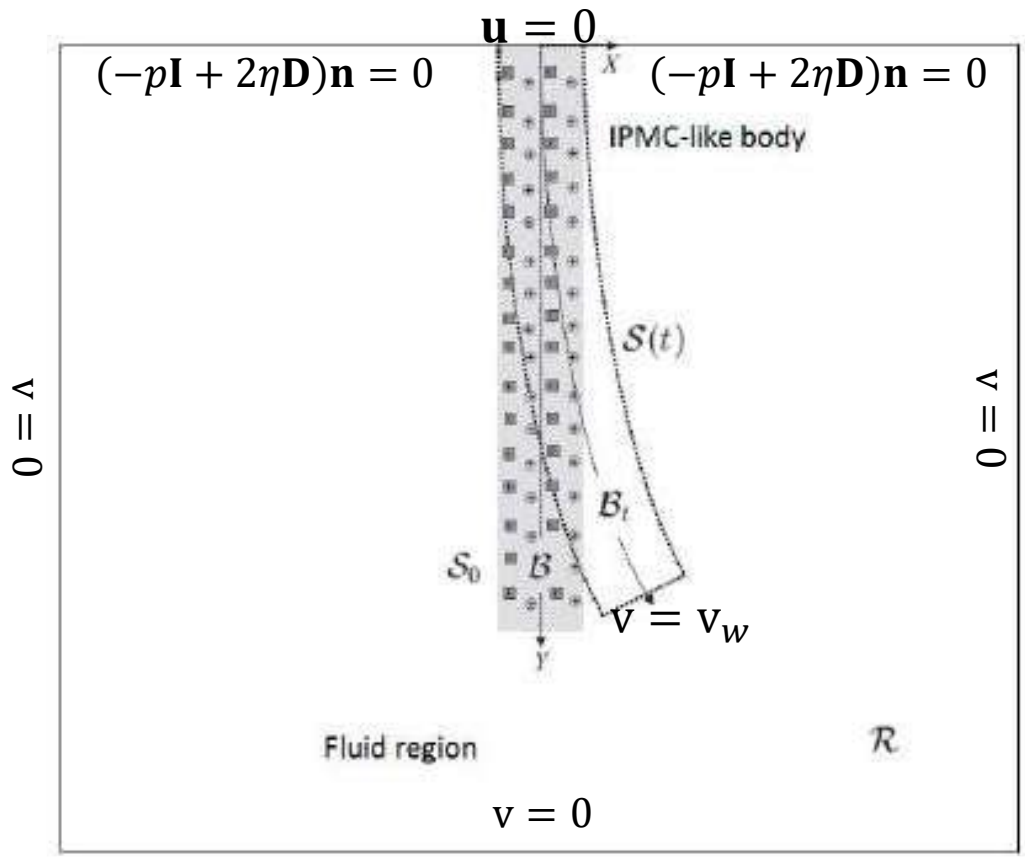

Figure 4.5: A sketch of the general fluid-structure problem.

We consider a situation that is a fluid-structure interaction analysis, where the surrounding fluid flow is due to the deformation of the IPMC domain B. Accordingly, a moving-mesh Arbitrary-Lagrangian-Eulerian (ALE) mode is used to make sure that the flow domain R is deformed along with the IPMC body. Further, transient effects are taken into account in the fluid, and the deformations in the IPMC are modeled using reference configuration, say, material frame in the plane strain application mode. Thus, the weak form of the Navier-Stokes equation (26), solving for the velocity field and the pressure in the spatial (deformed) moving coordinate system. Fluid and IPMC structure interaction requires simultaneous two-way coupling of shared fluid and deformable solid boundary interfaces S(t). On shared boundary interfaces (i.e, fluid-IPMC-like body S), the IPMC deformation domain provides a loading condition given by (26) to the fluid domain and a velocity constraint given by (27) to the flow.

In the moving mesh, the motion of the deformed mesh is modeled using Winslow smoothing, which is the default smoothing when using the predefined Fluid-Structure Interaction coupled application modes. See the Moving Mesh Application Mode in the COMSOL Multiphysics Modeling Guide for implementation details. The boundary conditions control the displacement of the moving mesh with respect to the

initial geometry. At the boundaries of the IPMC-like body B, this displacement is the same as the structural deformation. At the exterior boundaries of the flow domain S, the deformation is set to zero in all directions. In all simulations, we use two-dimensional quadratic Lagrange elements to interpolate the displacement **u** and the solute concentration *c* in each layer. We use linear elements approximation for the pressure *p* and approximate the velocity u by means of continuous quadratic elements, the so-called Taylor-Hood elements. For the time discretization, we employ second-order backward differentiation formula (BDF), with the time steps controlled by the numerical solver during the computations. At each time step, the corresponding discrete system is solved by using the default option of COMSOL (PARDISO solver), with residual tolerance levels of 10^{-4}. This was verified 8 to be sufficient since similar solutions were obtained at lower tolerance levels. Computations were carried out on a twelve-core 64 GB memory Dell PowerEdge T620. Required post processing performed to produce results.

CHAPTER V

5. RESULTS AND DISCUSSIONS

5.1. Introduction

This chapter presents four sections consisting of the results and numerical simulation obtained from COMSOL by solving the governing equations mentioned in chapter three. First section is related to simulating IPMC strip deformation under electro-potential and confirms the related equations with experimental and numerical results of available works. In the next three sections, different configurations of IPMC micropump are simulated and discussed with IPMC-fluid interaction model from chapter three and employing the numerical method described in chapter four. The first micropump is based on one IPMC diaphragms and developed for drug delivery application. The second micropump with the double IPMC diaphragm is suitable for extracting fluid in biomedical application. Last section concerns the new concept of micropump consists of IPMCs cilia attached inside the channel for application in highly miniaturized microfluid systems in order to size reduction. To investigate and analyze three mentioned type of micropumps, diaphragm deformation, fluid velocity, and pressure field results are presented and discussed.

5.1. Three-dimensional IPMC

Here, the ionic polymer metal composite is viewed as a thin, 3-D cantilever resembling the characteristics of a hydrated base polymer (Nafion) sandwiched between the two metallated layers. The modeling of the complex response of the IPMC-like body to electrical and mechanical stimuli is set within the context of the 3-D theory of linear elasticity. In solid mechanics, the chemically induced deformations of the IPMC cantilever are described in terms of volumetric distortion field induced by the redistribution of the ions, which carry with them the solvent's molecules.

A set of numerical experiments is employed through a specialized computational analysis in order to analyze the behavior of the IPMC cantilever in different circumstances. The computational analysis is employed with reference to a cantilever IPMC-like body having a length 17 mm, a width of 2 mm, and a thickness 180 μm, corresponding to the sample tested in the laboratory by Wallmersperger *et al*. [206] which includes Nafion-117 as the base ionomer and lithium as the mobile cations. All the parameters have been implemented as presented in Table 5.1.

The behavior of the IPMC-like cantilever as an actuator has been numerically tested by different parameters. Crucial parameters of IPMC investigation include concentration, electro-potential, charge density, and displacement profiles. The coupled

multiphysics problem has been solved through a commercial finite element code (Comsol Multiphysics 4.4) using a fixed multigrid with a refined mesh along the thickness. The response of the system to applied voltages is obtained through an application of the upper voltage starting from zero.

Table 5.1: Three-dimensional IPMC simulation parameters [214].

Parameter		**Value**	**Dimension**
Diffusion coefficient	D	6.0×10^{-11}	$m^2\ s^{-1}$
Poisson´s modulus	ν	0.3	-
Anion concentration	c_0	1073	$mol\ m^{-3}$
Temperature	T	300	K
Gas constant	R	8.3143	$J\ mol^{-1}K^{-1}$
Faraday constant	F	96487	$C\ mol^{-1}$
Permittivity	ε	0.0177	$C^2\ N^{-1}\ m^{-2}$
Young´s modulus	E	220	MPa

Figure 5.1 shows the elastic curves of the IPMC-like body when $\alpha=1.18\times10^{-5}$ m^3/mol at different times. The curves in figure 5.2 represent electric boundary layer and in figure 5.3 demonstrate charge density. Small figures attached in figures 5.1 and 5.2 were given from simulation work by Nardinocchi [214] and experimental work by Wallmersperger [206] to validate the mathematical model and the numerical simulation results.

Results show that the electrochemical feedback makes an initial fast electrically driven actuation followed by a slow actuation when the diffusive component of the chemical flux compensates for the effects of the electrical migrative component. The boundary layers corresponding to the excess of a charge related to the electric potential and to the difference $(c-c_0)$ are shown in the Figures 5.2 and 5.3 respectively.

The electrochemical effects have been extensively investigated and Figures 5.2 and 5.3 agree with the standard results concerning the evolution of the chemical concentration and the electric potential as well as the formation of the corresponding boundary layers. The steady mechanical solution, i.e., the value attained by the tip displacement in correspondence of the stationary solution for the mobile concentration, is depicted in figure 5.4. In the last part of this section, the active bending behavior

resulting from the applied electric field (after the 20s) is calculated and illustrated in figure 5.5. This figure presents initial geometry of IPMC (black and white sketch) and deformed geometry (colorful sketch). From dark blue (fixed part of IPMC strip) to red section of deformed IPMC, we can observe the exact displacement of IPMC under 50 mV electro-potential. This kind of simulation could deliver valuable information to predict deformation and critical parameters of IPMC in different dimension under a variety of electro-potential.

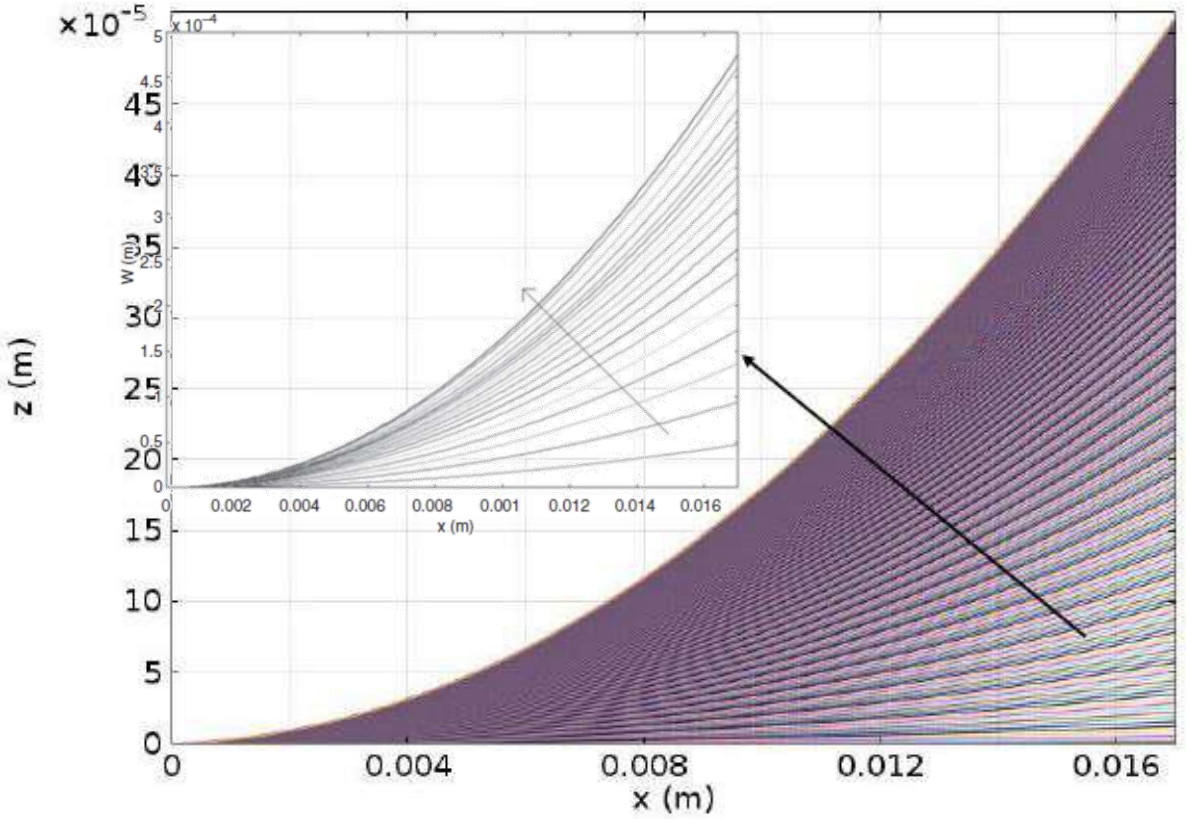

Figure 5.1: Elastic curves of IPMC cantilever corresponding to $\alpha=1.18\times10^{-5}$ m^3/mol and 50mV.

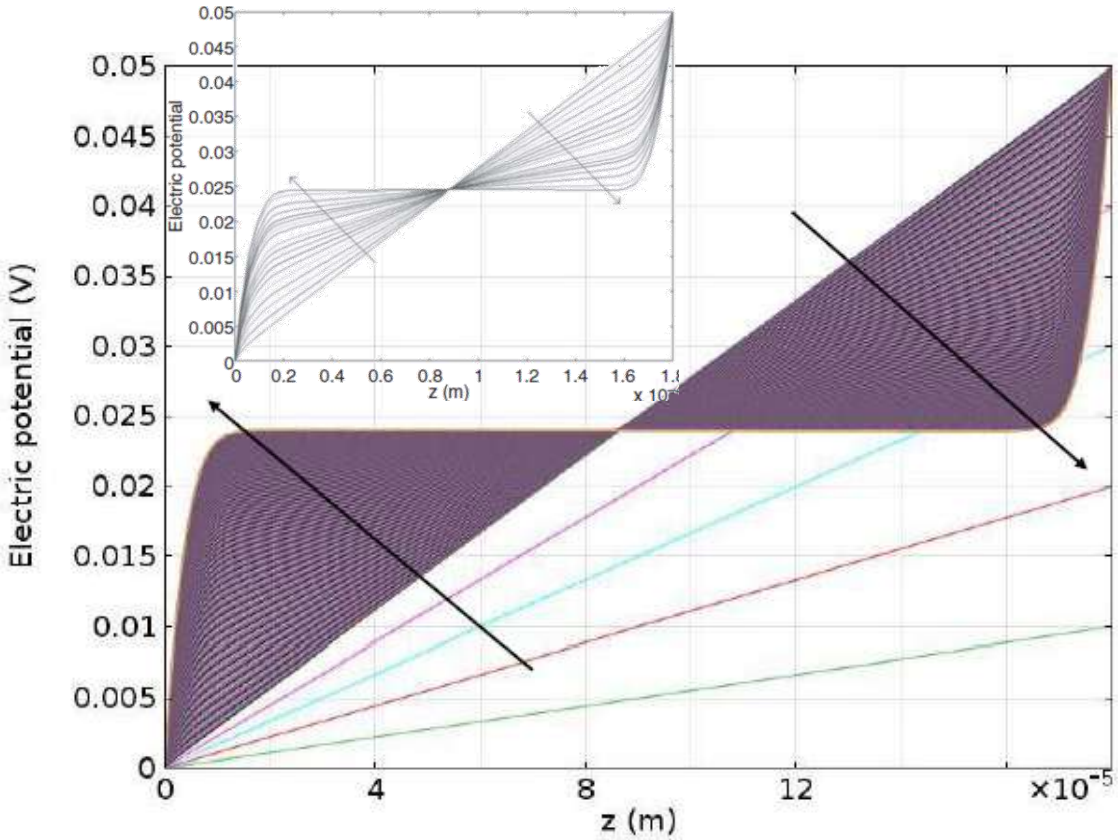

Figure 5.2: Electrical boundary layers of IPMC cantilever.

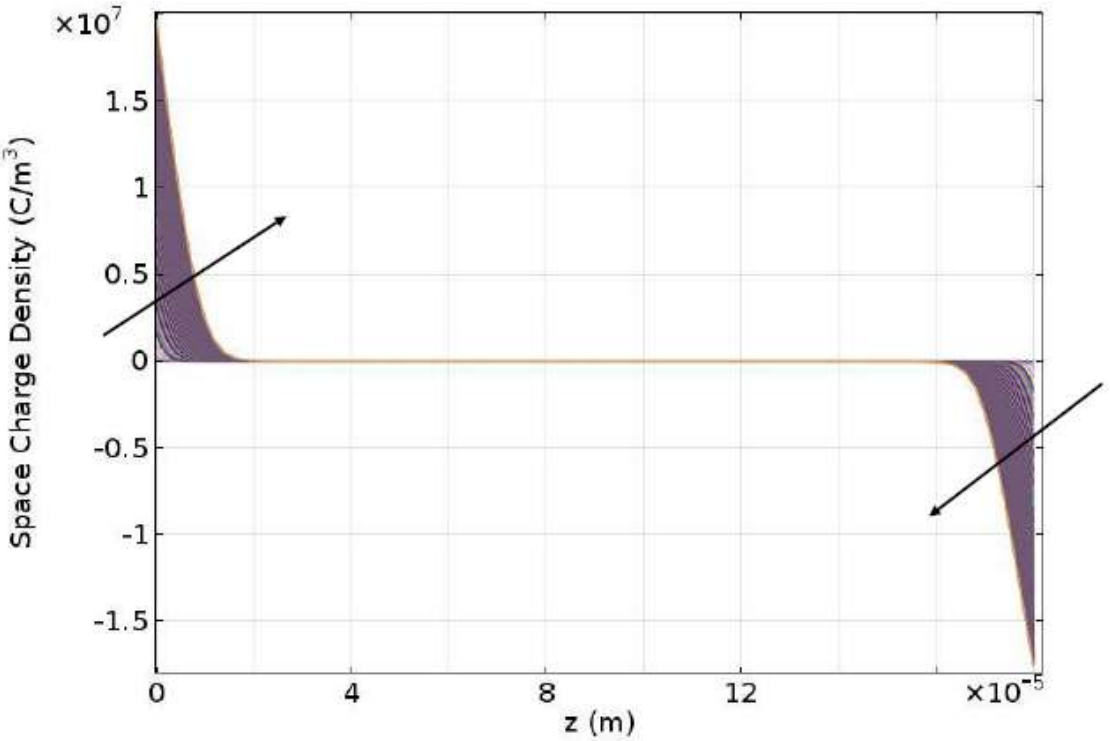

Figure 5.3: Chemical boundary layers of IPMC cantilever.

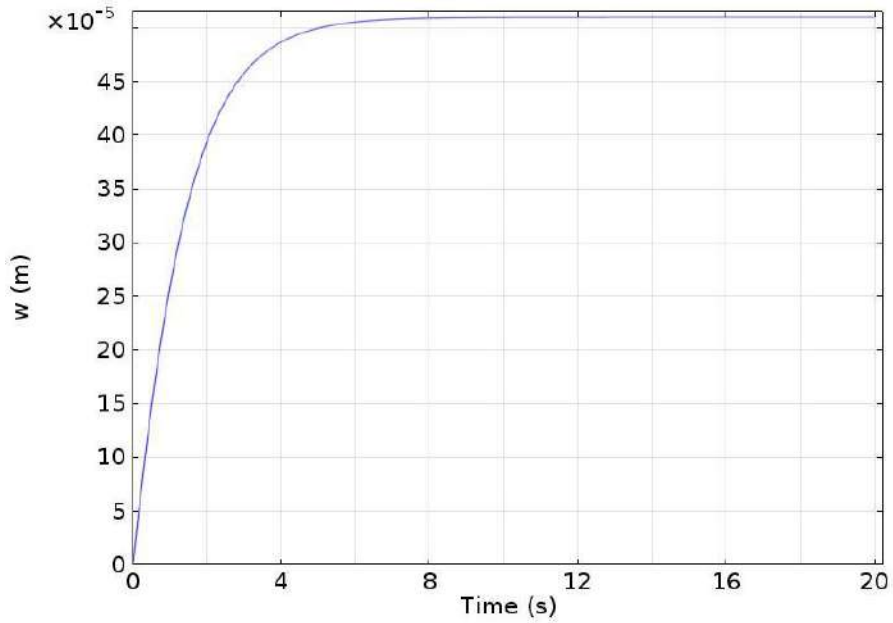

Figure 5.4: Tip displacement of IPMC cantilever corresponding to $\alpha=1.18\times10^{-5}$ m^3/mol.

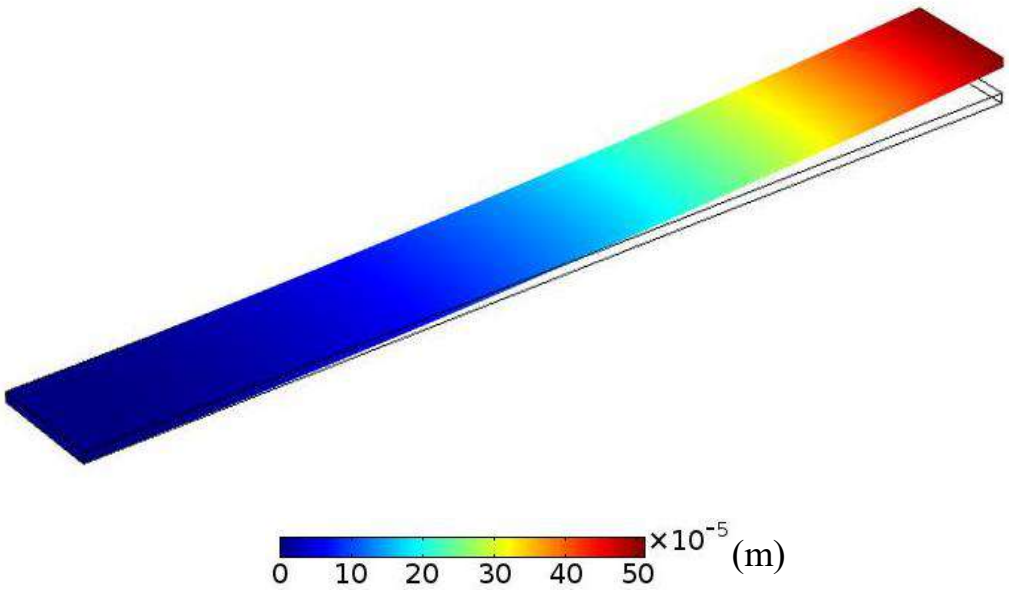

Figure 5.5: Deformation of IPMC cantilever.

5.2. IPMC micropump

As we explained in section 2.6, drug delivery for treatment of incurable diseases is very critical. In the case of diabetes, the best-known method for delivering insulin to the patient is insulin dispenser pump. Energy consumption and size of these insulin pumps is a challenge for researchers in the last years. In order to reduce size and energy consumption a lot of actuated and structures have been developed. One of the famous commercial insulin dispenser devices is called V-Go and produced in three different models for different types of patients (see table 5.2 for operational specification). Normally Diabetes patient needs 0.01 to 0.015 insulin unit (IU = 10 µl) per hour for each kilogram of his weight [61].

Table 5.2: Operational specification of different types of V-Go insulin pump [61].

Operational Specification			
Pump Model	V-Go 20	V-Go 30	V-Go 40
Reservoir Volume	560 µL (56 IU of insulin)	660 µL (66 IU of insulin)	760 µL (76 IU of insulin)
Basal Rate	8.3 µL/hr (0.6 IU/hr)	12.5 µL/hr (1.2 IU/hr)	16.7 µL/hr (1.8 IU/hr)
Bolus Increments	20 µL (2 IU) 18 Actuations	20 µL (2 IU) 18 Actuations	20 µL (2 IU) 18 Actuations
Nominal Bolus Volume	360 µL (36 IU)	360 µL (36 IU)	360 µL (36 IU)
Basal Volume (24 Hours)	200 µL (20 IU)	300 µL (30 IU)	400 µL (40 IU)
Accuracy	+/- 10%	+/- 10%	+/- 10%

In this section, the main goal of the study of IPMC micropump is to check if the IPMC diaphragm is able to provide enough deformation to generate the necessary pressure and flow of insulin by trying different electro potentials. According to current commercial insulin dispenser device and IPMC diaphragm, we suggest an IPMC based micropump for insulin dispenser device (see figure 2.2). Then, we simulate two dimensionally the micropump shown in figure 5.6 with mathematical equations mentioned in chapter three to prove the capability of micropump. Micropump made with

an 8 mm length IPMC strip and 100 µm width. Figure 5.6 shows the total displacement of IPMC diaphragm under 100, 200, and 300 mV electro-potential. The velocity of fluid inside the chamber under 100, 200 and 300 mV electro-potential demonstrate in figures 5.7. By increasing the applied electro-potential velocity of fluid increased. Flow rates of micropump at the outlet reach respectively 17 µl/hr, 40 µl/hr and 63 µl/hr under 100, 200 and 300 mV electro-potential. Compared to table 2.1 these flow rates are sufficient for insulin delivery in the treatment of Diabetes. Figure 5.8 presents the fluid pressure inside a chamber under 100 to 300 mV. Results show the pressure increased with increasing applied electro-potential. In general, a mathematical model of fluid-structure interaction predicts the behavior of IPMC and velocity of fluid in IPMC based micropump and compare the obtained results and data in table 5.2 prove the ability of IPMC micropump for application in insulin dispenser device.

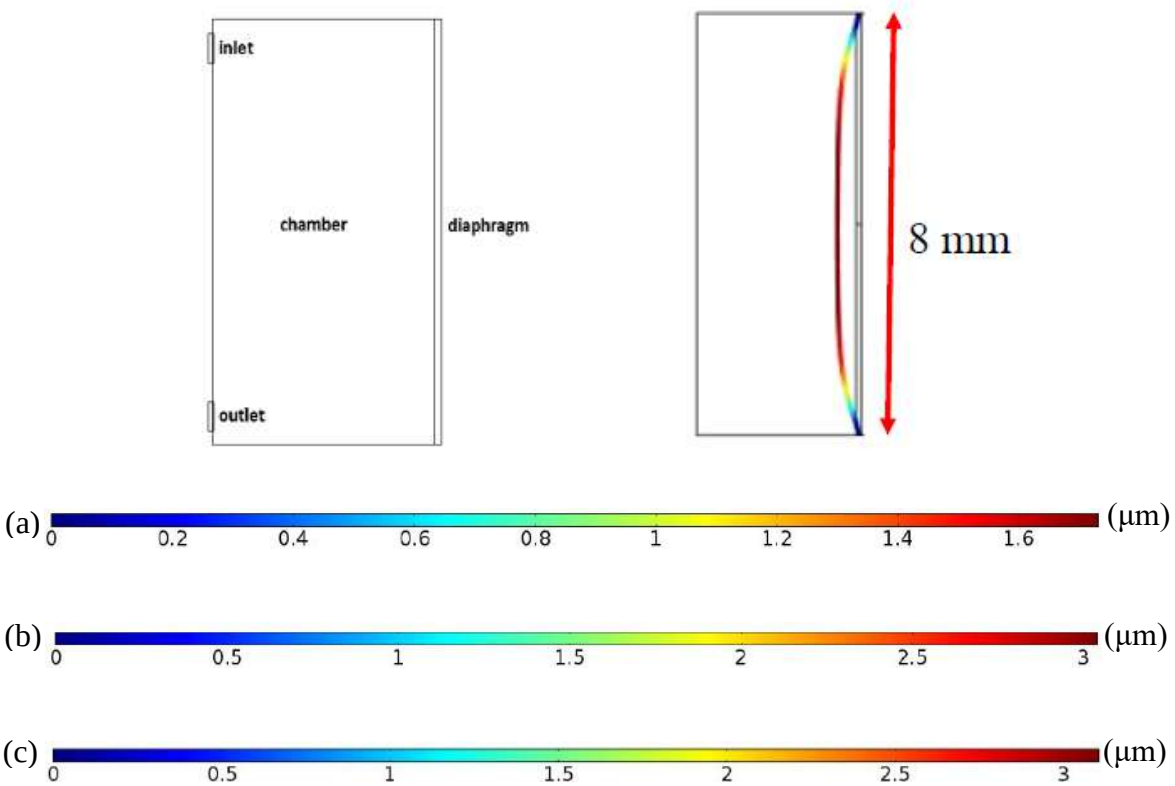

Figure 5.6: Total displacement of IPMC under a) 100 mV (1.31s), b) 200 mV (1.1s) and c) 300 mV (0.74s).

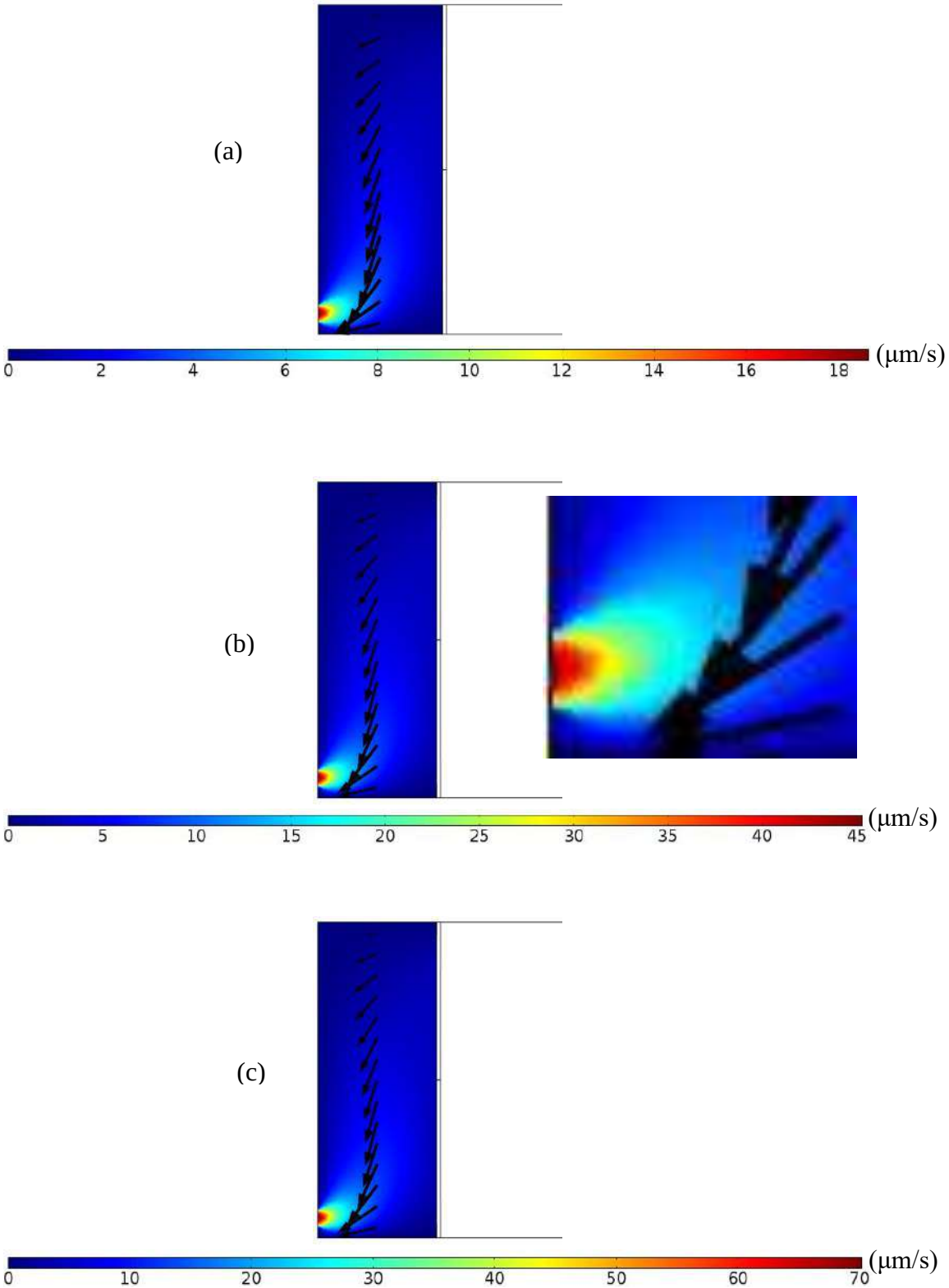

Figure 5.7: Fluid velocity inside chamber under a) 100 mV (1.31s), b) 200 mV (1.1s) and c) 300 mV (0.74s).

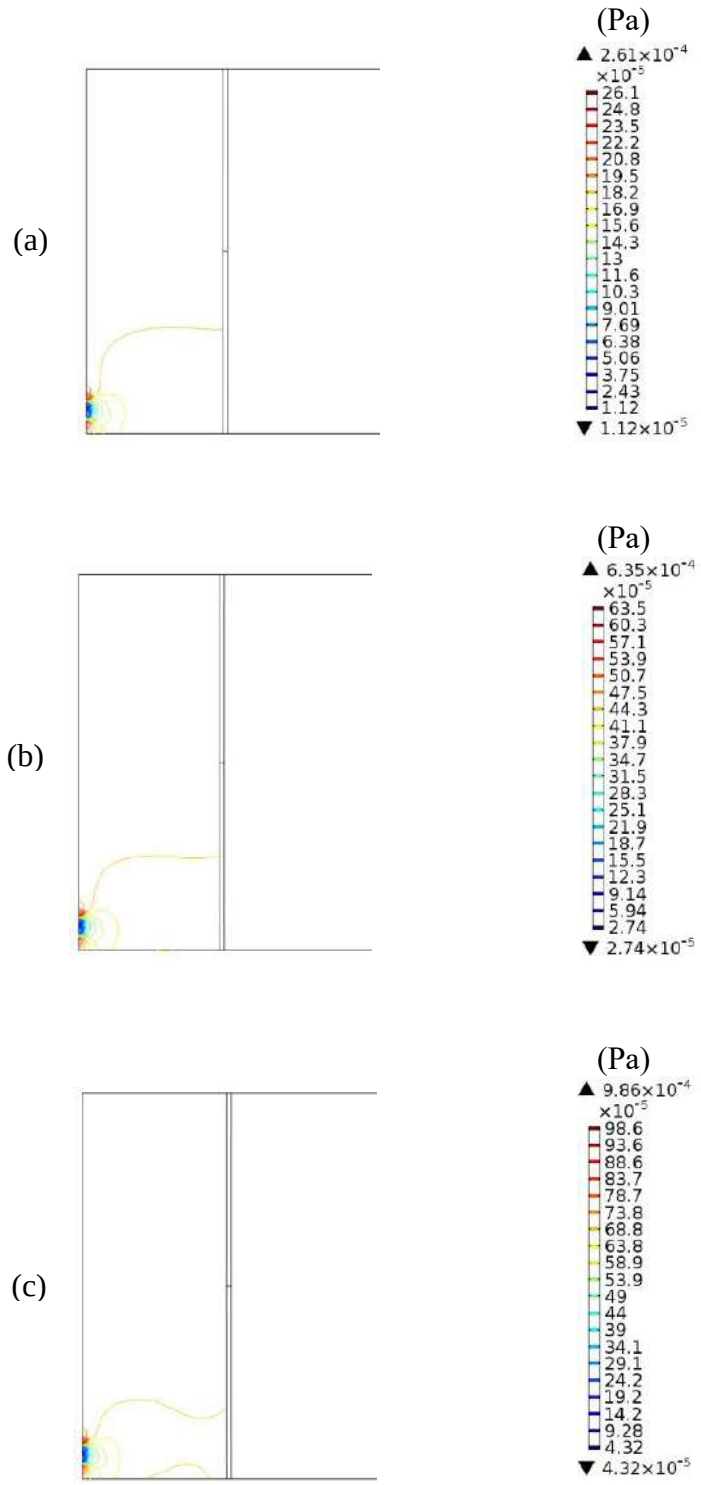

Figure 5.8: Fluid pressure inside chamber under a) 100 mV (1.31s), b) 200 mV (1.1s) and c) 300 mV (0.74s).

5.3. Double IPMC micropump

In recent years, treatment of Glaucoma by extracting accumulated fluid has been attracted huge attentions. There are some implants patents involved with the treatment of Glaucoma which drainage the aqueous humor and reduce the intraocular pressure (IOP). One of the successful commercial implants is invented by Ahmed Mateen and its detail and dimensions are shown in figure 5.9.

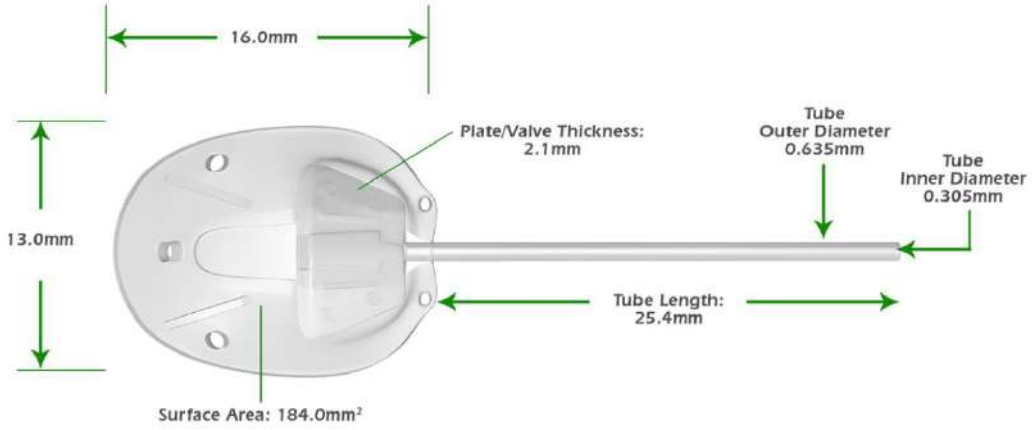

Figure 5.9: Ahmed flexible valve model FP7.

After study all patents and implants suggested before, we presented an IPMC micropump with a double IPMC diaphragm (with 100 μm thickness) as shown in figure 5.10. Micropump consists of a chamber, two IPMC diaphragms, inlet, outlet and IPMC microvalves. According to the patents and current implants, two diaphragms of IPMCs selected to reduce the dimension we need to generate the required flow rate. Compared to mentioned implants, dimension and energy consumption reduced with this structure. The main advantage of this IPMC implant would lie in control we have to change the flow rate, which depends on patient conditions. In current implants and surgical methods after 3 years, the path created for passing fluid start to narrowing (accumulation of tissues and particles) and aqueous humor will have difficulties to reach the implants and pump out of eye chamber. Here, by increasing electro potential applied to the implants and control the pump cycle it is possible to solve this problem and maintain the required flow rate. Due to the very low energy consumption of actuators, the maintenance cost decreases practically.

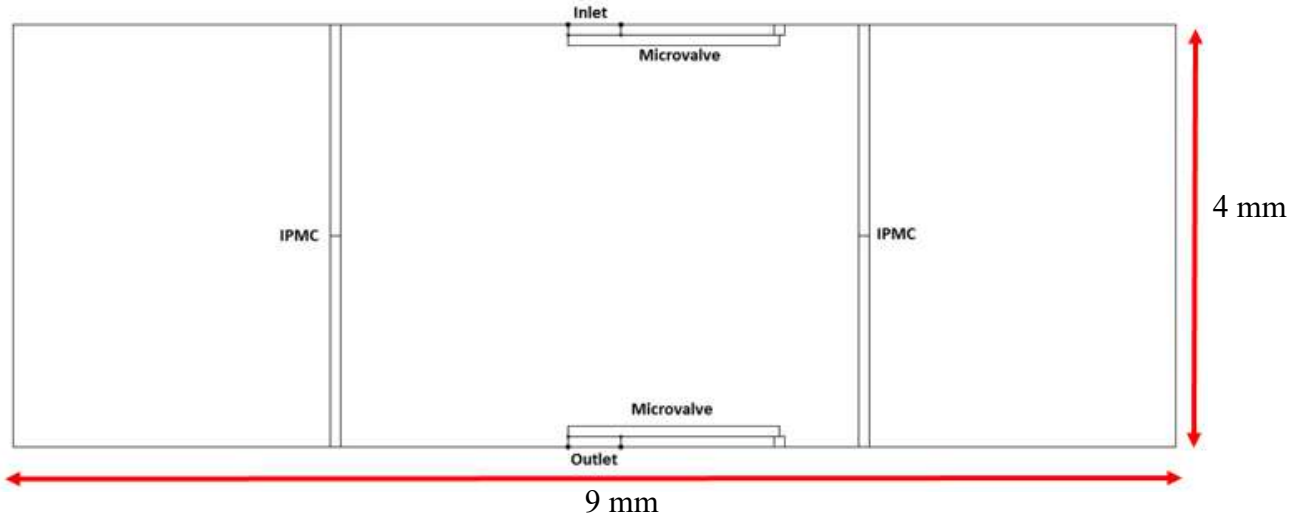

Figure 5.10: Schematic of IPMC based micropump with a double IPMC diaphragm.

A two-dimensional numerical simulation study has been performed using commercial software Comsol Multiphysics to simulate an IPMC based micropump. The numerical model solves the required governing equations to account for the electro-solid and fluid-solid coupling effects. In the electro-solid part, application of an electro-potential to the both IPMCs causes deflection of the diaphragms. In the fluid-solid interaction (FSI) approach, fluid flow described using Navier–Stokes equations are combined with the solid mechanics at the interface of FSI boundaries. The physics interface uses an Arbitrary Lagrangian–Eulerian (ALE) method to combine the fluid flow formulated using a Eulerian description and a spatial frame with solid mechanics formulated using a Lagrangian description and a material (reference) frame. The spatial frame also deforms with a mesh deformation that is equal to the displacements **u** of the solid within the solid domains. The mesh is free to move inside the fluid domains, and it adjusts to the motion of the solid walls. This geometric change of the fluid domain is automatically accounted for in COMSOL Multiphysics by the ALE method. IPMC diaphragms are fixed at its edges and considered as a zero-displacement boundary condition. The boundary conditions for the fluid model are no-slip at the fluid–wall interface and FSI and pressure boundary conditions at both inlet and outlet of the micropump. The flow is modeled using single-phase and incompressible flow assumptions via the Laminar Flow Module. In the present model, numerical investigations are carried out for IPMC diaphragms with 100 μm thickness and 4 mm length and fluid properties of water are used. The employed mesh is considered with an element size in the range of 1.6 μm to 112 μm for IPMCs diaphragm and fluid.

Figure 5.11 shows the deformation of IPMC diaphragms and the pumping mechanism of IPMC micropump with the application of 200 mV electro-potential. The result shows that the deformation is the maximum at the center and zero at the edges of IPMC diaphragms, as expected theoretically. So this deformation pushes the fluid out of the micropump chamber through the outlet. Figures 5.12 and 5.13 show simulation result for velocity and pressure field inside the pump chamber with the application of 200mV. Both velocity and pressure of the fluid observed at the maximum near the outlet. Figures 5.14 to 5.16 show result for deformation of IPMC, velocity, and pressure inside pump chamber with the application of 400 mV. Flow rate generated by the micropump increases with increasing the applied electro-potential. Our results show that during the pump mode, the membrane deflects into the chamber thus increasing the pressure of the fluid inside the chamber. As a result, the fluid in the chamber exits through the outlet.

Figures 5.17 to 5.19 demonstrate the simulation results in supply mode (suction) consist of IPMC deformation, fluid velocity and pressure contour in the pump chamber under 600mV electro-potential. From the results, it can be observed that during the supply mode, the IPMCs diaphragms deflects out of the chamber and thus creating a negative pressure inside the chamber. Due to this, the fluid enters the chamber through the inlet. These results confirm the function of IPMC micropump. The streamline of pressure in pump chamber show the formation of high pressure in inlet and outlet.

Figures 5.20 to 5.22 represent the velocity of the fluid under 600, 800 and 1000mV. These results confirm that the fluid velocity is influenced considerably by applied electro-potential (figure 5.23). The maximum fluid velocity of 175µm/s reached under 1000mV electro-potential. The relation between electro-potential and deformation of IPMC diaphragm can be seen in figure 5.24. In Figure 5.25, flow rates through the outlet of the micropump are shown under various electro potentials. Results show that by changing applied electro-potential we can reach required flow rate of micropump.

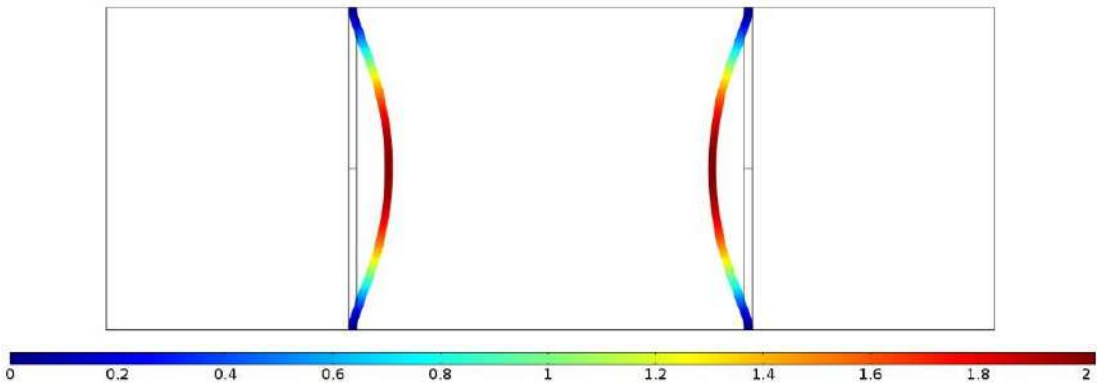

Figure 5.11: Total displacement of IPMC under 200 mV in 1s.

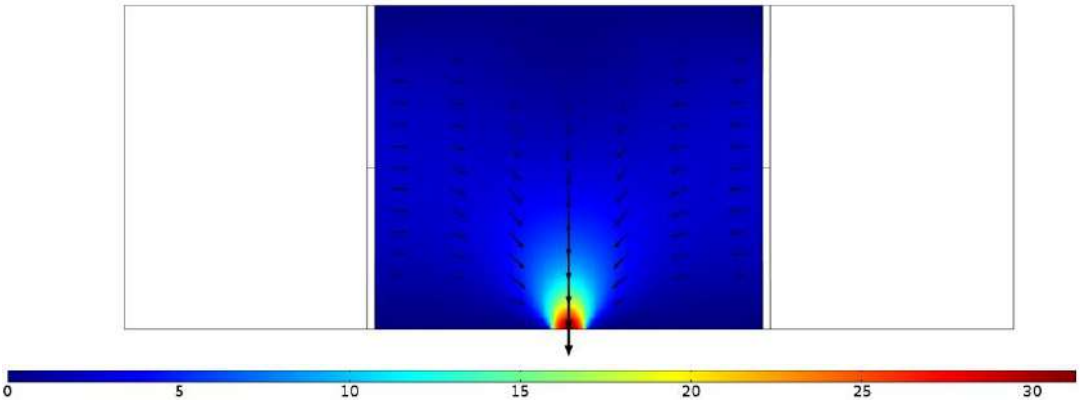

Figure 5.12: Fluid velocity under 200 mV in 1s.

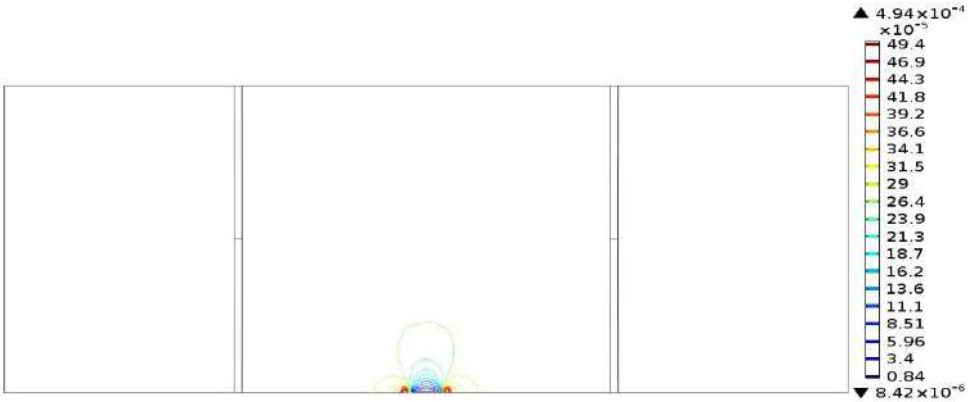

Figure 5.13: Pressure of fluid under 200 mV in 1s.

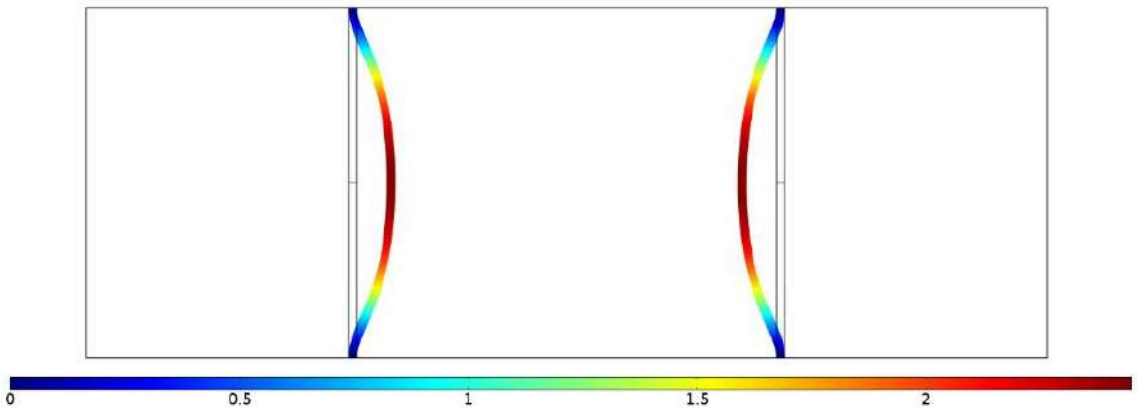

Figure 5.14: Total displacement of IPMC under 400 mV in 0.55s.

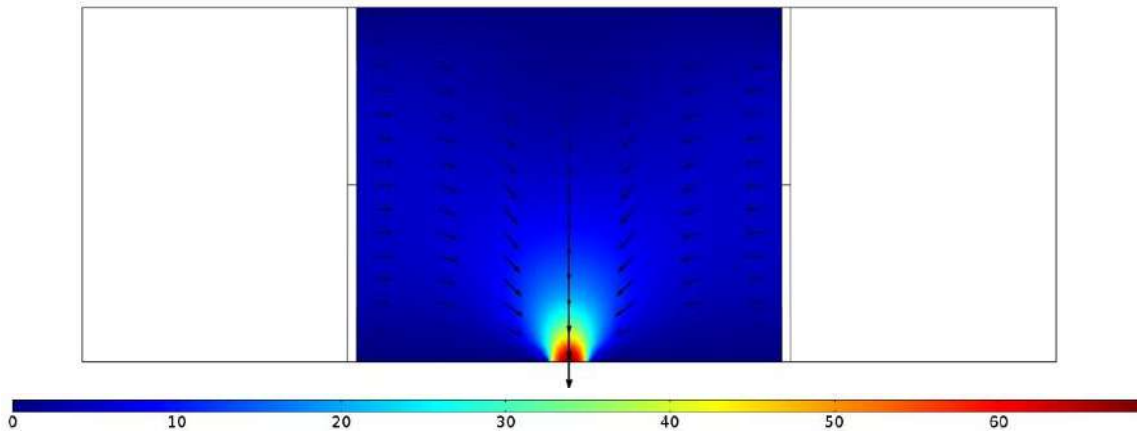

Figure 5.15: Fluid velocity under 400 mV in 0.55s.

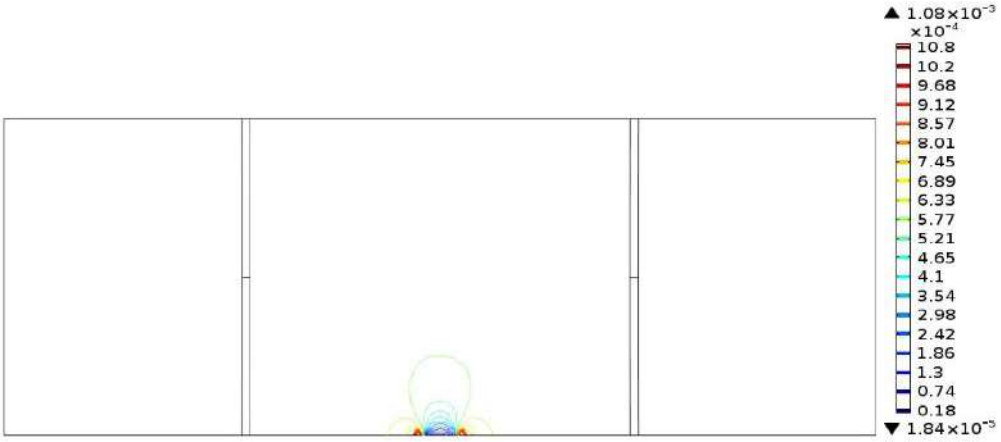

Figure 5.16: Pressure of fluid under 400 mV in 0.55s.

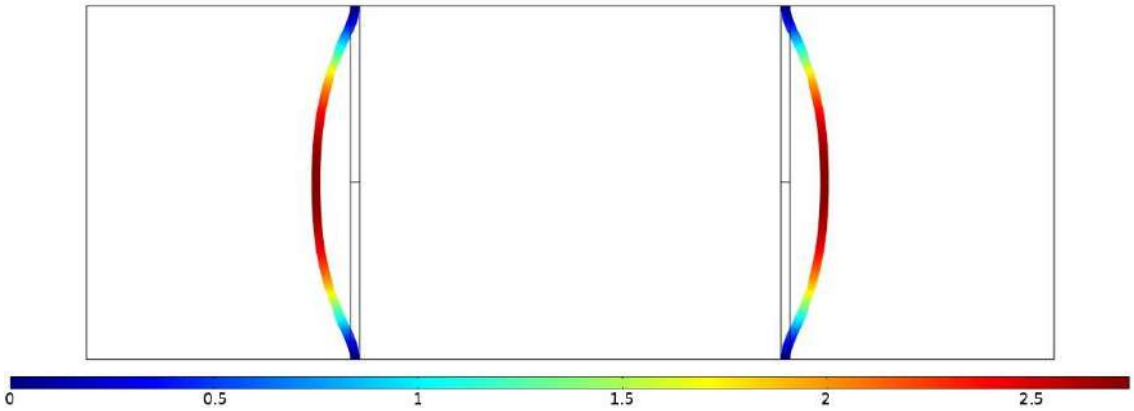

Figure 5.17. Total displacement of IPMC under 600 mV (supply mode) in 0.4s.

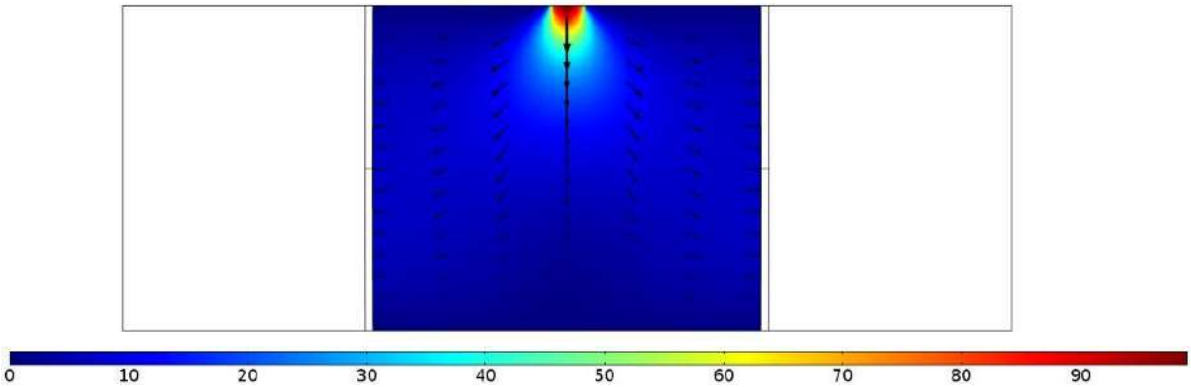

Figure 5.18: Fluid velocity under 600 mV (supply mode) in 0.4s.

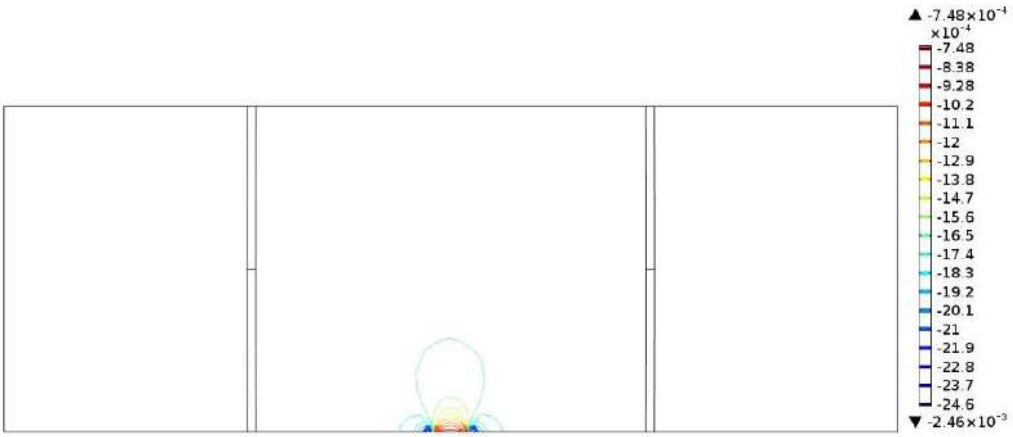

Figure 5.19: Pressure of fluid under 600 mV (supply mode) in 0.4s.

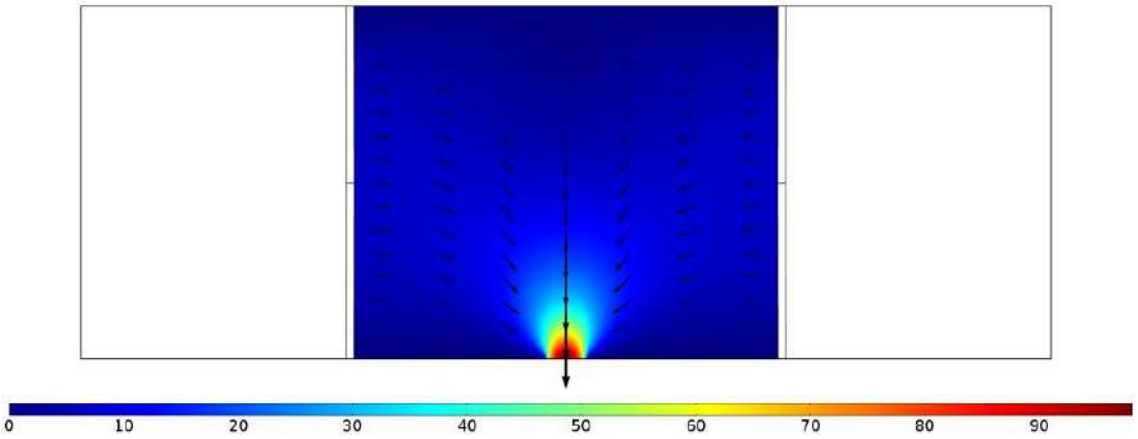

Figure 5.20: Fluid velocity under 600 mV in 0.4s.

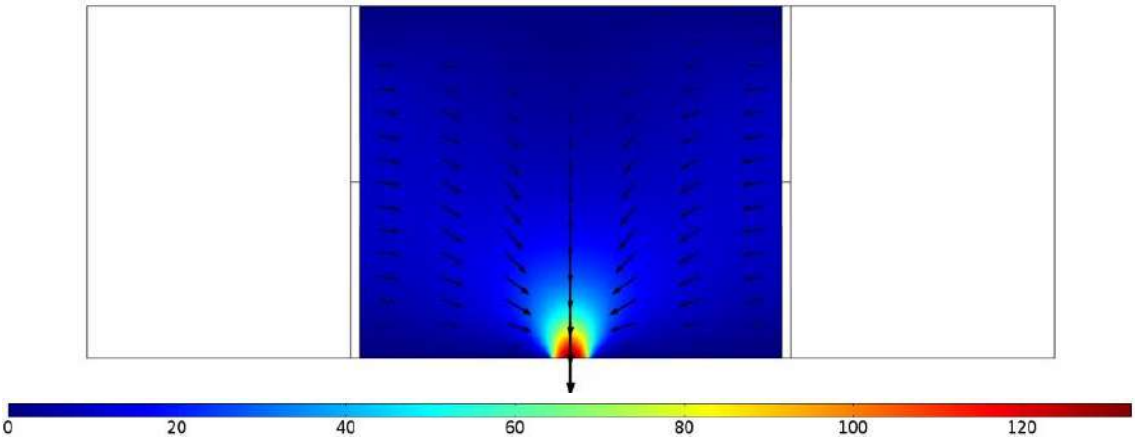

Figure 5.21: Fluid velocity under 800 mV in 0.15s.

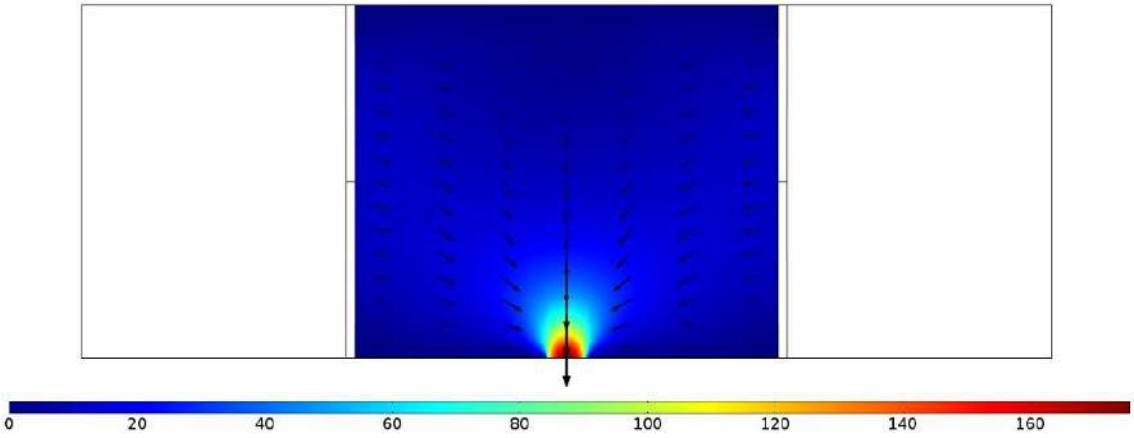

Figure 5.22: Fluid velocity under 1000 mV in 0.11s.

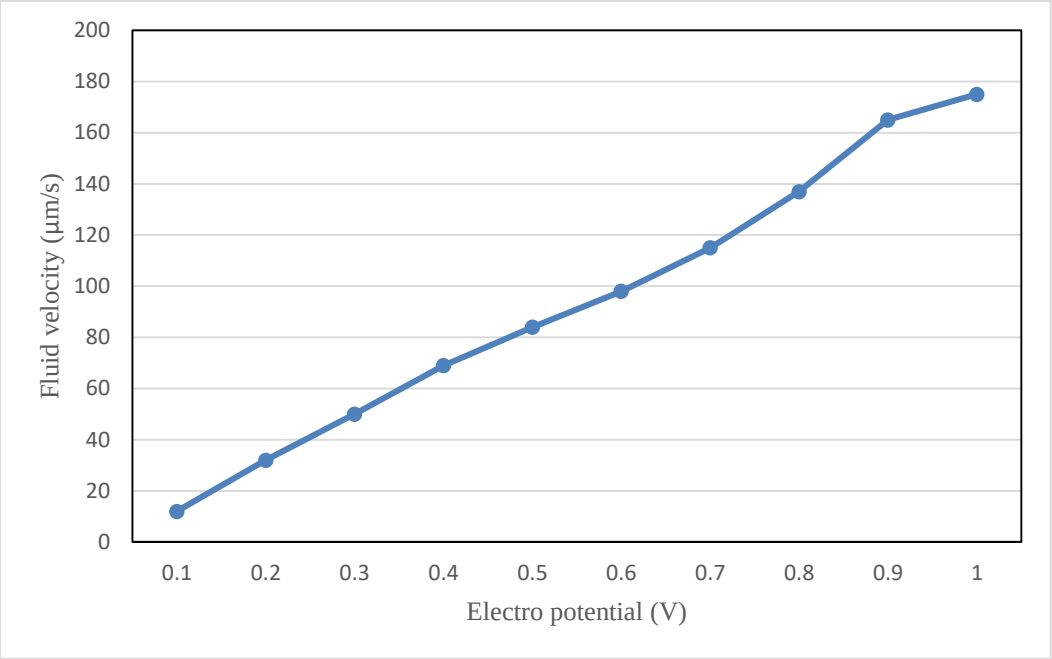

Figure 5.23: Fluid velocity as a function of electro-potential.

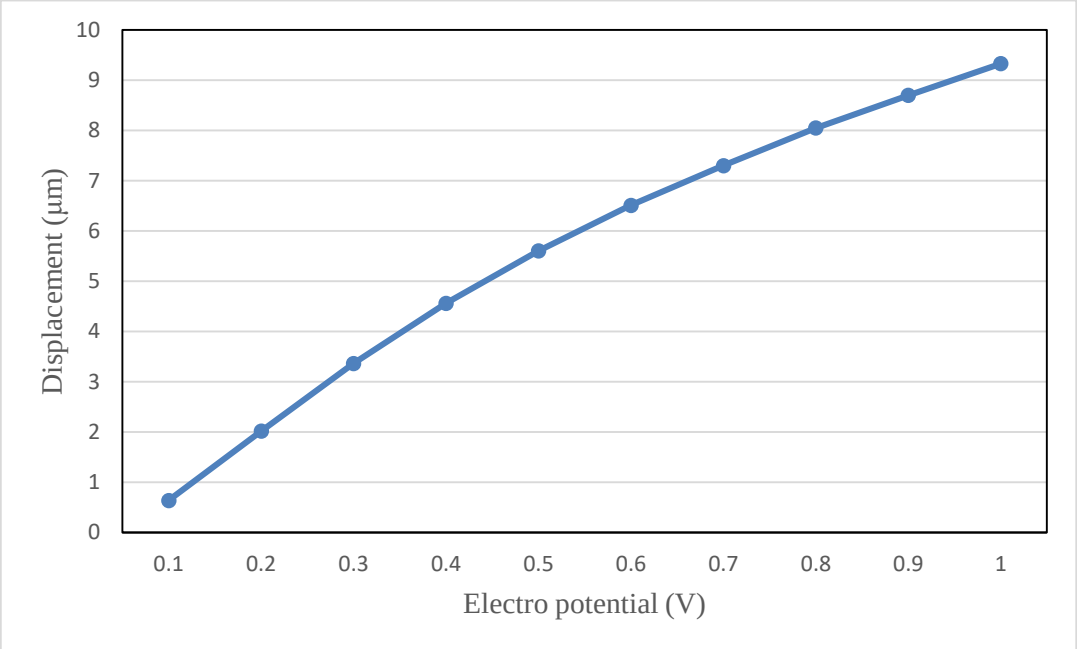

Figure 5.24: The relationship between displacement and electro-potential.

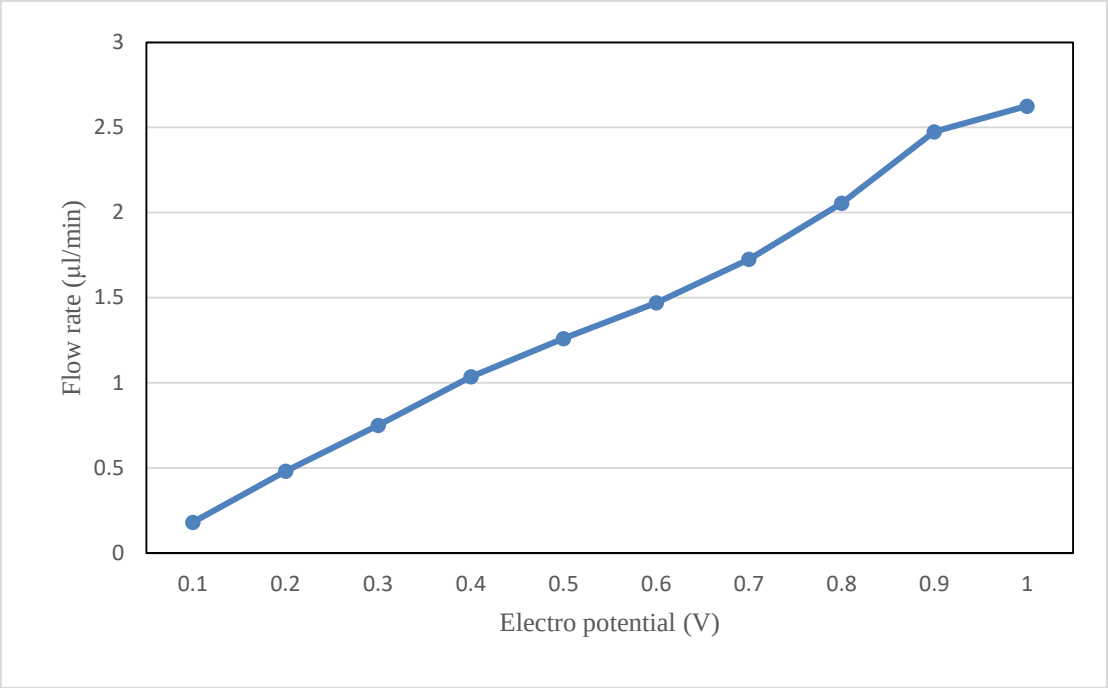

Figure 5.25: Flow rate as a function of electro-potential.

In this section, a novel low energy IPMC micropump is presented and simulated, in which the fluid is driven by deformation of two IPMC diaphragms. The flow fields generated in an IPMC micropump by deformation of diaphragms are simulated by considering the coupled electrical, mechanical and fluidic fields. The coupled model considers the deformation of IPMCs diaphragms simultaneously with the prediction of fluid flow. The simulation results show that IPMC micropump is able to generate a flow rate of 2.6 µl/min. These present results quantitatively provide the dependence of flow rates to the electro-potential. The pressure, velocity, and flow rate prediction models developed in the present study can be utilized to optimize the design of IPMC based micropumps that are being used for the treatment of Glaucoma. Considering all points mentioned about aqueous humor and its production IPMC micropump, we need to transfer the fluid at maximum 2.5 µl/min to the treatment of Glaucoma. It depends on the degree of Glaucoma we need to apply electro-potential up to 1V. By referring to figure 5.25 for each patient condition we can choose the applied electro-potential to extract the fluid and balance the IOP.

5.4. Mesh Convergence

In order to gauge how reasonable a finite element solution to a partial differential equation is a given mesh, a common strategy is to refine the mesh, compute the solution on the finer mesh, and use the solutions on the two meshes for a qualitative comparison. The theory of the finite element method (FEM) makes these comparisons quantitative by estimating the convergence order of the FEM error on a sequence of progressively finer meshes obtained by uniform mesh refinement.

Results obtained for different element sizes to validate the accuracy of numerical simulations. Related to study mesh convergence four element sizes from 0.6 μm to 8 μm employed to simulate a double IPMC micropump under 500 mV. Governing equations were a solver for three unknown variables including displacement, pressure, and velocity of the fluid. Results listed in table 5.2. Conducting the convergence study in this manner shows how to quantify the convergence of FEM solutions and brings out the potential benefit of using higher order elements. As shown in table 5.2 the changes in displacement of IPMC due to apply finer mesh elements are in order of 0.0003 to 0.001 μm. In addition, fluctuation of the velocity of the fluid and fluid pressure observed in the order of 4.5 μm/s and 0.05 Pa respectively.

This convergence study illuminates that the numerical solution obtained from COMSOL is reasonable and confirm the accuracy of results in higher order elements. Due to the similarity of presented examples for applications of IPMC in micropump (fluid-IPMC interaction), this study can be extended to all numerical simulations.

Table 5.3: Mesh convergence analysis detail for IPMC micropump under 500 mV electro potential.

Result / **Mesh**	Displacement (μm)	Pressure (Pa)	Velocity (μm/s)	Element Size (μm)	Element Size (μm)
Normal	5.6066	9.7×10^{-4}	73	8	180
Fine	5.6066	1.04×10^{-3}	74.4	4	140
Finer	5.6073	1.1×10^{-3}	70.8	1.6	112
Extra fine	5.6063	1.48×10^{-3}	69.7	0.6	52

5.5. IPMC cilia micropump

As we mentioned in section 2.7 understanding the hydrodynamics generated by an IPMC deformation underwater is central to the design of such biomimetic swimmers. In this chapter, we propose the study and simulation of IPMC cilia submerged in water to detail the fluid kinematics and kinetics in the vicinity of an IPMC deformation along its fundamental structural mode. The first time Toonder *et al.* suggested application of cilia actuators in micro channel structure for manipulation of fluid (see figure 5.26). In this section, we try to prove this concept with numerical simulation. IPMCs cilia deformation simulated by IPMC-fluid interaction mathematical model and results presented here confirm the ability of IPMCs cilia to manipulate and pump the fluid inside the channel.

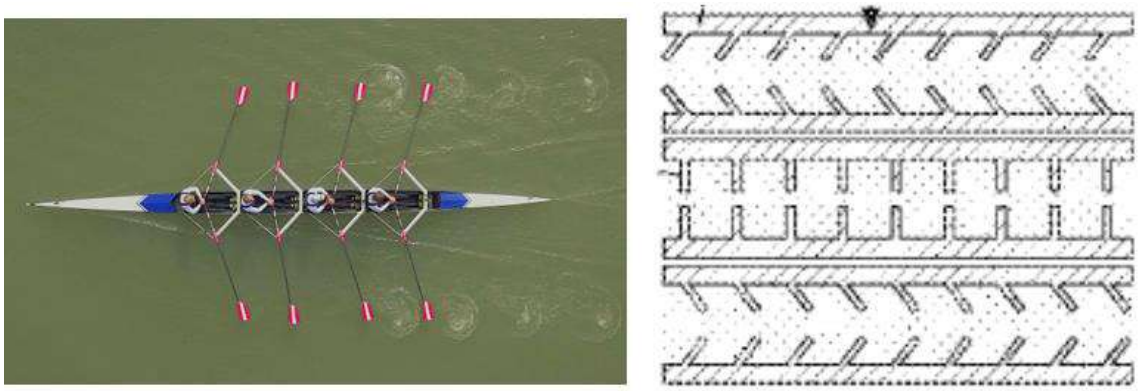

Figure 5.26: Schematic of concept IPMCs cilia attached in the microchannel. Cilia deformation is like paddle movement in boating.

We consider an IPMC cilia of thickness 100 μm, 3 mm length and a box of water with 20 mm width, 8 mm height. The coupled governing equations in chapter four with some change in boundary conditions employed to predict the behavior of IPMC cilia-fluid interaction under oscillation electro-potential. IPMC cilia excited by a sinusoidal voltage applied across its electrodes as shown in figure 5.27 to impose an oscillation deformation in IPMC cilia tip. Tip displacement of the IPMC at the driving frequency f = 1 Hz reaches a maximum of 100 μm. Figures 5.28-5.32 illustrate the instantaneous fluid velocity over one cycle of oscillation at f = 1 Hz for 5 consecutive time instants t = 0, t = T/4, t = T/2, t = 3T/4 and t = T where T = 1/f is the oscillation period. These figures show IPMC cilia have the ability to generate flow in fluid and it is possible to manipulate the fluid by oscillation movement of IPC cilia. Figures 5.33-5.37 present the pressure field in

the channel. The fluid flow is shown by the velocity vectors superimposed on the contours.

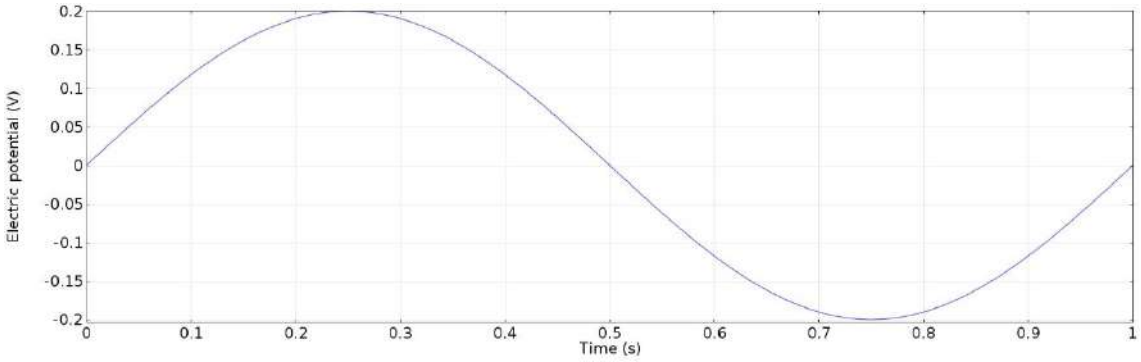

Figure 5.27: Electro potential applied to IPMC cilia under water.

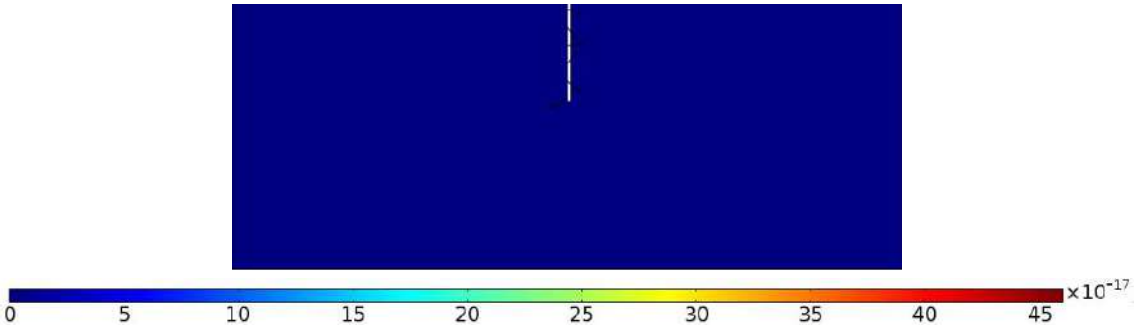

Figure 5.28: Fluid velocity inside a chamber under 200mV in 0s.

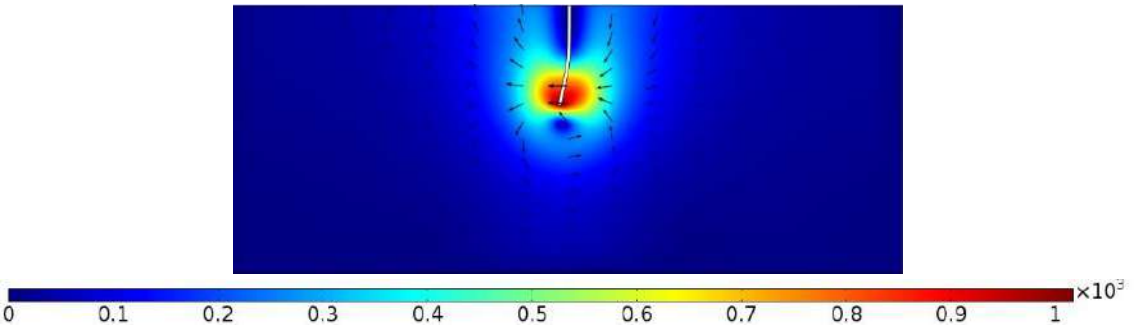

Figure 5.29: Fluid velocity inside chamber under 200mV in 0.25s.

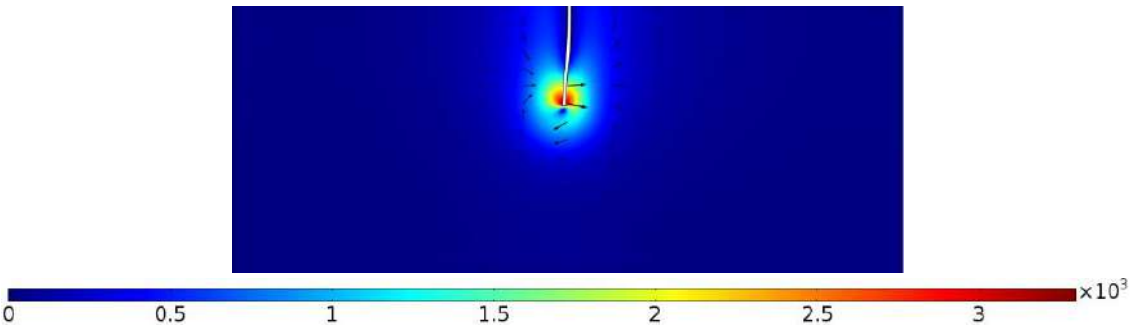

Figure 5.30: Fluid velocity inside chamber under 200mV in 0.5s.

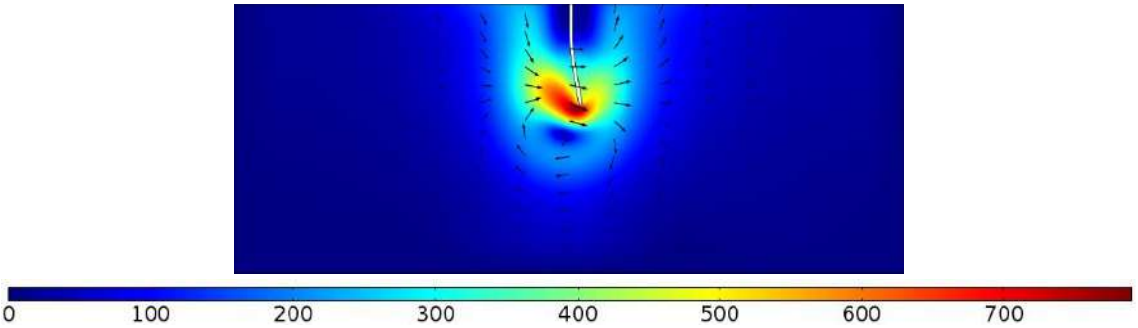

Figure 5.31: Fluid velocity inside chamber under 200mV in 0.75s.

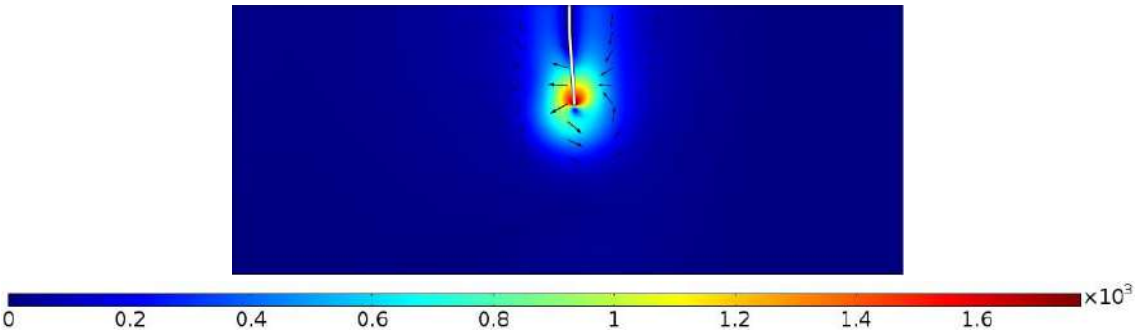

Figure 5.32: Fluid velocity inside a chamber under 200mV in 1s.

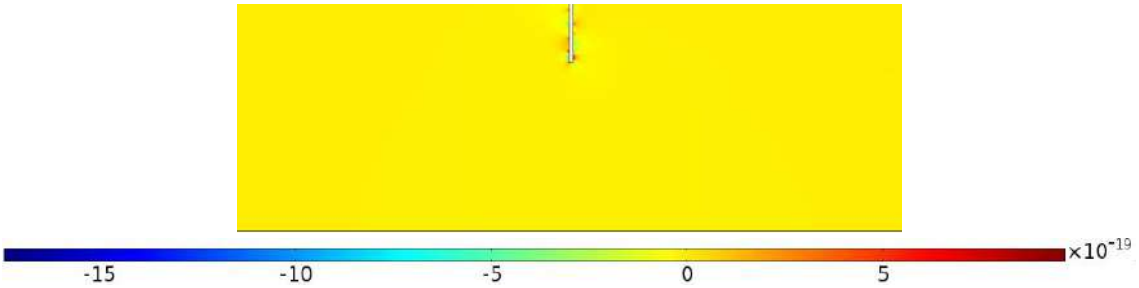

Figure 5.33: Pressure inside chamber under 200mV in 0s.

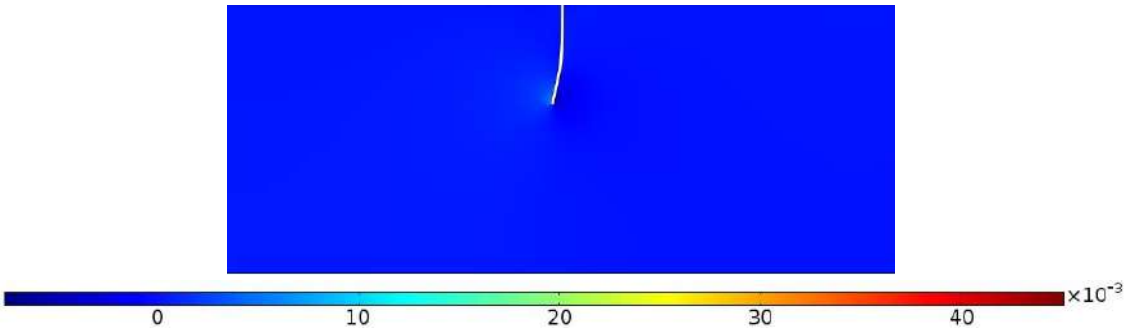

Figure 5.34: Pressure inside chamber under 200mV in 0.25s.

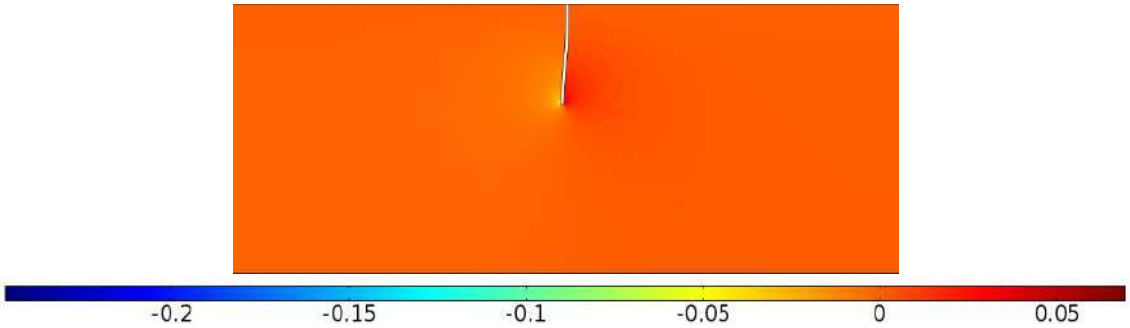

Figure 5.35: Pressure inside chamber under 200mV in 0.5s.

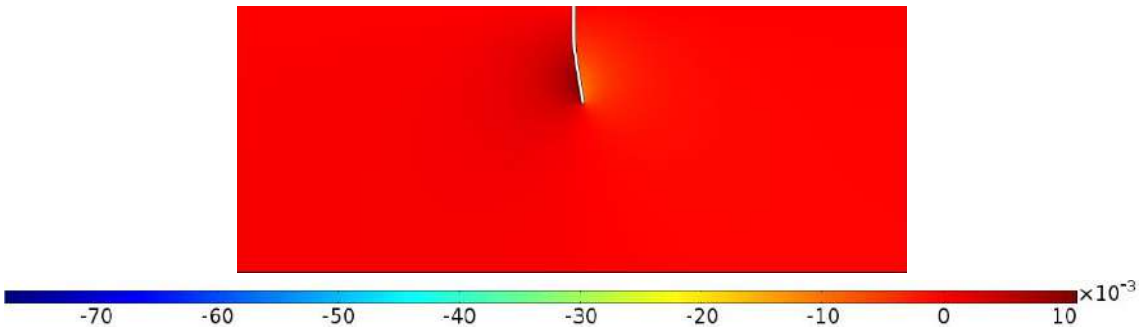

Figure 5.36: Pressure inside chamber under 200mV in 0.75s.

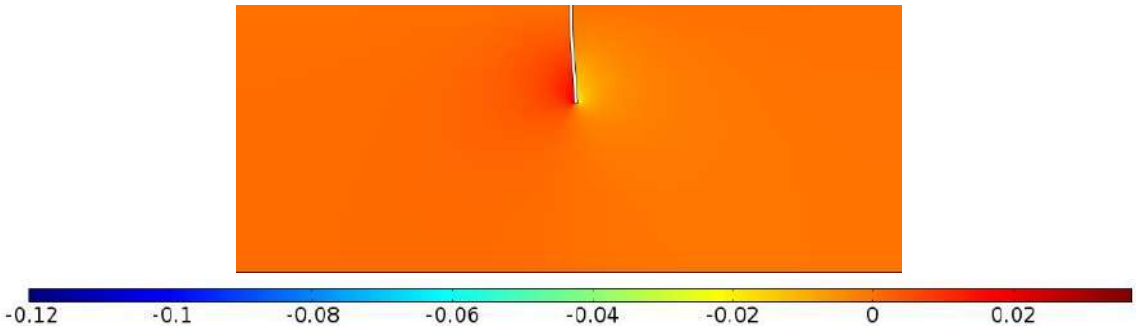

Figure 5.37: Pressure inside chamber under 200mV in 1s.

Here, the IPMC cilia integrated micropump is investigated in two different configurations. In first case ten IPMC cilia employed in the upper and bottom side of the channel. Then 800 mV electro-potential applied to IPMC cilia. Figure 5.38 presents schematic of a configuration of IPMC cilia integrated micropump and the mesh detail in IPMC and the fluid that we applied for simulating IPMC cilia micropump. Figures 5.39 to 5.43 illustrate fluid velocity inside the chamber of micropump under 800 mV electro-potential. Results show that IPMC cilia micropump generates a flow velocity of 100 µm/s at the outlet. In the all cases of IPMC cilia micropumps, open boundary conditions applied at the right side of the channels and the outlet defined at the left side.

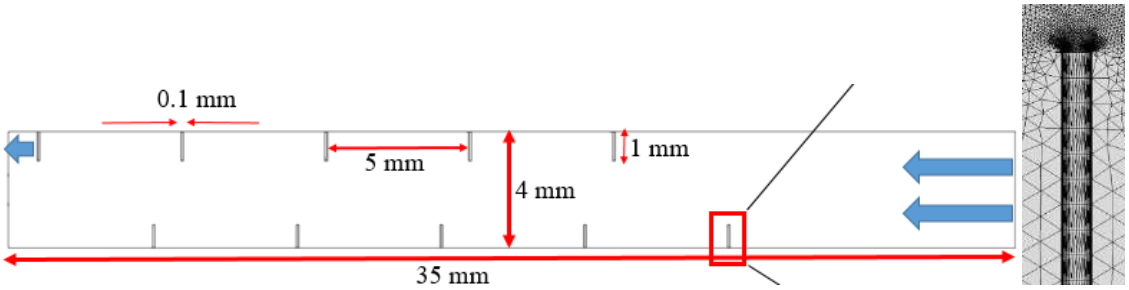

Figure 5.38: Schematic of IPMC cilia micropump case one.

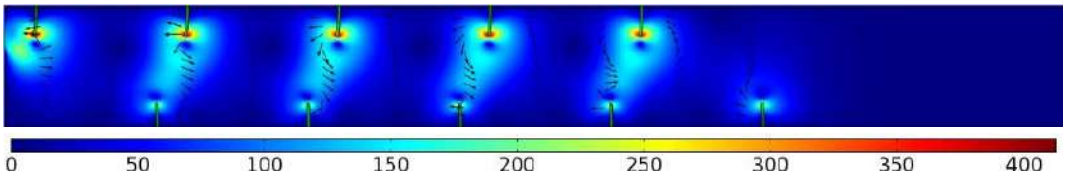

Figure 5.39: Fluid velocity inside a chamber under 800 mV in 0.1s.

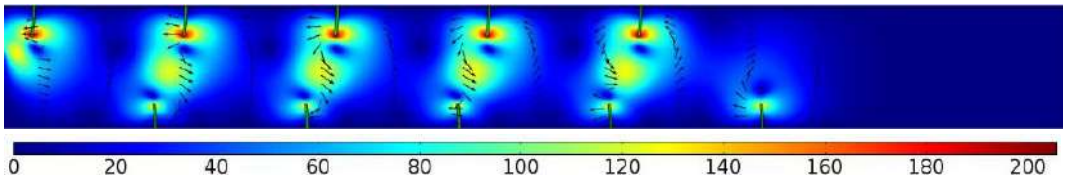

Figure 5.40: Fluid velocity inside a chamber under 800 mV in 0.2s.

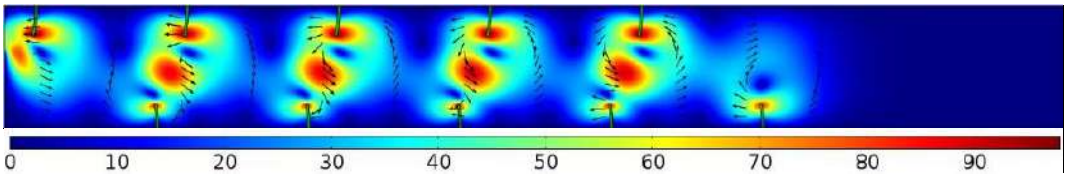

Figure 5.41: Fluid velocity inside a chamber under 800 mV in 0.3s.

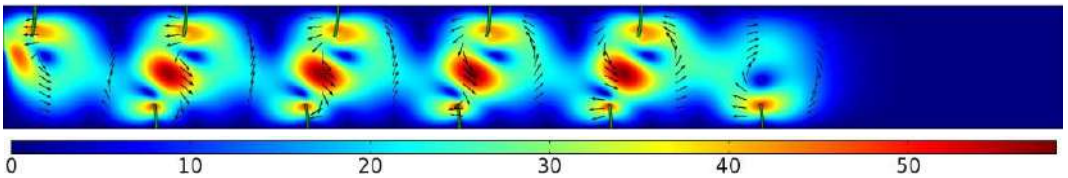

Figure 5.42: Fluid velocity inside a chamber under 800 mV in 0.4s.

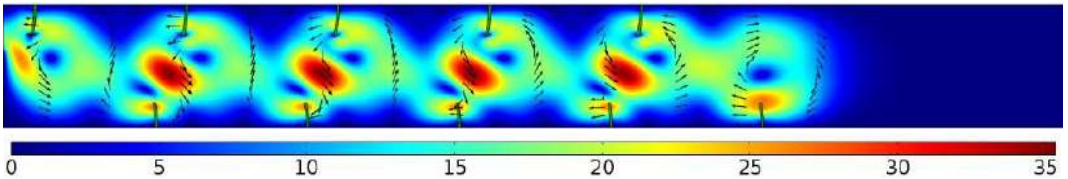

Figure 5.43: Fluid velocity inside a chamber under 800 mV in 0.5s.

Fluid velocity and pressure fields show fluid flow which is pumped by IPMCs cilia. Particle tracing analysis is performed with Particle Tracing Module in COMSOL to analyze pumping performance of IPMCs cilia. Figure 5.44 evaluates the pumping performance by computing the trajectory of suspended particles due to fluid flow in the channel. IPMCs cilia deforms and causes the particle to move toward the outlet.

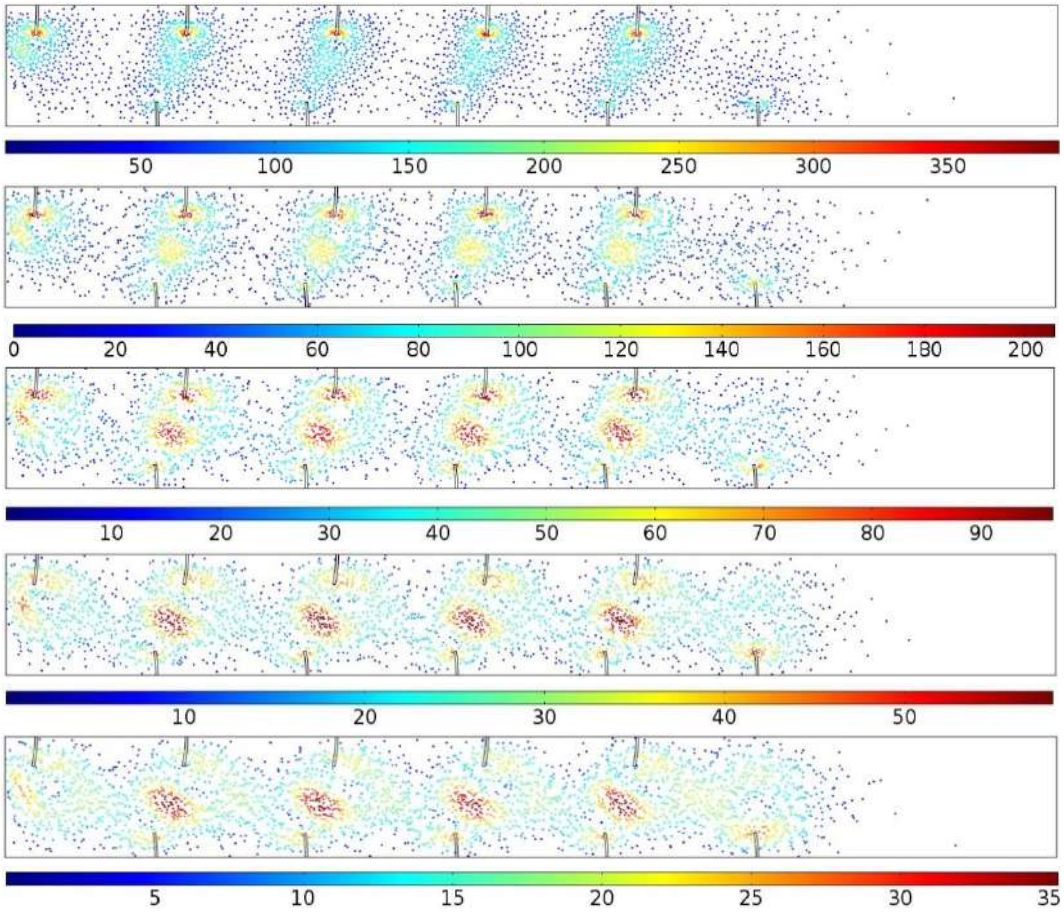

Figure 5.44: Particle trajectories inside channel under 800mV in 0.1-0.5s.

In another structure, due to increase the IPMC cilia number attached to the channel, the space between the cilia decreased, in result, the affected fluid area by IPMC cilia deformation joined together. The fluid velocity and pressure in the chamber are studied to investigate the effect of cilia deformation on the fluid in this structure. Figures 5.45 to 5.49 illustrate the velocity field in the chamber. Compared to the structure before, there is no recirculation center in fluid and fluid velocity is more homogenous through

the channel. At the beginning, the maximum of the velocity observed at the IPMCs tip because of highest displacement. So there is a fluid flow with highest velocity pass through the tip of IPMCs cilia which came from inlet flow at the upper side and down the side of the channel. Because of the outlet position, the velocity of the fluid at the upper side of the channel is higher than lower side of the channel. The fluid flow with highest velocity moves toward the center of the channel after 0.5 s.

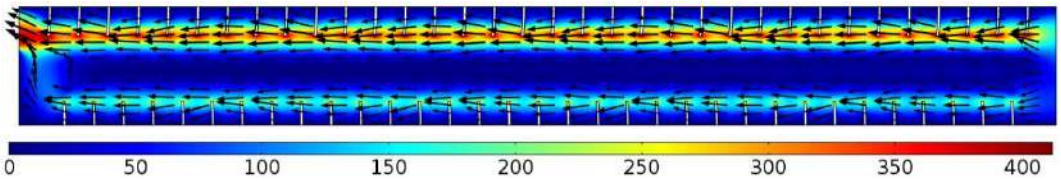

Figure 5.45: Fluid velocity inside a chamber under 800 mV in 0.1s.

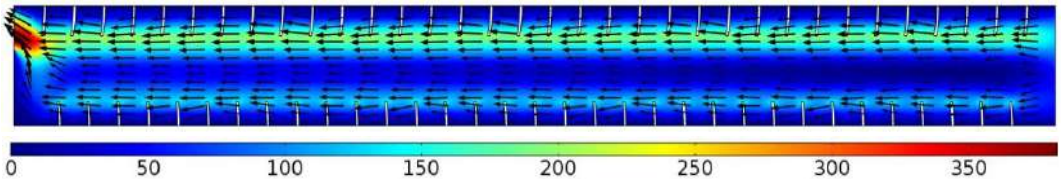

Figure 5.46: Fluid velocity inside a chamber under 800 mV in 0.2s.

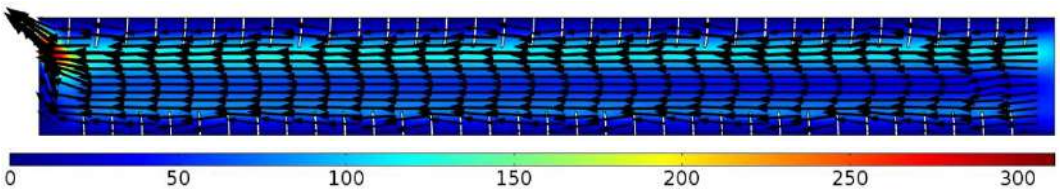

Figure 5.47: Fluid velocity inside a chamber under 800 mV in 0.3s.

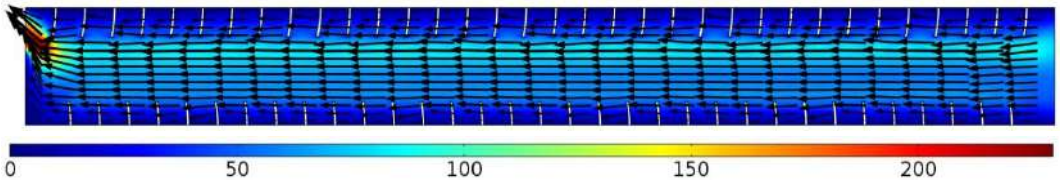

Figure 5.48: Fluid velocity inside a chamber under 800 mV in 0.4s.

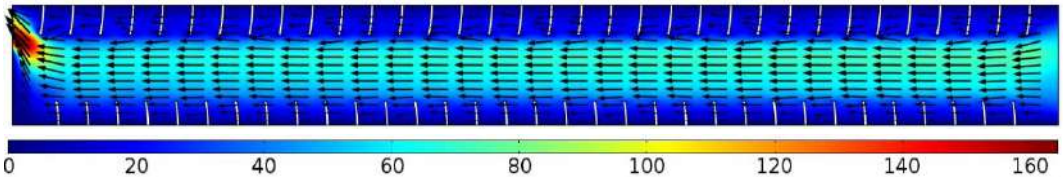

Figure 5.49: Fluid velocity inside a chamber under 800 mV in 0.5s.

To study the outlet location effect on fluid flow, in the last scenario of this configuration, the outlet moves toward the center. Figures 5.50 to 5.56 present the change of fluid flow during 0.7s. High-velocity route moves from near channel wall to center by passing time. Due to the outlet position, a symmetric fluid flow created near the channel wall and IPMCs cilia suck fluid equally into the channel. Compared to fewer cilia number configurations the fluid inside the channel is more homogeneous and continuous. The fix fluid region in front of each cilia breaks by the highest number of cilia and removes the recirculation area at the center of the channel between two cilia. Hence, depending on the type of fluid flow and velocity required for the specific application, the outlet position, number of IPMCs cilia, the distance between them, configurations and applied electro potential could be different.

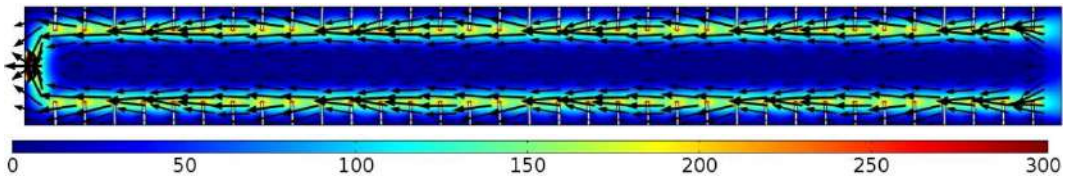

Figure 5.50: Fluid velocity inside a chamber under 800 mV in 0.1s.

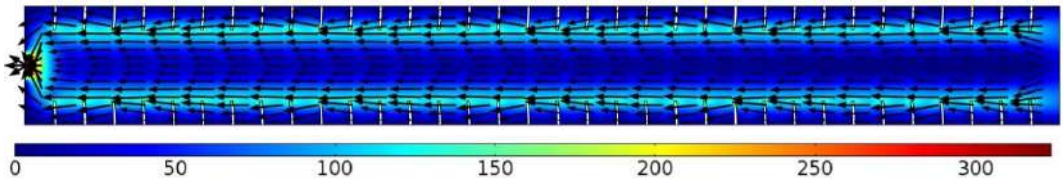

Figure 5.51: Fluid velocity inside a chamber under 800 mV in 0.2s.

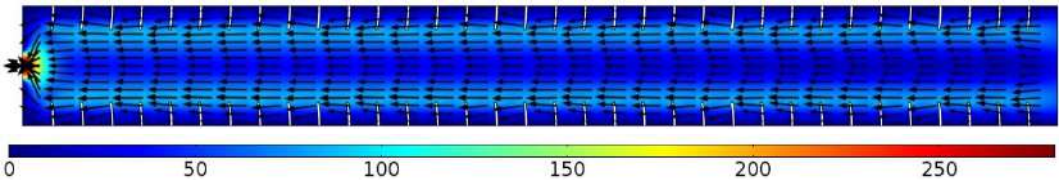

Figure 5.52: Fluid velocity inside a chamber under 800 mV in 0.3s.

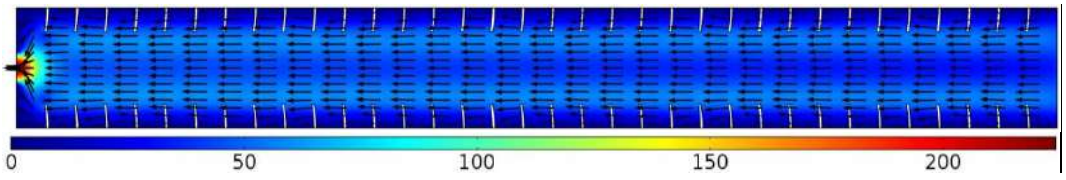

Figure 5.53: Fluid velocity inside a chamber under 800 mV in 0.4s.

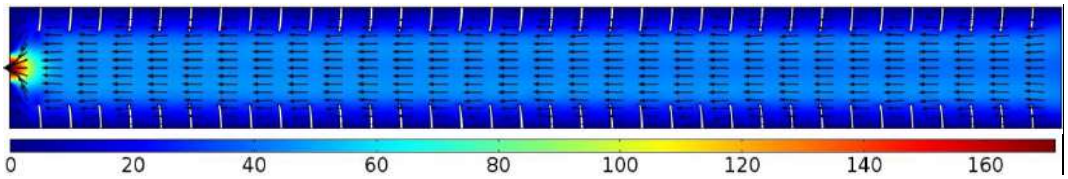

Figure 5.54: Fluid velocity inside a chamber under 800 mV in 0.5s.

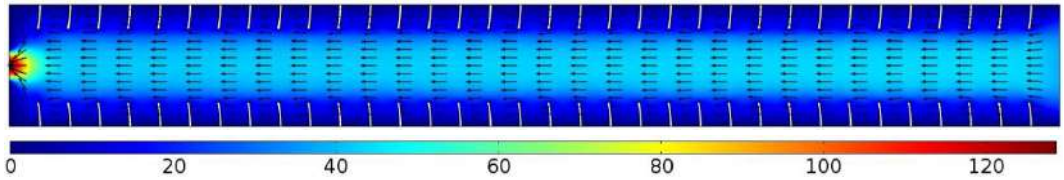

Figure 5.55: Fluid velocity inside a chamber under 800 mV in 0.6s.

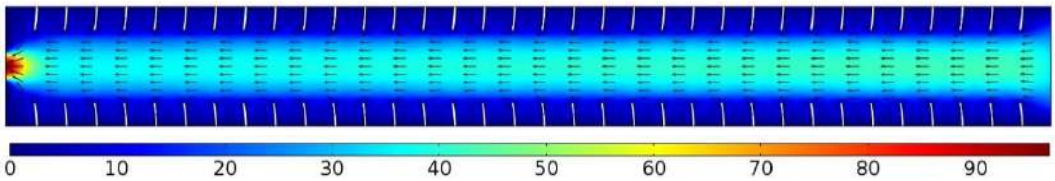

Figure 5.56: Fluid velocity inside a chamber under 200 mV in 0.7s.

In the second case, we investigate a smaller channel with 9 mm length and 2.5 mm height consist of ten IPMCs cilia attached to the inside wall. Figure 5.57 shows the configuration of cilia micropump, mesh detail and boundary conditions applied for simulation. The open boundary condition is applied to the right side of the channel and mapped mesh configuration with symmetric distribution option selected for IPMC and triangle for the fluid. In this case, the free space (for fluid flow) between two arrays of IPMCs cilia is less than the case one. External stimuli of 200 mV electro-potential applied to IPMCs cilia. Deformation of IPMCs under the electro-potential and working mechanism of cilia micropump illustrated in figure 5.58. Deformation of all cilia to the left sucks the fluid from the inlet (open boundary) at the right side of the channel and push to the outlet at the lower left side of the channel. The next four figures (5.59-5.62) demonstrated the fluid velocity due to tip displacement of cilia inside the channel. Recirculation area at the center of the channel with highest fluid velocity shown in figure 5.59 and 5.60. In addition, these results confirmed that IPMC cilia integrated micropump achieved a maximum fluid velocity of 7 µm/s at the outlet.

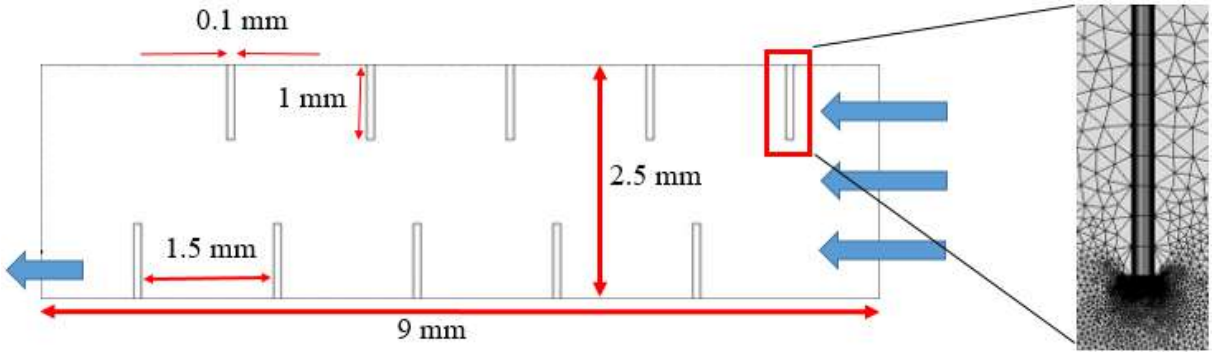

Figure 5.57: Schematic of IPMC cilia integrated micropump case two.

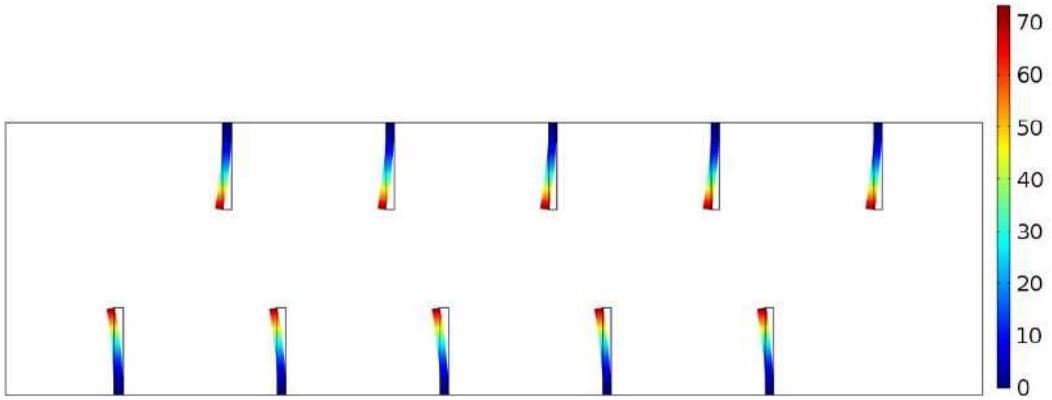

Figure 5.58: Total displacement of IPMC cilia under 200 mV inside the chamber.

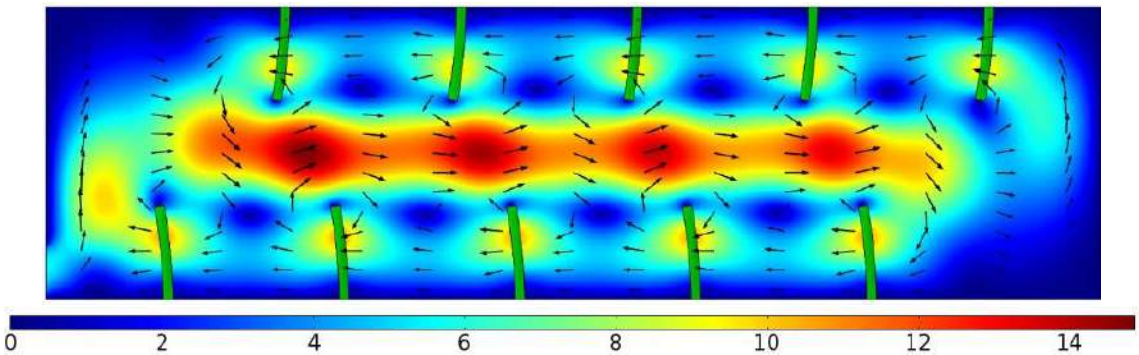

Figure 5.59: Fluid velocity inside a chamber under 200mV in 0.7s.

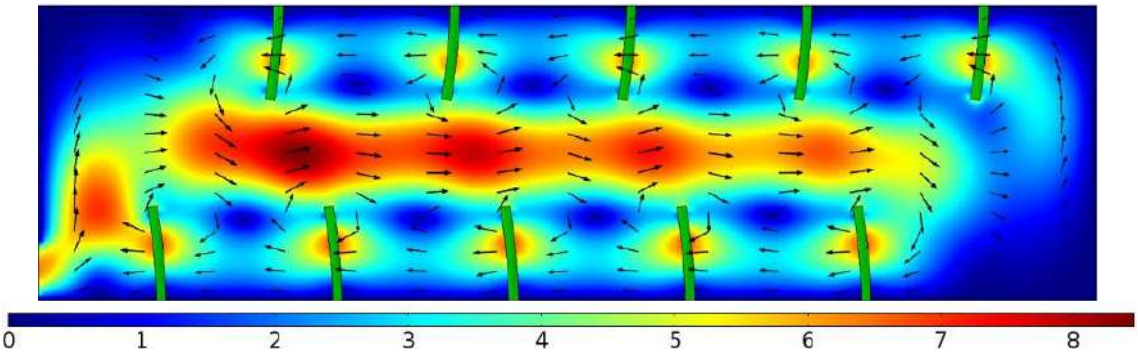

Figure 5.60: Fluid velocity inside a chamber under 200mV in 0.8s.

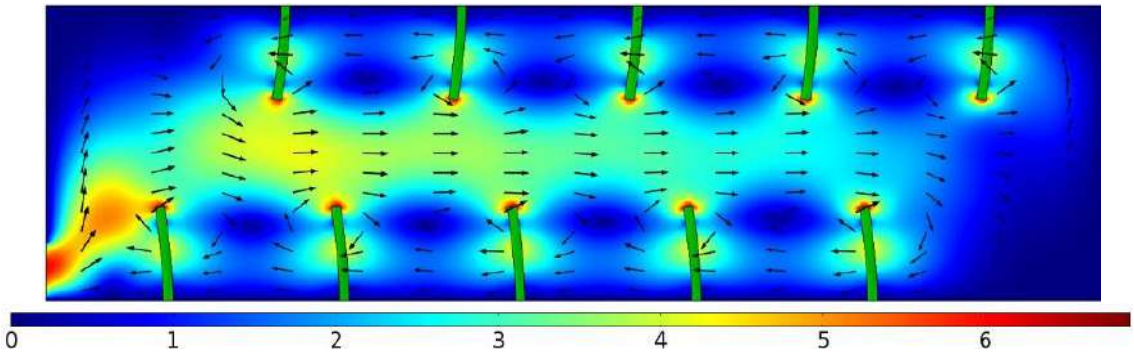

Figure 5.61: Fluid velocity inside a chamber under 200mV in 0.9s.

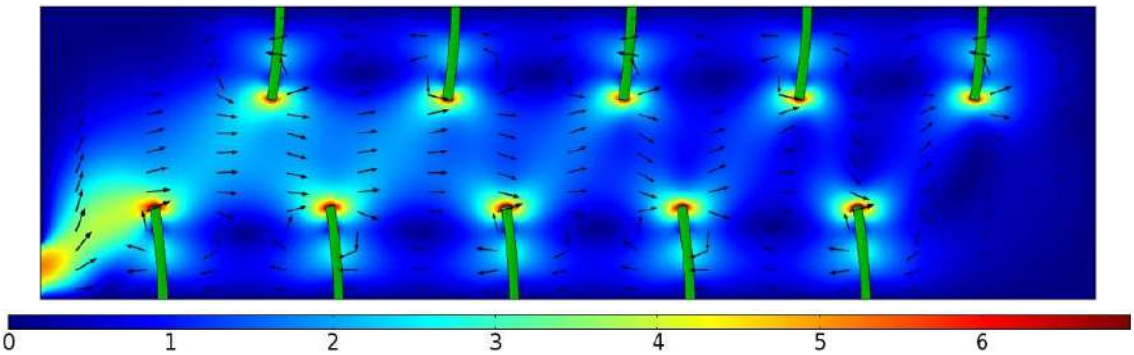

Figure 5.62: Fluid velocity inside a chamber under 200mV in 1s.

Particle tracing modeled in this case and the calculated particle trajectory due to deformation of IPMCs cilia and push the fluid into channel presented in Figure 5.63. Particles reached the velocity of 7 μm/s under 200 mV in the outlet. In the last section fluid velocity of cilia micropump with higher electro-potential (800 mV) presented in figures 5.64 to 5.68. Higher fluid velocity at the outlet without recirculation observed.

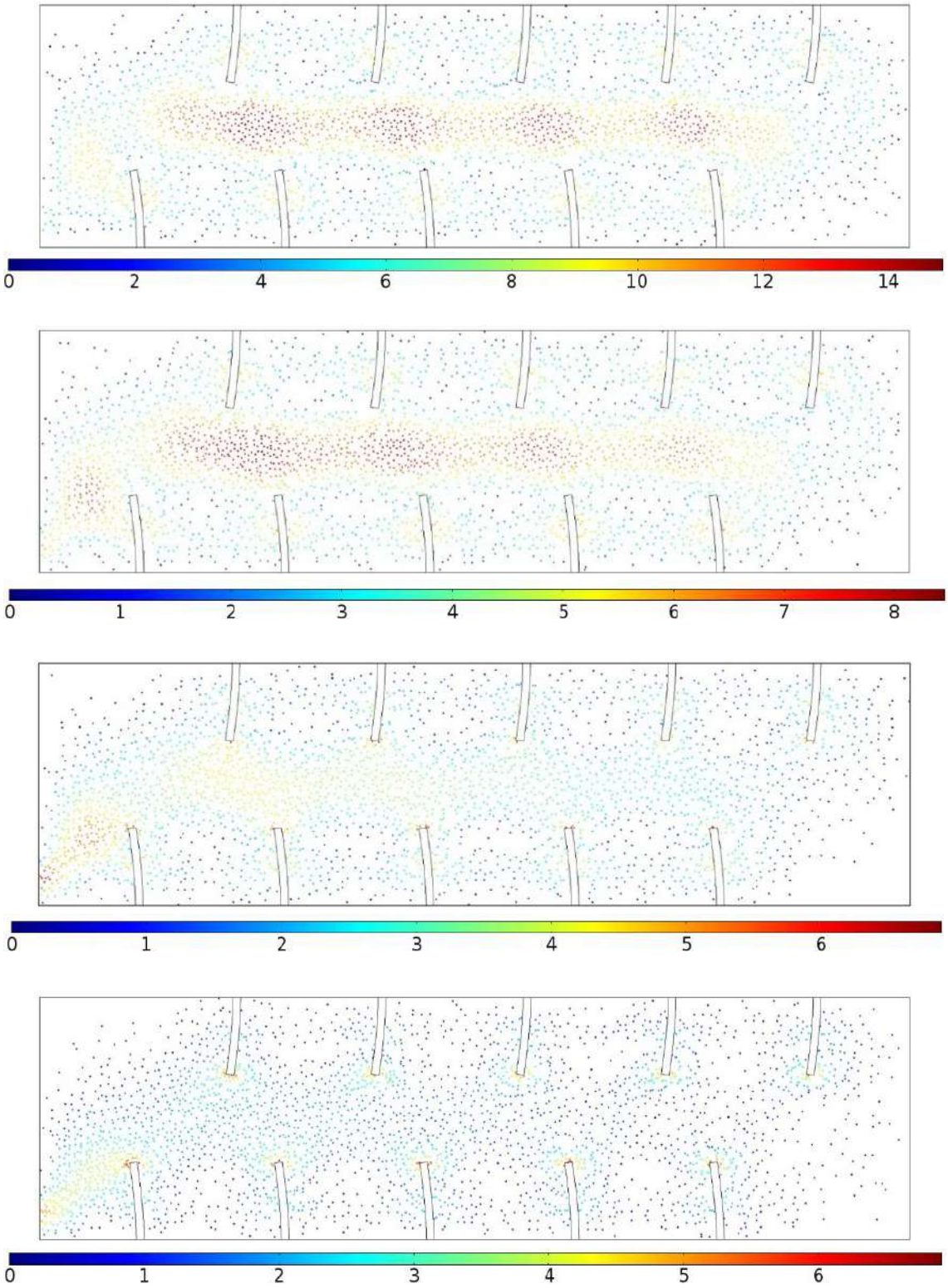

Figure 5.63: Particle trajectories inside chamber under 200 mV in 0.7-1 s.

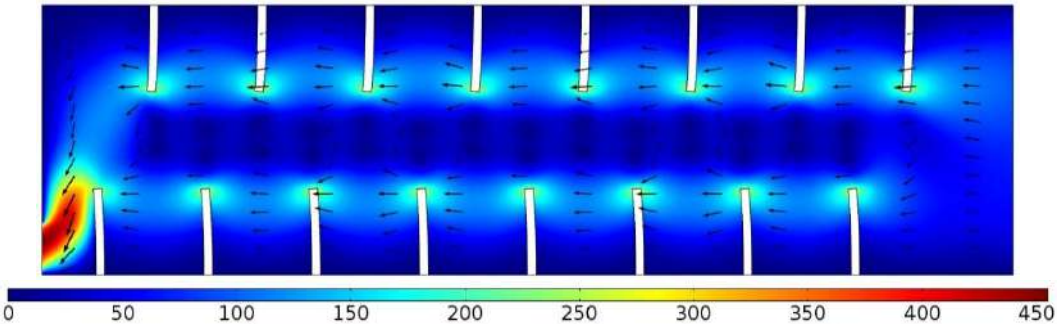

Figure 5.64: Fluid velocity inside a chamber under 800mV in 0.1s.

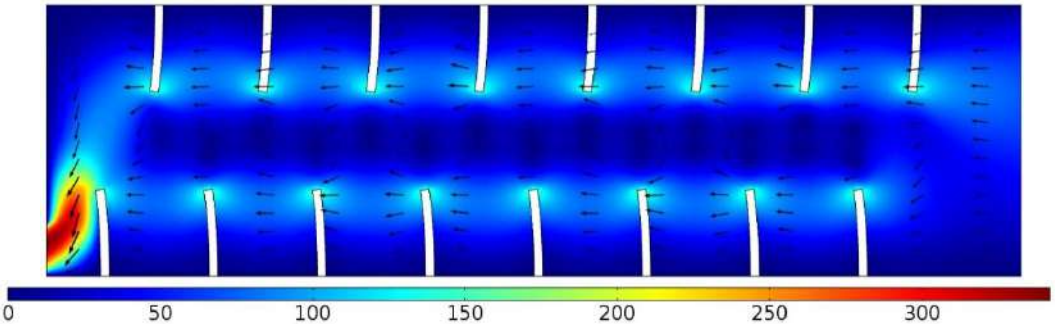

Figure 5.65: Fluid velocity inside a chamber under 800mV in 0.2s.

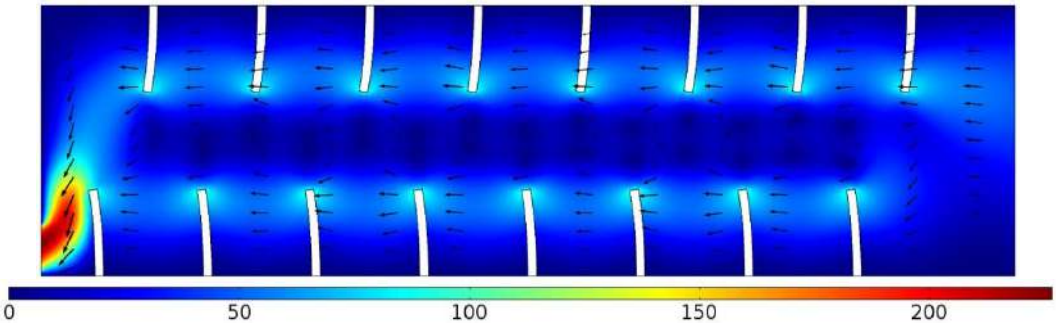

Figure 5.66: Fluid velocity inside a chamber under 800mV in 0.3s.

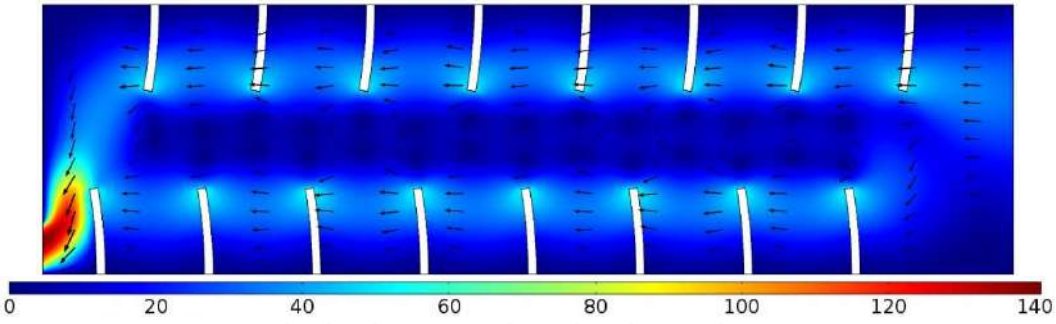

Figure 5.67: Fluid velocity inside a chamber under 800mV in 0.4s.

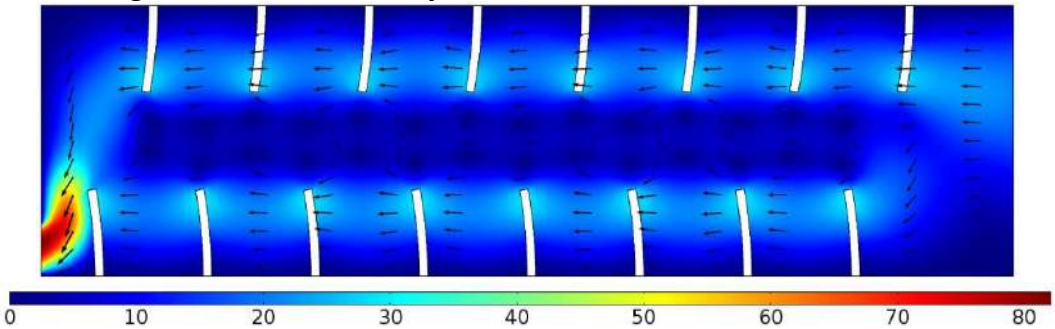

Figure 5.68: Fluid velocity inside a chamber under 800mV in 0.5s.

A disadvantage of using the micro-pump assembly and of using micropumps, in general, is that they have to be, in some way, integrated into microfluidic systems. This means that a large area must be devoted to the micro pump, which results in the bigger microfluidic device. This means that the size of the microfluidic systems will increase. It would, therefore, be useful to have a microfluidic system by IPMC cilia flow controller, which is compact and cheap, and nevertheless easy to process. The beam-shaped cilia of IPMC can change shape and orientation as a response to an external electric potential. Through this configuration, the flow of a fluid in a microchannel can be manipulated and controlled as shown in the last section of this chapter.

CHAPTER VI

6. CONCLUSIONS

In this study, a multi-physics mathematical model is presented and analyzed for simulation of the behaviors of ionic polymer metal composites strips immersed into the fluid, subject to an externally applied electric field. The balance law of chemo-electro-mechanics and constitutive equations of the involved fields were depicted. The formulation is capable of describing the bending deformation of the IPMC, the distributions of diffusive ionic concentrations, and electric potential in the IPMC strip. Three-dimensional numerical simulations are carried out for an IPMC strip. The numerically simulated results are in good agreements with published FEM solutions, which validates the presently developed models. With the derived coupled formulation, the IPMC behavior in the sensor as well as in actuator applications can be described. By utilizing this model, we are able to explore some applications of IPMC, and by coupling governing equation of this model with Navier-Stokes equation, we are able to simulate IPMC-fluid interaction and IPMC micropump for the medical applications. These coupled equations explained the fluid velocity and pressure field in the exterior fluid. Furthermore, we focused on application of IPMC as a micropump in treatment of Diabetes and Glaucoma and analyzed the IPMC micropump as a device in the treatment procedure. The simulation was done in both cases and results show IPMC micropump can generate sufficient flow rate with low electric potential for insulin delivery in Diabetes case and removing excess aqueous humor in Glaucoma case. In the last part, we successfully simulated and proved a new concept for IPMC cilia integrated micropump. The result showed IPMC cilia attached inside the channel can deform and generate a flow rate of the fluid at very low electro-potential. Also, this structure can be employed as a micro flow controller to manipulate and control the fluid by altering the electric potential. Simulation results collected valuable data for fabricating microfluidic device by IPMC cilia. We believe that investigation of IPMC cilia micropump in detail and deeper is necessary for future research.

Future Works

- Explore IPMC cilia micropump and related key parameters
- Simulation and modeling of IPMC-Multi fluid interaction
- Study the possibility of using IPMC cilia attached in channel for mixing different fluids
- Investigation of IPMCs cilia as a sensor in micro channel
- Analysis IPMC valve for application in micropump
- Verifying the results of the present study experimentally, specially IPMC cilia micropump
- Introducing new application for IPMC-fluid interaction

REFERENCES

[1] Chu, Won-Shik et al. "Review of biomimetic underwater robots using smart actuators." *International journal of precision engineering and manufacturing* 13, no. 7 (2012): 1281-1292.

[2] Frecker, Mary I. "Recent advances in optimization of smart structures and actuators." *Journal of Intelligent Material Systems and Structures* 14, no. 4-5 (2003): 207-216.

[3] Shahinpoor, Mohsen, Yoseph Bar-Cohen, J. O. Simpson, and J. Smith. "Ionic polymer-metal composites (IPMCs) as biomimetic sensors, actuators, and artificial muscles-a review." Smart materials and structures 7, no. 6 (1998): R15.

[4] Osada, Yoshihito, Hidenori Okuzaki, and Hirofumi Hori. "A polymer gel with electrically driven motility." *Nature* 355, no. 6357 (1992): 242-245.

[5] Bar-Cohen, Yoseph. Electroactive polymer (EAP) actuators as artificial muscles: reality, potential, and challenges. Vol. 136. SPIE press, 2004.

[6] De Rossi, Danilo, Kanji Kajiwara, Yoshihito Osada, and Aizo Yamauchi. "Polymer gels." *Fundamentals and Biomedical Applications, Plenum Press, New York* (1991).

[7] Osada, Yoshihito, and Simon B. Ross-Murphy. "Intelligent gels." *Scientific American* 268, no. 5 (1993): 42-47.

[8] Kim, Kwang J., and Satoshi Tadokoro. "Electroactive polymers for robotic applications." Artificial Muscles and Sensors (2007).

[9] Kim, Kwang J., David Pugal, and Kam K. Leang. "A twistable ionic polymer-metal composite artificial muscle for marine applications." Marine Technology Society Journal 45, no. 4 (2011): 83-98.

[10] Shahinpoor, Mohsen, and Kwang J. Kim. "Ionic polymer-metal composites: I. Fundamentals." *Smart materials and structures* 10.4 (2001): 819.

[11] Bao, Xiaoqi, Yoseph Bar-Cohen, and Shyh-Shiuh Lih. "Measurements and macro models of ionomeric polymer-metal composites (IPMC)." SPIE's 9th Annual International Symposium on Smart Structures and Materials. International Society for Optics and Photonics, 2002.

[12] Shahinpoor, Mohsen, and Kwang J. Kim. "Ionic polymer–metal composites: IV. Industrial and medical applications." Smart materials and structures 14.1 (2005): 197.

[13] Bar-Cohen, Y., et al. "Challenges to the transition of IPMC artificial muscle actuators to practical application." MRS Symposium Proceedings. 1999.

[14] Menciassi, Arianna, and Paolo Dario. "Bio-inspired solutions for locomotion in the gastrointestinal tract: background and perspectives." Philosophical Transactions of the Royal Society of London A: Mathematical, Physical and Engineering Sciences 361.1811 (2003): 2287-2298.

[15] Bar-Cohen, Yoseph. "Electroactive polymers as artificial muscles-capabilities, potentials and challenges." Handbook on biomimetics section 11, chapter8 (2000).

[16] Nemat-Nasser, S., and C. Thomas. "Ionomeric Polymer–Metal Composites Electroactive Polymer (EAP) Actuators as Artificial Muscles—Reality, Potential and Challenges (Bellingham, WA: SPIE Optical Engineering Press) chapter 6." (2004).

[17] Del Bufalo, Giovanni, Luca Placidi, and Maurizio Porfiri. "A mixture theory framework for modeling the mechanical actuation of ionic polymer metal composites." *Smart Materials and Structures* 17.4 (2008): 045010.

[18] Paquette, Jason W., and Kwang J. Kim. "Ionomeric electroactive polymer artificial muscle for naval applications." *IEEE Journal of Oceanic Engineering* 29.3 (2004): 729-737.

[19] Cha, Youngsu, and Maurizio Porfiri. "Mechanics and electrochemistry of ionic polymer metal composites." *Journal of the Mechanics and Physics of Solids* 71 (2014): 156-178.

[20] Nagpure, Tushar, and Zheng Chen. "Control-oriented modeling of ionic polymer-metal composite enabled hydrogen gas production." International Journal of Hydrogen Energy 41, no. 16 (2016): 6619-6629.

[21] Nemat-Nasser, Sia, and Yongxian Wu. "Comparative experimental study of ionic polymer–metal composites with different backbone ionomers and in various cation forms." *Journal of Applied Physics* 93.9 (2003): 5255-5267.

[22] Nemat-Nasser, Sia, Shahram Zamani, and Yitzhak Tor. "Effect of solvents on the chemical and physical properties of ionic polymer-metal composites." *Journal of Applied Physics* 99.10 (2006): 104902.

[23] Kim, Kwang J., and Mohsen Shahinpoor. "Ionic polymer–metal composites: II. Manufacturing techniques." *Smart materials and structures* 12, no. 1 (2003): 65.

[24] Bahramzadeh, Yousef, and Mohsen Shahinpoor. "A review of ionic polymeric soft actuators and sensors." *Soft Robotics* 1, no. 1 (2014): 38-52.

[25] Bar-Cohen, Yoseph. "Electroactive polymers: current capabilities and challenges." In *SPIE's 9th Annual International Symposium on Smart Structures and Materials*, pp. 1-7. International Society for Optics and Photonics, 2002.

[26] Bar-Cohen, Yoseph, and Qiming Zhang. "Electroactive polymer actuators and sensors." *MRS bulletin* 33, no. 03 (2008): 173-181.

[27] Bar-Cohen, Yoseph, Sean P. Leary, Mohsen Shahinpoor, Joycelyn S. Harrison, and Joseph G. Smith. "Electroactive polymer (EAP) actuators for planetary applications." In *1999 Symposium on Smart Structures and Materials*, pp. 57-63. International Society for Optics and Photonics, 1999.

[28] Bar-Cohen, Yoseph. "Electroactive polymers as artificial muscles: Capabilities, potentials and challenges." In *Robotics 2000*, pp. 188-196. 2000.

[29] Bar-Cohen, Yoseph. "Electroactive polymers as artificial muscles: a review." *Journal of Spacecraft and Rockets* 39, no. 6 (2002): 822-827.

[30] Bar-Cohen, Yoseph, Kwang J. Kim, Hyouk Ryeol Choi, and John DW Madden. "Electroactive polymer materials." *Smart Materials and Structures* 16, no. 2 (2007).

[31] Keshavarzi, Amid, Mohsen Shahinpoor, Kwang J. Kim, and Jeffrey W. Lantz. "Blood pressure, pulse rate, and rhythm measurement using ionic polymer-metal composite sensors." In *1999 Symposium on Smart Structures and Materials*, pp. 369-376. International Society for Optics and Photonics, 1999.

[32] McDaid, A. J., K. C. Aw, E. Haemmerle, M. Shahinpoor, and S. Q. Xie. "Adaptive tuning of a 2DOF controller for robust cell manipulation using IPMC actuators." *Journal of Micromechanics and Microengineering* 21, no. 12 (2011): 125004.

[33] Shahinpoor, Mohsen. "Smart thin sheet batteries made with ionic polymer metal composites (IPMC'S)." In *ASME 2004 International Mechanical Engineering Congress and Exposition*, pp. 97-102. American Society of Mechanical Engineers, 2004.

[34] Bahramzadeh, Y., and M. Shahinpoor. "Ionic Polymer-Metal Composites (IPMCs) as dexterous manipulators and tactile sensors for minimally invasive robotic surgery." In *SPIE Smart Structures and Materials+ Nondestructive Evaluation and Health Monitoring*, pp. 83402O-83402O. International Society for Optics and Photonics, 2012.

[35] Van De Pol, F. C. M., and J. Branebjerg. "Micro liquid-handling devices-A review." In *Micro System Technologies 90*, pp. 799-805. Springer Berlin Heidelberg, 1990.

[36] Singh, S., N. Kumar, D. George, and A. K. Sen. "Analytical modeling, simulations and experimental studies of a PZT actuated planar valveless PDMS micropump." *Sensors and Actuators A: Physical* 225 (2015): 81-94.

[37] Huang, Xiaoyang, and Toh Kok Chuan. "MEMS-micropumps: a review." In *Journal of Fluids Engineering-Transactions of the ASME*. 2002.

[38] Laser, Daniel J., and Juan G. Santiago. "A review of micropumps." *Journal of micromechanics and microengineering* 14, no. 6 (2004): R35.

[39] Guo, Shuxiang, and Kinji Asaka. "Polymer-based new type of micropump for bio-medical application." *Proceedings. ICRA'03. IEEE International Conference on Robotics and Automation*, vol. 2, (2003): 1830-1835.

[40] Pak, James J., Jihong Kim, Sang Woo Oh, Jee Hee Son, Sung Hwan Cho, Seung-Ki Lee, Jong-Yeon Park, and Byungkyu Kim. "Fabrication of ionic-polymer-metal-composite (IPMC) micropump using a commercial Nafion." In *Smart Structures and Materials*, (2004): 272-280. International Society for Optics and Photonics.

[41] Lee, Sangki, and Kwang J. Kim. "Design of IPMC actuator-driven valve-less micropump and its flow rate estimation at low Reynolds numbers." *Smart materials and structures* 15, no. 4 (2006): 1103-1109.

[42] Nguyen, Thanh Tung, Nam Seo Goo, Vinh Khanh Nguyen, Youngtai Yoo, and Seungbae Park. "Design, fabrication, and experimental characterization of a flap valve IPMC micropump with a flexibly supported diaphragm." *Sensors and Actuators A: Physical* 141, no. 2 (2008): 640-648.

[43] Santos, J., B. Lopes, and PJ Costa Branco. "Ionic polymer–metal composite material as a diaphragm for micropump devices." *Sensors and Actuators A: Physical* 161, no. 1 (2010): 225-233.

[44] Nam, Doan Ngoc Chi, and Kyoung Kwan Ahn. "Design of an IPMC diaphragm for micropump application." *Sensors and Actuators A: Physical* 187 (2012): 174-182.

[45] Kawun, Paul, Stephane Leahy, and Yongjun Lai. "A thin PDMS nozzle/diffuser micropump for biomedical applications." *Sensors and Actuators A: Physical* 249 (2016): 149-154.

[46] Angueira, Eugenio. "Non-insulin treatments for diabetes." *American journal of therapeutics* 20, no. 4 (2013): 377-384.

[47] Bagnasco, Annamaria, Patrizia Di Giacomo, Roberta Da Rin Della Mora, Gianluca Catania, Carlo Turci, Gennaro Rocco, and Loredana Sasso. "Factors influencing self-

management in patients with type 2 diabetes: a quantitative systematic review protocol." *Journal of advanced nursing* 70, no. 1 (2014): 187-200.

[48] Bascones-Martinez, Antonio, Paula Matesanz-Perez, Marta Escribano-Bermejo, Miguel-Ángel González-Moles, Jaime Bascones-Ilundain, and Jukka-H. Meurman. "Periodontal disease and diabetes Review of the Literature." *Med Oral Patol Oral Cir Bucal* 16, no. 6 (2011): e722-729.

[49] Blair, Meg. "Diabetes mellitus review." *Urologic nursing* 36, no. 1 (2016): 27-37.

[50] Brunton, Stephen, and Jaime A. Davidson. "Exenatide once weekly: a review of pharmacology and treatment considerations in type 2 diabetes." *Clinical therapeutics* 38, no. 3 (2016): 582-594.

[50] Brunton, S. "Insulin Delivery Systems: Reducing Barriers to Insulin Therapy and Advancing Diabetes Mellitus Treatment. " *The American Journal of Medicine* 121, no. 6 (2008): S35–S41.

[51] Fonseca, Vivian A., and Karmeen D. Kulkarni. "Management of type 2 diabetes: oral agents, insulin, and injectables." *Journal of the American Dietetic Association* 108, no. 4 (2008): S29-S33.

[52] Goo, Alvin KY, Deborah Stier Carson, and Aleksandra Bjelajac. "Metformin: a new treatment option for non-insulin-dependent diabetes mellitus." *Journal of family practice* 42, no. 6 (1996): 612-619.

[53] Iser, Betine Pinto Moehlecke, Sheila Rizzato Stopa, Patrícia Sampaio Chueiri, Célia Landmann Szwarcwald, Deborah Carvalho Malta, Helena Oliveira da Cruz Monteiro, Bruce Bartholow Duncan, and Maria Inês Schmidt. "Prevalência de diabetes autorreferido no Brasil: resultados da Pesquisa Nacional de Saúde 2013." *Epidemiologia e Serviços de Saúde* 24, no. 2 (2015): 305-314.

[54] Marrero, David G. "Overcoming patient barriers to initiating insulin therapy in type 2 diabetes mellitus." *Clinical cornerstone* 8, no. 2 (2007): 33-43.

American Diabetes Association. "Standards of medical care in diabetes—2007." *Diabetes care* 30, no. suppl 1 (2007): S4-S41.

[55] American Diabetes Association. "Standards of medical care in diabetes—2013." *Diabetes care* 36, no. Supplement 1 (2013): S11-S66.

[56] Nathan, David M. "Diabetes: advances in diagnosis and treatment." *Jama* 314, no. 10 (2015): 1052-1062.

[57] Pickup, John C. "Insulin-pump therapy for type 1 diabetes mellitus." *New England Journal of Medicine* 366, no. 17 (2012): 1616-1624.

[58] Reznik, Yves, Ohad Cohen, Ronnie Aronson, Ignacio Conget, Sarah Runzis, Javier Castaneda, Scott W. Lee, and OpT2mise Study Group. "Insulin pump treatment compared with multiple daily injections for treatment of type 2 diabetes (OpT2mise): a randomised open-label controlled trial." *The Lancet* 384, no. 9950 (2014): 1265-1272.

[59] McMahon, Graham T., and Ronald A. Arky. "Inhaled insulin for diabetes mellitus." *New England Journal of Medicine* 356, no. 5 (2007): 497-502.

[60] Skyler, Jay S., Ruth S. Weinstock, Philip Raskin, Jean-François Yale, Eugene Barrett, John E. Gerich, and Hertzel C. Gerstein. "Use of inhaled insulin in a basal/bolus insulin regimen in type 1 diabetic subjects." *Diabetes care* 28, no. 7 (2005): 1630-1635.

[61] Chemitiganti, Ramachandra Rahul V., and Craig W. Spellman. "Management of progressive type 2 diabetes: role of insulin therapy." *Osteopathic medicine and primary care* 3, no. 1 (2009): 5.

[62] Van Belle, Tom L., Ken T. Coppieters, and Matthias G. Von Herrath. "Type 1 diabetes: etiology, immunology, and therapeutic strategies." *Physiological reviews* 91, no. 1 (2011): 79-118.

[63] Yousri, Noha A., Dennis O. Mook-Kanamori, Mohammed M. El-Din Selim, Ahmed H. Takiddin, Hala Al-Homsi, Khoulood AS Al-Mahmoud, Edward D. Karoly et al. "A systems view of type 2 diabetes-associated metabolic perturbations in saliva, blood and urine at different timescales of glycaemic control." *Diabetologia* 58, no. 8 (2015): 1855-1867.

[64] 1. Sia, Samuel K., and George M. Whitesides. "Microfluidic devices fabricated in poly (dimethylsiloxane) for biological studies." *Electrophoresis* 24, no. 21 (2003): 3563-3576.

[65] McClain, Maxine A., Christopher T. Culbertson, Stephen C. Jacobson, Nancy L. Allbritton, Christopher E. Sims, and J. Michael Ramsey. "Microfluidic devices for the high-throughput chemical analysis of cells." *Analytical chemistry* 75, no. 21 (2003): 5646-5655.

[66] González-Guerrero, Maria José, F. Javier del Campo, Juan Pablo Esquivel, Fabien Giroud, Shelley D. Minteer, and Neus Sabaté. "Paper-based enzymatic microfluidic fuel cell: From a two-stream flow device to a single-stream lateral flow strip." *Journal of Power Sources* 326 (2016): 410-416.

[67] Björnmalm, Mattias, Yan Yan, and Frank Caruso. "Engineering and evaluating drug delivery particles in microfluidic devices." *Journal of Controlled Release* 190 (2014): 139-149.

[68] Wang, Qi, Ting Yu, and Zhe Guo. "Cancer Associated Fibroblast Promotes Non-Small Cell Lung Cancer Invasiveness By Activating GRP78 Expression On An Integreated Bionic Microfluidic Device." In B30. *MOLECULAR AND IMMUNOLOGICAL ASPECTS OF LUNG CANCER*, pp. A3132-A3132. American Thoracic Society, 2016.

[69] Tseng, Hsiu-Yang, Scott Malfesi, Nadia Tehranchi, Mona Rahbar, John Jones, and Bonnie L. Gray. "On-Board Array for Multiplexed Semi-Active Cooling-Rate-Controlled Cryopreservation of Living Cells." *Journal of Medical and Biological Engineering* 36, no. 2 (2016): 206-213.

[70] Zhang, Chunsun, Da Xing, and Yuyuan Li. "Micropumps, microvalves, and micromixers within PCR microfluidic chips: advances and trends." *Biotechnology advances* 25, no. 5 (2007): 483-514.

[71] Chang, Yi-Hsien, Gwo-Bin Lee, Fu-Chun Huang, Yi-Yu Chen, and Jr-Lung Lin. "Integrated polymerase chain reaction chips utilizing digital microfluidics." *Biomedical microdevices* 8, no. 3 (2006): 215-225.

[72] Lin, Yi-Chen, Chung-Yi Yu, Chung-Min Li, Chin-Heng Liu, Jiun-Peng Chen, Tah-Hsiung Chu, and Guo-Dung John Su. "An ionic-polymer-metallic composite actuator for reconfigurable antennas in mobile devices." *Sensors* 14, no. 1 (2014): 834-847.

[73] Seiler, T., and J. Wollensak. "The resistance of the trabecular meshwork to aqueous humor outflow." *Graefe's archive for clinical and experimental ophthalmology* 223, no. 2 (1985): 88-91.

[74] Toris, Carol B., Scott A. Koepsell, Michael E. Yablonski, and Carl B. Camras. "Aqueous humor dynamics in ocular hypertensive patients." *Journal of glaucoma* 11, no. 3 (2002): 253-258.

[75] Weinreb, Robert N., Tin Aung, and Felipe A. Medeiros. "The pathophysiology and treatment of glaucoma: a review." *Jama* 311, no. 18 (2014): 1901-1911.

[76] Willoughby, Colin E., Diego Ponzin, Stefano Ferrari, Aires Lobo, Klara Landau, and Yadollah Omidi. "Anatomy and physiology of the human eye: effects of mucopolysaccharidoses disease on structure and function–a review." *Clinical & Experimental Ophthalmology* 38, no. s1 (2010): 2-11.

[77] Adatia, Feisal A., and Karim F. Damji. "Chronic open-angle glaucoma. Review for primary care physicians." *Canadian family physician* 51, no. 9 (2005): 1229-1237.

[78] Gedde, Steven J., Kuldev Singh, Joyce C. Schiffman, William J. Feuer, and Tube Versus Trabeculectomy Study Group. "The Tube Versus Trabeculectomy Study:

interpretation of results and application to clinical practice." *Current opinion in ophthalmology* 23, no. 2 (2012): 118-126.

[79] Quigley, Harry A. "Open-angle glaucoma." *New England Journal of Medicine* 328, no. 15 (1993): 1097-1106.

[80] Villamarin, Adan, Sylvain Roy, Reda Hasballa, Orestis Vardoulis, Philippe Reymond, and Nikolaos Stergiopulos. "3D simulation of the aqueous flow in the human eye." *Medical engineering & physics* 34, no. 10 (2012): 1462-1470.

[81] Kwon, Young H., John H. Fingert, Markus H. Kuehn, and Wallace LM Alward. "Primary open-angle glaucoma." *New England Journal of Medicine* 360, no. 11 (2009): 1113-1124.

[82] Fitt, A. D., and G. Gonzalez. "Fluid mechanics of the human eye: aqueous humour flow in the anterior chamber." *Bulletin of mathematical biology* 68, no. 1 (2006): 53-71.

[83] Greco, Antonio, Maria Ida Rizzo, Armando De Virgilio, Andrea Gallo, Massimo Fusconi, and Marco de Vincentiis. "Emerging concepts in glaucoma and review of the literature." *The American journal of medicine* 129, no. 9 (2016): 1000-e7.

[84] Wimmer, Iris, Ulrich Welge-Luessen, Greda Picht, and Franz Grehn. "Influence of argon laser trabeculoplasty on transforming growth factor-beta 2 concentration and bleb scarring following trabeculectomy." *Graefe's archive for clinical and experimental ophthalmology* 241, no. 8 (2003): 631-636.

[85] Modi, Neil, Kaveh Vahdani, and Adam P. Booth. "Glaucoma surgery." *The Journal of Perioperative Practice* 21, no. 1 (2011): 33-37.

[86] Hong, Chian-Huey, Analisa Arosemena, David Zurakowski, and Ramesh S. Ayyala. "Glaucoma drainage devices: a systematic literature review and current controversies." *Survey of ophthalmology* 50, no. 1 (2005): 48-60.

[87] Sarkisian Jr, Steven R. "Tube shunt complications and their prevention." *Current opinion in ophthalmology* 20, no. 2 (2009): 126-130.

[88] Reiss, George R., Jacob T. Wilensky, and Eve J. Higginbotham. "Laser trabeculoplasty." Survey of ophthalmology 35, no. 6 (1991): 407-428.

[89] Molteno, A. C. "New implant for drainage in glaucoma. Clinical trial." *The British journal of ophthalmology* 53, no. 9 (1969): 606.

[90] Fellenbaum, Paul S., Paul A. Sidoti, Dale K. Heuer, Don S. Minckler, George Baerveldt, and Paul P. Lee. "Experience with the Baerveldt implant in young patients with complicated glaucomas." Journal of glaucoma 4, no. 2 (1995): 91-97.

[91] Krupin, Theodore, Paul Kaufman, Alan Mandell, Robert Ritch, Carl Asseff, Steven M. Podos, and Bernard Becker. "Filtering valve implant surgery for eyes with neovascular glaucoma." American journal of ophthalmology 89, no. 3 (1980): 338-343.

[92] http://www.newworldmedical.com.

[93] Weinreb, Robert N., and Peng Tee Khaw. "Primary open-angle glaucoma." The Lancet 363, no. 9422 (2004): 1711-1720.

[94] Gardiner, Stuart K., Shaban Demirel, Mae O. Gordon, Michael A. Kass, and Ocular Hypertension Treatment Study Group. "Seasonal changes in visual field sensitivity and intraocular pressure in the ocular hypertension treatment study." *Ophthalmology* 120, no. 4 (2013): 724-730.

[95] Shahinpoor, M. "Conceptual design, kinematics and dynamics of swimming robotic structures using ionic polymeric gel muscles." *Smart Materials and Structures* 1, no. 1 (1992): 91.

[96] Guo, Shuxiang, Yarning Ge, Lingfei Li, and Sheng Liu. "Underwater swimming micro robot using IPMC actuator." In Mechatronics and Automation, Proceedings of the 2006 IEEE International Conference on, pp. 249-254. IEEE, 2006.

[97] Yeom, Sung-Weon, and Il-Kwon Oh. "A biomimetic jellyfish robot based on ionic polymer metal composite actuators." Smart materials and structures 18, no. 8 (2009): 085002.

[98] Shen, Qi, Tiammiao Wang, Jianhong Liang, and Li Wen. "Hydrodynamic performance of a biomimetic robotic swimmer actuated by ionic polymer–metal composite." *Smart Materials and Structures* 22, no. 7 (2013): 075035.

[99] Kim, Byungkyu, Deok-Ho Kim, Jaehoon Jung, and Jong-Oh Park. "A biomimetic undulatory tadpole robot using ionic polymer–metal composite actuators." *Smart materials and structures* 14, no. 6 (2005): 1579.

[100] Kim, Kwang J., Woosoon Yim, Jason W. Paquette, and Doyeon Kim. "Ionic polymer-metal composites for underwater operation." *Journal of Intelligent Material Systems and Structures* 18, no. 2 (2007): 123-131.

[101] Chen, Zheng, Tae I. Um, and Hilary Bart-Smith. "A novel fabrication of ionic polymer–metal composite membrane actuator capable of 3-dimensional kinematic motions." *Sensors and Actuators A: Physical* 168, no. 1 (2011): 131-139.

[102] Hubbard, Joel J., Maxwell Fleming, Viljar Palmre, David Pugal, Kwang J. Kim, and Kam K. Leang. "Monolithic IPMC fins for propulsion and maneuvering in

bioinspired underwater robotics." *IEEE Journal of Oceanic Engineering* 39, no. 3 (2014): 540-551.

[103] Cha, Youngsu, Jeffrey Laut, Paul Phamduy, and Maurizio Porfiri. "Swimming robots have scaling laws, too." *IEEE/ASME Transactions on Mechatronics* 21, no. 1 (2016): 598-600.

[104] Abdelnour, Karl, Elisa Mancia, Sean D. Peterson, and Maurizio Porfiri. "Hydrodynamics of underwater propulsors based on ionic polymer–metal composites: a numerical study." *Smart Materials and Structures* 18, no. 8 (2009): 085006.

[105] Lee, Joon Soo, Shivakanth Gutta, and Woosoon Yim. "Open-loop control of ionic polymer metal composite (IPMC) based underwater actuator using a network of neural oscillator." *Intelligent Robots and Systems, 2007. IROS 2007. IEEE/RSJ International Conference on*, pp. 2132-2137. IEEE, 2007.

[106] Hamlen, R. P., C. E. Kent, and S. N. Shafer. "Electrolytically activated contractile polymer." (1965): 1149-1150.

[107] Tanaka, Toyoichi, et al. "Collapse of gels in an electric field." *Science* 218.4571 (1982): 467-469.

[108] Osada, Yoshihito, and Mariko Hasebe. "Electrically activated mechanochemical devices using polyelectrolyte gels." *Chemistry Letters* 9 (1985): 1285-1288.

[109] Osada, Yoshihito. "Conversion of chemical into mechanical energy by synthetic polymers (chemomechanical systems)." *Polymer Physics*. Springer Berlin Heidelberg, (1987): 1-46.

[110] Osada, Yoshihito, Kayo Umezawa, and Aizo Yamauchi. "Entrained responses of the current oscillation of polymer gels to sinusoidal stimulation." *Bulletin of the Chemical Society of Japan* 62.10 (1989): 3232-3238.

[111] Osada, Yoshihito. "Chemical valves and gel actuators." *Advanced Materials* 3.2 (1991): 107-108.

[112] Shiga, Tohru, and Toshio Kurauchi. "Deformation of polyelectrolyte gels under the influence of electric field." *Journal of Applied Polymer Science* 39.11-12 (1990): 2305-2320.

[113] Shiga, Tohru, et al. "Bending of poly (vinyl alcohol)–poly (sodium acrylate) composite hydrogel in electric fields." *Journal of applied polymer science* 44.2 (1992): 249-253.

[114] Shiga, Tohru, et al. "Electric field-associated deformation of polyelectrolyte gel near a phase transition point." *Journal of applied polymer science* 46.4 (1992): 635-640.

[115] Shahinpoor, Mohsen. "Micro-electro-mechanics of ionic polymeric gels as electrically controllable artificial muscles." *Journal of Intelligent Material Systems and Structures* 6.3 (1995): 307-314.

[116] Nemat-Nasser, Sia, and Jiang Yu Li. "Electromechanical response of ionic polymer-metal composites." *Journal of Applied Physics* 87.7 (2000): 3321-3331.

[117] De Rossi, D., et al. "Pseudomuscular gel actuators for advanced robotics." *Journal of intelligent material systems and structures* 3.1 (1992): 75-95.

[118] Chiarelli, P., and D. De Rossi. "Determination of mechanical parameters related to the kinetics of swelling in an electrically activated contractile gel." *Relationships of Polymeric Structure and Properties*. Steinkopff, 1988. 4-8.

[119] Shiga, T., et al. "Bending of high strength polymer gel in an electric field." *Polymer Preparation* 46.11 (1989): 709-713.

[120] O'Grady, Megan L., Po-ling Kuo, and Kevin Kit Parker. "Optimization of electroactive hydrogel actuators." *ACS applied materials & interfaces* 2, no. 2 (2009): 343-346.

[121] Calvert, Paul. "Electroactive polymer gels." *Electroactive Polymer (EAP) Actuators as Artificial Muscles—Reality, Potential and Challenges, ed. Y. Bar-Cohen, SPIE Press, Vol. PM98, 123* 138 (2001).

[122] Yoshioka, Yuka, and Paul Calvert. "Epoxy-based electroactive polymer gels." *Experimental Mechanics* 42, no. 4 (2002): 404-408.

[123] Tanaka, Toyoichi, Shao-Tang Sun, and Izumi Nishio. "Phase Transition in Gels." *Scattering Techniques Applied to Supramolecular and Nonequilibrium Systems*. Springer US, (1981): 321-336.

[124] Flory, Paul J. "Thermodynamics of high polymer solutions." *The Journal of Chemical Physics* 9.8 (1941): 660-660.

[125] Huggins, Maurice L. "Solutions of long chain compounds." *The Journal of Chemical Physics* 9.5 (1941): 440-440.

[126] Flory, Paul J., and John Rehner Jr. "Statistical Mechanics of Cross-Linked Polymer Networks I. Rubberlike Elasticity." *The Journal of Chemical Physics* 11.11 (1943): 512-520.

[127] Flory, Paul J., and John Rehner Jr. "Statistical mechanics of cross-linked polymer networks II. Swelling." *The Journal of Chemical Physics* 11.11 (1943): 521-526.

[128] Dušek, K., et al. "Are cured epoxy resins inhomogeneous?" *Polymer* 19.4 (1978): 393-397.

[1229] Patterson, Donald, and Andrée Robard. "Thermodynamics of polymer compatibility." *Macromolecules* 11.4 (1978): 690-695.

[130] Tanaka, Toyoichi. "Collapse of gels and the critical endpoint." *Physical Review Letters* 40.12 (1978): 820.

[131] Doi, Masao, Mitsuhiro Matsumoto, and Yoshiharu Hirose. "Deformation of ionic polymer gels by electric fields." *Macromolecules* 25.20 (1992): 5504-5511.

[132] Brock, David, et al. "A dynamic model of a linear actuator based on polymer hydrogel." *Journal of intelligent material systems and structures* 5.6 (1994): 764-771.

[133] Grimshaw, P. E., et al. "Kinetics of electrically and chemically induced swelling in polyelectrolyte gels." *The Journal of Chemical Physics* 93.6 (1990): 4462-4472.

[134] De Gennes, P. G., et al. "Mechanoelectric effects in ionic gels." *EPL (Europhysics Letters)* 50.4 (2000): 513.

[135] Tamagawa, Hirohisa, and Minoru Taya. "A theoretical prediction of the ions distribution in an amphoteric polymer gel." *Materials Science and Engineering: A* 285.1 (2000): 314-325.

[136] Li, Hua, Rongmo Luo, and K. Y. Lam. "Modeling of ionic transport in electric-stimulus-responsive hydrogels." *Journal of membrane science* 289.1 (2007): 284-296.

[137]. De, Sudipto K., and N. R. Aluru. "A chemo-electro-mechanical mathematical model for simulation of pH sensitive hydrogels." *Mechanics of materials* 36.5 (2004): 395-410.

[138]. Li, Hua, and Fukun Lai. "Transient analysis of the effect of the initial fixed charge density on the kinetic characteristics of the ionic-strength-sensitive hydrogel by a multi-effect-coupling model." *Analytical and bioanalytical chemistry* 399.3 (2011): 1233-1243.

[139] Wallmersperger, Thomas, et al. "Coupled multifield formulation for ionic polymer gels in electric fields." *SPIE's 8th Annual International Symposium on Smart Structures and Materials*. International Society for Optics and Photonics, 2001.

[140] Wallmersperger, Thomas, Bernd Kröplin, and Rainer W. Gülch. "Coupled chemo-electro-mechanical formulation for ionic polymer gels—numerical and experimental investigations." *Mechanics of Materials* 36.5 (2004): 411-420.

[141]. Wallmersperger, Thomas, Dirk Ballhause, Bernd Kröplin, Margarita Günther, and Gerald Gerlach. "Coupled multi-field formulation in space and time for the simulation of intelligent hydrogels." *Journal of Intelligent Material Systems and Structures* 20, no. 12 (2009): 1483-1492.

[142] Keller, Karsten, et al. "Modeling of temperature-sensitive polyelectrolyte gels by the use of the coupled chemo-electro-mechanical formulation." *Mechanics of Advanced Materials and Structures* 18.7 (2011): 511-523.

[143] Gerlach, Gerald, et al. "Chemical and pH sensors based on the swelling behavior of hydrogels." *Sensors and Actuators B: Chemical* 111 (2005): 555-561.

[144] Orlov, Yury, Xiaoping Xu, and Gerd Maurer. "Equilibrium swelling of N-isopropyl acrylamide based ionic hydrogels in aqueous solutions of organic solvents: Comparison of experiment with theory." *Fluid phase equilibria* 249.1 (2006): 6-16.

[145] Orlov, Yury, Xiaoping Xu, and Gerd Maurer. "An experimental and theoretical investigation on the swelling of N-isopropyl acrylamide based ionic hydrogels in aqueous solutions of (sodium chloride or di-sodium hydrogen phosphate)." *Fluid phase equilibria* 254.1 (2007): 1-10.

[146] Ermatchkov, Viktor, Luciana Ninni, and Gerd Maurer. "Thermodynamics of phase equilibrium for systems containing N-isopropyl acrylamide hydrogels." *Fluid Phase Equilibria* 296.2 (2010): 140-148.

[147] Maurer, G., and J. M. Prausnitz. "Thermodynamics of phase equilibrium for systems containing gels." *Fluid phase equilibria* 115.1 (1996): 113-133.

[148] Scharfer, Philip, Wilhelm Schabel, and Matthias Kind. "Mass transport measurements in membranes by means of in situ Raman spectroscopy-first results of methanol and water profiles in fuel cell membranes." *Journal of Membrane Science* 303.1 (2007): 37-42.

[149] Scharfer, Philip, Wilhelm Schabel, and Matthias Kind. "Modelling of alcohol and water diffusion in fuel cell membranes—experimental validation by means of in situ Raman spectroscopy." *Chemical Engineering Science* 63.19 (2008): 4676-4684.

[150] Yoon, Jinhwan, et al. "Poroelastic swelling kinetics of thin hydrogel layers: comparison of theory and experiment." *Soft Matter* 6.23 (2010): 6004-6012.

[151] Prudnikova, Katsiaryna, and Marcel Utz. "Electromechanical equilibrium properties of poly (acrylic acid/acrylamide) hydrogels." *Macromolecules* 45.2 (2012): 1041-1045.

[152] Mann, Bernward A., Kurt Kremer, and Christian Holm. "The swelling behavior of charged hydrogels." *Macromolecular symposia*. Vol. 237. No. 1. WILEY-VCH Verlag, 2006.

[153] Quesada-Pérez, Manuel, et al. "Gel swelling theories: the classical formalism and recent approaches." *Soft Matter* 7.22 (2011): 10536-10547.

[154] Sun, D. N., et al. "A mixed finite element formulation of triphasic mechano-electrochemical theory for charged, hydrated biological soft tissues." *International Journal for Numerical Methods in Engineering* 45.10 (1999): 1375-1402.

[155] Van Loon, R., et al. "3D FE implementation of an incompressible quadriphasic mixture model." *International Journal for Numerical Methods in Engineering* 57.9 (2003): 1243-1258.

[156] Ehlers, "Wolfgang. Foundations of multiphasic and porous materials." *Springer* Berlin Heidelberg, 2002.

[157] Acartürk, Ayhan Yusuf. "Simulation of charged hydrated porous materials." PhD Thesis, Stuttgart University (2009).

[158] Walter, Jonathan, et al. "Molecular dynamics and experimental study of conformation change of poly (N-isopropylacrylamide) hydrogels in water." *Fluid Phase Equilibria* 296.2 (2010): 164-172.

[159] Wallmersperger, Thomas, et al. "Multiscale Modeling of Polymer Gels—Chemo-Electric Model versus Discrete Element Model." *Mechanics of Advanced Materials and Structures* 15.3-4 (2008): 228-234.

[160] Guenther, Margarita, Gerald Gerlach, and Thomas Wallmersperger. "Non-linear effects in hydrogel-based chemical sensors: experiment and modeling." *Journal of Intelligent Material Systems and Structures* 20.8 (2009): 949-961.

[161] Bouklas, Nikolaos, and Rui Huang. "Swelling kinetics of polymer gels: comparison of linear and nonlinear theories." *Soft Matter* 8.31 (2012): 8194-8203.

[162] Lucantonio, A., and P. Nardinocchi. "Reduced models of swelling-induced bending of gel bars." *International Journal of Solids and Structures* 49.11 (2012): 1399-1405.

[163] Sadowski, Gabriele. "Special themed issue on “Responsive gels”." *Colloid and Polymer Science* 289.5-6 (2011): 453-453.

[164] Li, Daming, HongLiu Yang, and Heike Emmerich. "Phase field model simulations of hydrogel dynamics under chemical stimulation." *Colloid and Polymer Science* 289.5-6 (2011): 513-521.

[165] Tabatabaei, Fatemeh, Olaf Lenz, and Christian Holm. "Simulational study of anomalous tracer diffusion in hydrogels." *Colloid and Polymer Science* 289.5-6 (2011): 523-534.

[166] Wallmersperger, Thomas, et al. "Modeling and simulation of pH-sensitive hydrogels." *Colloid and Polymer Science* 289.5-6 (2011): 535-544.

[167] Poggendorf, Stefanie, et al. "Diffusion of poly (ethylene glycol) and ectoine in NIPAAm hydrogels with confocal Raman spectroscopy." *Colloid and Polymer Science* 289.5-6 (2011): 545-559.

[168] Duda, Fernando P., Angela C. Souza, and Eliot Fried. "A theory for species migration in a finitely strained solid with application to polymer network swelling." *Journal of the Mechanics and Physics of Solids* 58.4 (2010): 515-529.

[169] Wu, Shunnian, et al. "Modeling investigation of hydrogel volume transition." *Macromolecular theory and simulations* 13.1 (2004): 13-29.

[170] Gibbs, Josiah Willard. *Scientific Papers: Thermodynamics*. Vol. 1. Dover Publications, 1961.

[171] Truesdell, C. "Thermodynamics of diffusion." *Rational thermodynamics*. Springer New York, 1984. 219-236.

[172] Morland, L. W. "A simple constitutive theory for a fluid-saturated porous solid." *Journal of Geophysical Research* 77.5 (1972): 890-900.

[173] Lai, W. M., J. S. Hou, and V. C. Mow. "A triphasic theory for the swelling and deformation behaviors of articular cartilage." *Journal of biomechanical engineering* 113.3 (1991): 245-258.

[174] Gu, W. Y., W. M. Lai, and V. C. Mow. "A triphasic analysis of negative osmotic flows through charged hydrated soft tissues." *Journal of biomechanics* 30.1 (1997): 71-78.

[175] Sun, D. N., et al. "A mixed finite element formulation of triphasic mechano-electrochemical theory for charged hydrated biological soft tissues." *International Journal for Numerical Methods in Engineering* 45.10 (1999): 1375-1402.

[176] Li, Hua, et al. "Model development and numerical simulation of electric-stimulus-responsive hydrogels subject to an externally applied electric field." *Biosensors and Bioelectronics* 19.9 (2004): 1097-1107.

[177] Lu, X. Lux, et al. "Indentation determined mechanoelectrochemical properties and fixed charge density of articular cartilage." *Annals of biomedical engineering* 32.3 (2004): 370-379.

[178] Setton, Lori A., Wenbo Zhu, and Van C. Mow. "The biphasic poroviscoelastic behavior of articular cartilage: role of the surface zone in governing the compressive behavior." *Journal of biomechanics* 26.4 (1993): 581-592.

[179] Lai, W. Michael, et al. "On the electric potentials inside a charged soft hydrated biological tissue: streaming potential versus diffusion potential." *Journal of biomechanical engineering* 122.4 (2000): 336-346.
[180] Biot, Maurice A. "General theory of three-dimensional consolidation." *Journal of applied physics* 12.2 (1941): 155-164.
[181] Hong, Wei, et al. "A theory of coupled diffusion and large deformation in polymeric gels." *Journal of the Mechanics and Physics of Solids* 56.5 (2008): 1779-1793.
[182] Zhao, Xuanhe, and Zhigang Suo. "Electrostriction in elastic dielectrics undergoing large deformation." *Journal of Applied Physics* 104.12 (2008): 123530.
[183] Hong, Wei, et al. "A theory of coupled diffusion and large deformation in polymeric gels." *Journal of the Mechanics and Physics of Solids* 56.5 (2008): 1779-1793.
[184] Oguro, K., Y. Kawami, and H. Takenaka. "Bending of an ion-conducting polymer film-electrode composite by an electric stimulus at low voltage." *Journal of Micromachine Society* 5.1 (1992): 27-30.
[185] Sadeghipour, K., R. Salomon, and S. Neogi. "Development of a novel electrochemically active membrane and 'smart' material based vibration sensor/damper." *Smart Materials and Structures* 1.2 (1992): 172.
[186] Shahinpoor, Mohsen, et al. "Ionic polymer-metal composites (IPMCs) as biomimetic sensors, actuators and artificial muscles-a review." *Smart materials and structures* 7.6 (1998): R15-R30.
[187] Nemat-Nasser, S., and C. Thomas. "Ionomeric Polymer–Metal Composites Electroactive Polymer (EAP) Actuators as Artificial Muscles—Reality, Potential and Challenges (Bellingham, WA: SPIE Optical Engineering Press) chapter 6." (2004): 171-230.
[188] Shahinpoor, Mohsen, and Kwang J. Kim. "Ionic polymer–metal composites: III. Modeling and simulation as biomimetic sensors, actuators, transducers, and artificial muscles." Smart materials and structures 13.6 (2004): 1362-1388.
[189] Kanno, Ryu, et al. "Linear approximate dynamic model of ICPF (ionic conducting polymer gel film) actuator." IEEE International Conference on Robotics and Automation Proceedings Vol. 1. (1996): 219-225.
[190] Tadokoro, Satoshi, et al. "Modeling of Nafion-Pt composite actuators (ICPF) by ionic motion." SPIE's 7th Annual International Symposium on Smart Structures and Materials (2000): 92-102.

[191] Mallavarapu, Kiran, Kenneth M. Newbury, and Donald J. Leo. "Feedback control of the bending response of ionic polymer-metal composite actuators." SPIE's 8th Annual International Symposium on Smart Structures and Materials (2001): 301-310.

[192] Mallavarapu, Kiran, and Donald J. Leo. "Feedback control of the bending response of ionic polymer actuators." *Journal of Intelligent Material Systems and Structures* 12.3 (2001): 143-155.

[193] Newbury, Kenneth M., and Donald J. Leo. "Linear electromechanical model of ionic polymer transducers-part I: model development." *Journal of Intelligent Material Systems and Structures* 14.6 (2003): 333-342.

[194] Farinholt, Kevin, and Donald J. Leo. "Modeling of electromechanical charge sensing in ionic polymer transducers." *Mechanics of Materials* 36.5 (2004): 421-433.

[195] Nemat-Nasser, Sia, and Jiang Yu Li. "Electromechanical response of ionic polymer-metal composites." *Journal of Applied Physics* 87.7 (2000): 3321-3331.

[196] Nemat-Nasser, Sia. "Micromechanics of actuation of ionic polymer-metal composites." *Journal of Applied Physics* 92.5 (2002): 2899-2915.

[197] Nemat-Nasser, Siavouche, and Yongxian Wu. "Tailoring actuation of ionic polymer metal composites through cation combination." *Smart Structures and Materials. International Society for Optics and Photonics* (2003): 245-253.

[198] Nemat-Nasser, Sia, Shahram Zamani, and Yitzhak Tor. "Effect of solvents on the chemical and physical properties of ionic polymer-metal composites." *Journal of Applied Physics* 99.10 (2006): 104902.

[199] Branco, PJ Costa, and J. A. Dente. "Derivation of a continuum model and its electric equivalent-circuit representation for ionic polymer–metal composite (IPMC) electromechanics." *Smart Materials and Structures* 15.2 (2006): 378-392.

[200] Lee, Sangki, Hoon Cheol Park, and Kwang Jin Kim. "Equivalent modeling for ionic polymer–metal composite actuators based on beam theories." *Smart materials and structures* 14.6 (2005): 1363.

[201] Xiao, Yu, and Kaushik Bhattacharya. "Modeling electromechanical properties of ionic polymers." SPIE's 8th Annual International Symposium on Smart Structures and Materials (2001): 292-300.

[202] Weiland, Lisa Mauck, and Donald J. Leo. "Computational analysis of ionic polymer cluster energetics." *Journal of Applied physics* 97.1 (2005): 013541.

[203] Weiland, Lisa Mauck, and Donald J. Leo. "Ionic polymer cluster energetics: Computational analysis of pendant chain stiffness and charge imbalance." *Journal of Applied physics* 97.12 (2005): 123530.

[204] Farinholt, Kevin M., and Donald J. Leo. "Modeling the electrical impedance response of ionic polymer transducers." *Journal of Applied Physics* 104.1 (2008): 014512.

[205] Leo, Donald J., Kevin Farinholt, and Thomas Wallmersperger. "Computational models of ionic transport and electromechanical transduction in ionomeric polymer transducers." *Smart Structures and Materials* (2005): 170-181.

[206] Wallmersperger, Thomas, Donald J. Leo, and Curt S. Kothera. "Transport modeling in ionomeric polymer transducers and its relationship to electromechanical coupling." *Journal of Applied Physics* 101.2 (2007): 024912.

[207] Wallmersperger, Thomas, et al. "Electrochemical response in ionic polymer transducers: An experimental and theoretical study." *Composites Science and Technology* 68.5 (2008): 1173-1180.

[208] Wallmersperger, Thomas, et al. "Chemo-electric characterization and modeling of the high surface area electrodes in ionic polymer transducers." The 14th International Symposium on: Smart Structures and Materials & Nondestructive Evaluation and Health Monitoring (2007): 65240S.

[209] Akle, Barbar J., et al. "High surface area electrodes in ionic polymer transducers: numerical and experimental investigations of the chemo-electric behavior." The 15th International Symposium on: Smart Structures and Materials & Nondestructive Evaluation and Health Monitoring (2008): 69290N.

[210] Akle, Barbar J., et al. "High surface area electrodes in ionic polymer transducers: numerical and experimental investigations of the electro-chemical behavior." *Journal of Applied Physics* 109.7 (2011): 074509.

[211] He, Xingxi, Donald J. Leo, and Thomas Wallmersperger. "Modeling of ion transport in high strain ionomers by Monte Carlo simulation compared to continuum model." Proceedings of the ASME International Mechanical Engineering Congress and Exposition, (Paper number IMECE2006-13928) 71 (2006): 119-126.

[212] Pugal, D., et al. "An advanced finite element model of IPMC." The 15th International Symposium on: Smart Structures and Materials & Nondestructive Evaluation and Health Monitoring (2008): 692711.

[213] Pugal, Deivid, et al. "A self-oscillating ionic polymer-metal composite bending actuator." *Journal of Applied Physics* 103.8 (2008): 084908.

[214] Nardinocchi, Paola, Matteo Pezzulla, and Luca Placidi. "Thermodynamically based multiphysic modeling of ionic polymer metal composites." *Journal of Intelligent Material Systems and Structures* 22.16 (2011): 1887-1897.

[215] Enikov, Eniko T., and Geon S. Seo. "Numerical Analysis of Muscle-Like Ionic Polymer Actuators." *Biotechnology progress* 22.1 (2006): 96-105.

[216] Chen, Zheng, et al. "A dynamic model for ionic polymer–metal composite sensors." *Smart Materials and Structures* 16.4 (2007): 1477-1488.

[217] Bonomo, C., et al. "A nonlinear model for ionic polymer metal composites as actuators." *Smart Materials and Structures* 16.1 (2007): 1-12.

[218] Porfiri, Maurizio. "Charge dynamics in ionic polymer metal composites." *Journal of Applied Physics* 104.10 (2008): 104915.

[219] Porfiri, Maurizio. "An electromechanical model for sensing and actuation of ionic polymer metal composites." *Smart Materials and Structures* 18.1 (2009): 015016.

[220] Cha, Youngsu, and Maurizio Porfiri. "Bias-dependent model of the electrical impedance of ionic polymer-metal composites." *Physical Review E* 87.2 (2013): 022403.

[221] Aureli, Matteo, and Maurizio Porfiri. "Nonlinear sensing of ionic polymer metal composites." *Continuum Mechanics and Thermodynamics* 25.2-4 (2013): 273-310.

[222] Davidson, Jacob D., and N. C. Goulbourne. "Nonlinear capacitance and electrochemical response of ionic liquid-ionic polymers." *Journal of Applied Physics* 109.8 (2011): 084901.

[223] Comsol Manual Guide version 4.4 (www.comsol.com)

[224] J.M. Coulson and J.F. Richardson, "Particle Technology and Separation Processes," *Chemical Engineering, Volume 2*, Butterworth-Heinemann, 2002.